

Award Number: W81XWH-12-1-0125

TITLE: "Zebrafish Model of NF1 for Structure-Function Analysis, Mechanisms of Glial Tumorigenesis, and Chemical Biology"

PRINCIPAL INVESTIGATOR: Dr. Thomas Look, M.D.

CONTRACTING ORGANIZATION: Dana-Farber Cancer Institute
Boston, MA 02115-6013

REPORT DATE: August 2015

TYPE OF REPORT: Final

PREPARED FOR: U.S. Army Medical Research and Materiel Command
Fort Detrick, Maryland 21702-5012

DISTRIBUTION STATEMENT: Approved for Public Release;
Distribution Unlimited

The views, opinions and/or findings contained in this report are those of the author(s) and should not be construed as an official Department of the Army position, policy or decision unless so designated by other documentation.

REPORT DOCUMENTATION PAGE

Form Approved
OMB No. 0704-0188

Public reporting burden for this collection of information is estimated to average 1 hour per response, including the time for reviewing instructions, searching existing data sources, gathering and maintaining the data needed, and completing and reviewing this collection of information. Send comments regarding this burden estimate or any other aspect of this collection of information, including suggestions for reducing this burden to Department of Defense, Washington Headquarters Services, Directorate for Information Operations and Reports (0704-0188), 1215 Jefferson Davis Highway, Suite 1204, Arlington, VA 22202-4302. Respondents should be aware that notwithstanding any other provision of law, no person shall be subject to any penalty for failing to comply with a collection of information if it does not display a currently valid OMB control number. **PLEASE DO NOT RETURN YOUR FORM TO THE ABOVE ADDRESS.**

1. REPORT DATE August 2015			2. REPORT TYPE Final		3. DATES COVERED 1May2012 - 30Apr2015	
4. TITLE AND SUBTITLE "Zebrafish Model of NF1 for Structure-Function Analysis, Mechanisms of Glial Tumorigenesis, and Chemical Biology"					5a. CONTRACT NUMBER	
					5b. GRANT NUMBER W81XWH-12-1-0125	
					5c. PROGRAM ELEMENT NUMBER	
6. AUTHOR(S) Dr. Thomas Look, M.D. E-Mail: thomas_look@dfci.harvard.edu					5d. PROJECT NUMBER	
					5e. TASK NUMBER	
					5f. WORK UNIT NUMBER	
7. PERFORMING ORGANIZATION NAME(S) AND ADDRESS(ES) Dana-Farber Cancer Institute Office of Grants and Contracts 450 Brookline Avenue, BP3 Boston, MA 02215-5450					8. PERFORMING ORGANIZATION REPORT NUMBER	
9. SPONSORING / MONITORING AGENCY NAME(S) AND ADDRESS(ES) U.S. Army Medical Research and Materiel Command Fort Detrick, Maryland 21702-5012					10. SPONSOR/MONITOR'S ACRONYM(S)	
					11. SPONSOR/MONITOR'S REPORT NUMBER(S)	
12. DISTRIBUTION / AVAILABILITY STATEMENT Approved for Public Release; Distribution Unlimited						
13. SUPPLEMENTARY NOTES						
14. ABSTRACT In collaboration with the Granato lab at Penn, the Epstein lab has discovered striking learning and memory defects in mutant fish. Our data provide compelling evidence that neurofibromin regulates learning and memory by distinct molecular pathways in vertebrates and that deficits produced by genetic loss of function are reversible. These findings support the investigation of cAMP signaling enhancers as a companion therapy to Ras inhibition in the treatment of cognitive dysfunction in NF1. In the Look lab, the zebrafish models of the NF1 tumor suppressor linked cancers of MPNST and glioma have been completely updated to make them optimal for the structure function studies. We established new transgenic lines with overexpression of the receptor tyrosine kinase PDGFRA, which accelerates disease onset and increases the penetrance of MPNST in nf1/p53 deficient zebrafish, to increase the precision of the structure function studies to elucidate the mechanism of tumor suppression by NF1. We also established a faithful model of high-risk neuroblastoma with loss of nf1 and successfully performed in vivo structure-function analysis of NF1. Our results demonstrated that the GAP activity of the GRD domain is required to mediate the tumor suppressor function of <i>nf1</i> in MYCN-induced neuroblastoma tumorigenesis.						
15. SUBJECT TERMS Neurofibromatosis; learning and memory; glioma; MPNST						
16. SECURITY CLASSIFICATION OF:			17. LIMITATION OF ABSTRACT	18. NUMBER OF PAGES	19a. NAME OF RESPONSIBLE PERSON	
a. REPORT	b. ABSTRACT	c. THIS PAGE			USAMRMC	
U	U	U	UU	55	19b. TELEPHONE NUMBER (include area code)	

Table of Contents

	<u>Page</u>
Introduction.....	4
Body.....	4
Key Research Accomplishments.....	11
Conclusion.....	11
Reportable Outcomes.....	13
References.....	16
Appendices.....	17

INTRODUCTION

Neurofibromatosis type 1 (NF1) is a common genetic disorder caused by mutations in the *NF1* gene. Patients exhibit pigmentation abnormalities, learning disorders, bone abnormalities and multiple benign and malignant tumors, including tumors of neural crest origin such as glioma and malignant peripheral nerve sheath tumors (MPNSTs). The *NF1* gene encodes neurofibromin, a protein of over 4,000 amino acids. So far, only a 360 aa region of neurofibromin has been functionally characterized as a GAP-related domain (GRD) which is capable of accelerating the hydrolysis of GTP bound to Ras, thus down-regulating Ras activity. Additional important functions of neurofibromin are yet to be discovered. The purpose of this study is to exploit a new vertebrate animal model of NF1. We capitalize on the advantages of zebrafish as a model system to address pressing questions relevant to the generation of new and effective therapies for NF1. The zebrafish model system will allow the Epstein lab in Aim 1 to perform rapid *in vivo* rescue “structure-function” experiments using wild type and mutant *NF1* genes, as well as constructs expressing portions of the *NF1* protein, in order to determine the functional domains of neurofibromin that have not been previously identified or evaluated. These structure-function mutants will also be used by the Look lab in Aim 2 to understand the role of *nf1* in glioma and MPNST tumorigenesis, which will reveal clinically relevant mechanistic information about neurofibromin function and identify unrecognized functional domains of neurofibromin appropriate for therapeutic targeting.

BODY

Aim 1: To fully characterize *nf1a/b* compound null zebrafish and to perform structure-function studies of *Nf1* *in vivo* by performing rescue experiments in *zn1a/b* loss-of function zebrafish to determine which aspects of the mutant phenotype are regulated by GAP and non-GAP domains (Epstein lab).

Over the past three years, the Epstein laboratory has completed the behavioral evaluation of *nf1a/b* mutant zebrafish. An exciting phenotype has been identified that is relevant to the human disease and to the potential development of meaningful therapies. In collaboration with the Granato lab at Penn, these studies have identified learning and memory defects in mutant fish. We are pleased to report that our work in this area has been published in *Cell Reports* (volume 8, pages 1265-70) in a manuscript entitled: “Modulation of cAMP and ras signaling pathways improves distinct behavioral deficits in a zebrafish model of neurofibromatosis type 1” by Wolman, de Groh, McBride, Jongens and Epstein. The manuscript summarizes our findings that mutant larval zebrafish have dramatic learning and memory defects that can be markedly improved by adding appropriate chemicals (drugs) to the water.

The key findings rely upon a learning and memory assay in which fish are habituated to an acoustic or visual stimulus (a loud noise or a moment of darkness, Figure 1) (1, 2). At first, the fish will respond to the stimulus with a characteristic bending and movement. However, after repeated stimuli, the fish habituate, and respond more slowly or not at all. Interestingly, *nf1a/b* mutant fish habituate (learn) poorly, but this poor learning behavior can be improved by drugs that elevate cAMP (Figure 2). If fish are once again tested after a period of an hour or more, trained fish “remember” the past experience and respond more slowly to renewed stimuli. Mutant fish lacking either 3 or 4 of the *nf1a/b* alleles have poor memory in this assay. This impaired memory phenotype can be improved with drugs that block ras or mapk (but not cAMP; Figure 3).

These results have several important implications for learning and memory deficits in humans with NF1, if the fish prove to be good models of the human disease. First, the defects

are not “hard-wired” or developmental abnormalities, but rather appear to be functional defects that can be modified by chemicals. (We treated the fish for only 30 minutes before testing). This provides reason for hope that proper medications will be beneficial. Second, this completed study strongly suggests that some aspects of neurofibromin function in zebrafish are unrelated to Ras-GAP activity. The work supports a growing body of literature that implicates a function of neurofibromin in the regulation of cAMP (Figure 4). In particular, this work suggests that behavioral abnormalities in neurofibromatosis may be caused or contributed to by aberrations of cAMP signaling and therefore those medications which target Ras alone may not be successful in treating ADHD and other behavioral or learning deficits in affected patients. In the future, it will be important to determine if these findings can be reproduced in mouse models, and if they predict successful treatments for learning disorders in humans with NF1.

The Epstein lab has also prepared the necessary clones for the genetic rescue experiments described in the original proposal. We are now actively proceeding with the structure-function studies by making stable transgenic lines expressing full-length or partial-length human NF1 and breeding them with the *nf1a*;*nf1b* compound mutant zebrafish. We are actively screening embryos to look for the clones that can at least partially rescue the learning and/or memory defect of *nf1a*^{-/-};*nf1b*^{-/-} compound null embryos.

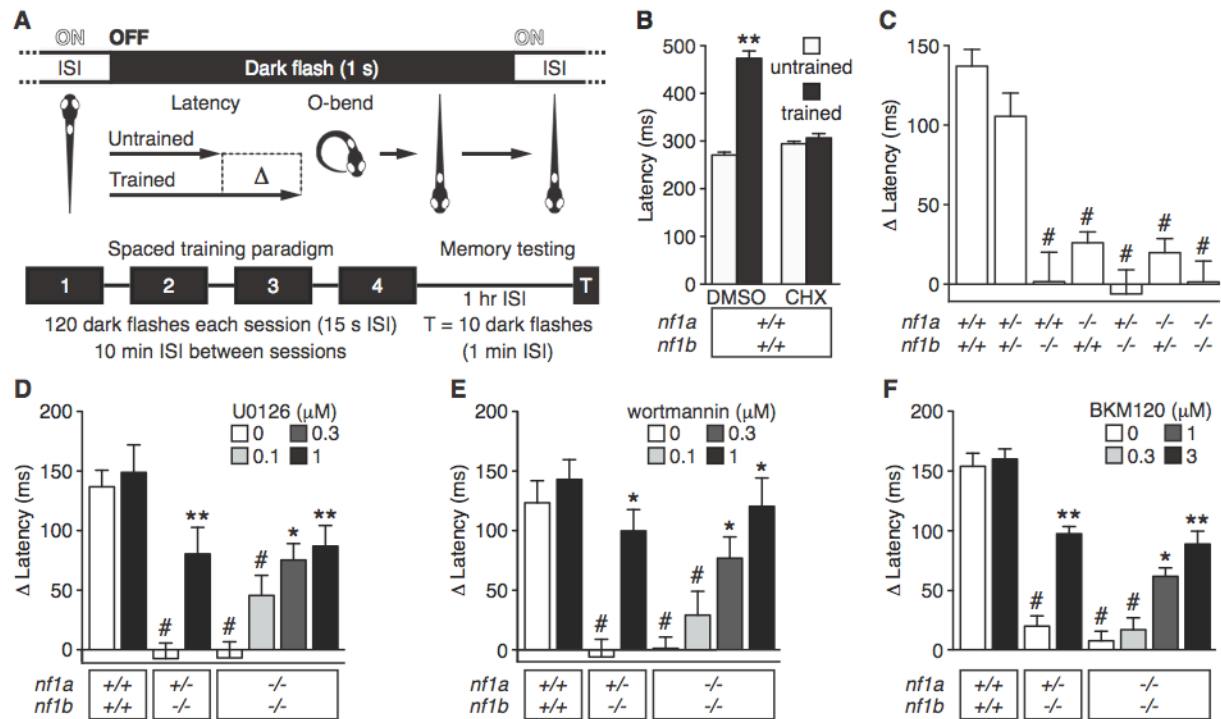


Figure 1. *nf1*-Mutant Larvae Exhibit Reduced Memory Recall

(A) Schematic representation of visual memory assay. ISI: interstimulus interval. (B-F) Mean O-bend latency (B) or latency change (C-F) 1 h after spaced training (test) versus untrained controls (n = 26 to 130 O-bend maneuvers per genotype/treatment). #P < 0.001 versus wild-type untreated (C) or DMSO-treated (B, D-F). *P < 0.01, **P < 0.001 versus same genotype, DMSO-treated. One-way ANOVA. Error bars denote SEM.

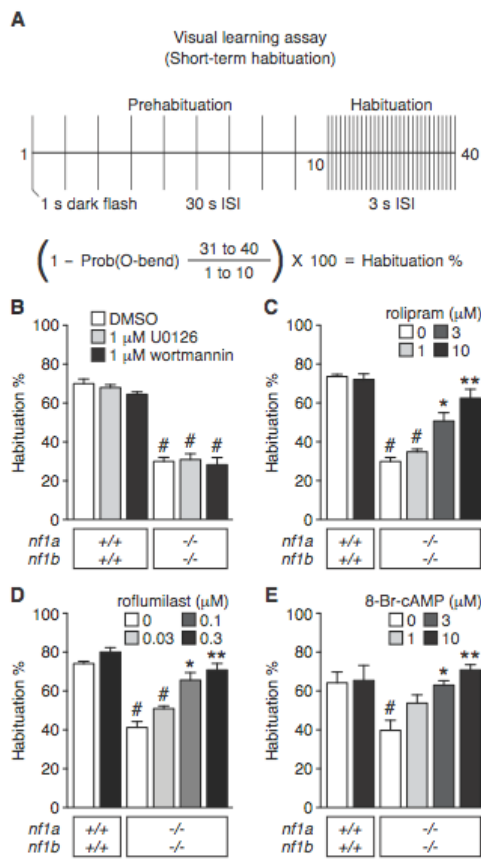


Figure 2. cAMP Signaling Mediates *nf1*-Dependent Visual Learning

(A) Schematic representation of visual learning assay. ISI: interstimulus interval. (B-E) Mean habituation percentage to repeated dark flash stimulation ($n = 3$ groups of 15-20 larvae for all genotype/treatment groups). # $P < 0.001$ versus DMSO-treated wild-type larvae. * $P < 0.01$, ** $P < 0.001$ versus DMSO-treated *nf1a*^{-/-}; *nf1b*^{-/-} larvae. One-way ANOVA. Error bars denote SEM.

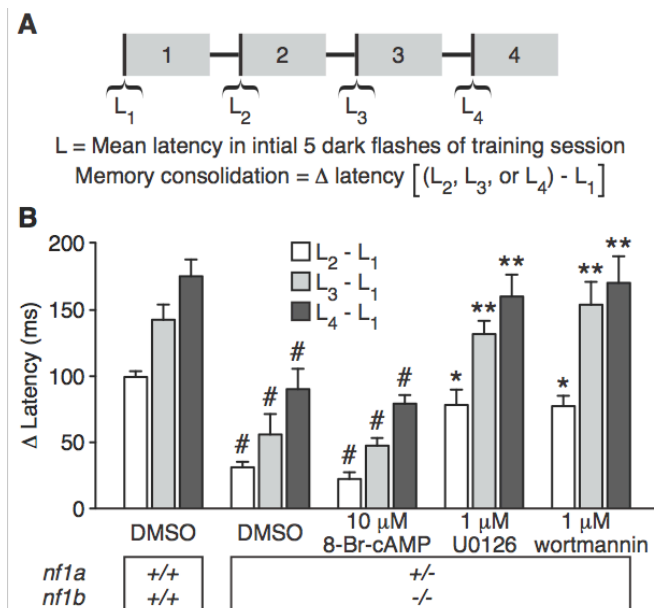


Figure 3. Inhibition of Ras Signaling Improves Memory Consolidation Deficits in *nf1* Mutants

(A) Schematic representation of visual memory consolidation measurement. (B) Mean O-bend latency change comparing responses to dark flash stimuli 1-5 of sessions 2-4 versus stimuli 1-5 of session 1 ($n = 30$ to 139 O-bend maneuvers per genotype/treatment). # $P < 0.001$ versus DMSO-treated wild-type larvae. * $P < 0.01$, ** $P < 0.001$ versus DMSO-treated *nf1a*^{+/-}; *nf1b*^{-/-} larvae. One-way ANOVA. Error bars denote SEM.

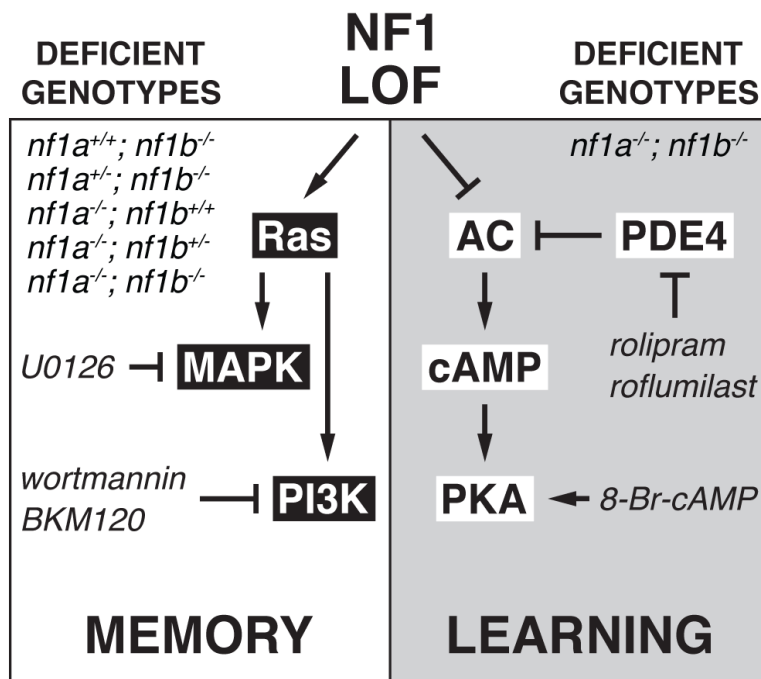


Figure 4. Effects of NF1 Loss of Function on the Ras and cAMP Pathways.

The genotypes of the zebrafish *nf1* larvae that exhibited significant memory or learning deficits are shown. The pharmacological agents (*italicized*) that were used to improve memory or learning in these genotypes, as well as the molecular targets of the agents, are indicated. LOF, loss of function.

Aim 2: To analyze the contributions of Nf1 GAP and other functional domains, based on Nf1 structure function analysis in Aim 1, to the suppression of malignant glioblastomas (CNS) and MPNSTs (PNS), which we have shown to develop in conjunction with p53 loss (Look lab).

Over the past three years, the Look lab has continued efforts to analyze the consequence of loss of NF1 in solid tumors *in vivo* and we are pleased to report that our work in this area has resulted in two manuscripts (one submitted and one in preparation).

The Look lab has crossed the *nf1a/b* mutant lines with the p53 mutant zebrafish to generate *nf1a+/-;nf1b-/-;p53-/-* fish and monitored for tumorigenesis. The current *nf1a+/-;nf1b-/-;p53-/-* fish line began to develop tumors from the age of 17 weeks (Figure 5). To improve monitoring tumor initiation and progression *in vivo* in the *nf1/p53* mutant zebrafish lines, we have crossed the *nf1/p53* mutant fish to a *sox10:EGFP* line (early neural crest cells are labeled with GFP), as *sox10* is consistently expressed in schwannian tumors (3, 4). As shown in Figure 6, the GFP driven by the *sox10* promoter is highly expressed in the high-grade gliomas and MPNSTs, but not in the non-malignant neural crest-derived tissues, in the *nf1a+/-;nf1b-/-;p53-/-;sox10:GFP* adult zebrafish. This result indicates that *sox10* is highly expressed in high-grade gliomas and MPNSTs in our zebrafish model of type I neurofibromatosis.

Initial structure-function studies of NF1 was performed using the human NF1 gene for transgenic rescue experiments. As *sox10* is highly expressed in high-grade gliomas and MPNSTs in our zebrafish model of type I neurofibromatosis (Figure 6), we co-injected *sox10:mcherry* plus the *sox10:NF1* mutant cDNAs to see which protein domains and amino acids of this very large protein are required for tumor suppression. The first domain that we tested was the GRD, which encodes the GAP function of NF1. We received cDNA coding the wild-type GRD domain of the human NF1 (GRDwt), as well as the GRD domain with an inactivating point mutation (R1276P, refer as GRDmut), from the Epstein lab, and sub-cloned the GRD domains downstream of the zebrafish *sox10* promoter. *Sox10:GRDwt* or *sox10:GRDmut* was co-injected with a *sox10:mCherry* construct into the progeny of the *nf1a+/-*

nf1b^{-/-};*p53*^{-/-};*sox10:EGFP* zebrafish (Figure 7). We have generated stable transgenic lines that have stably integrated the transgenes into the germline.

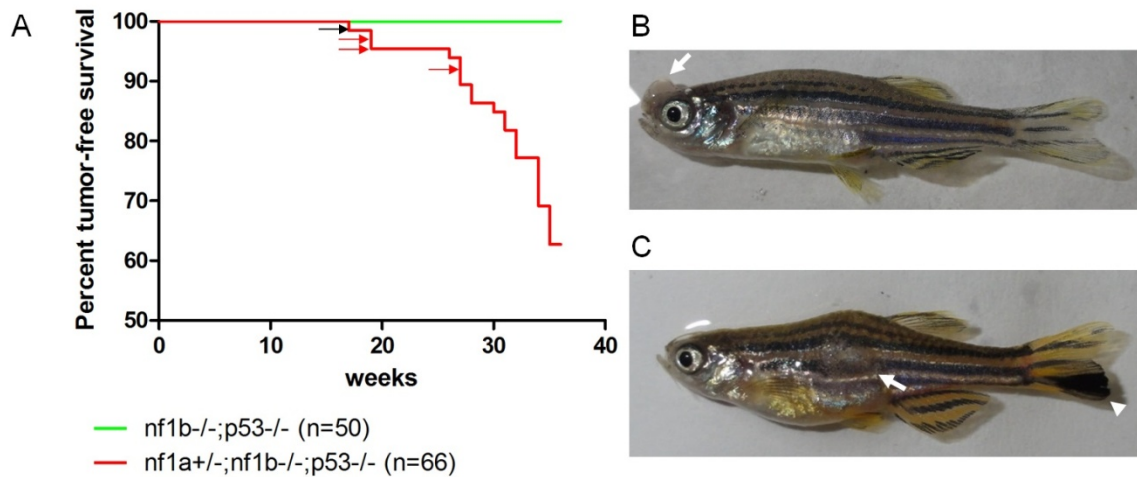


Figure 5: (A) Tumor surveillance results for *nf1b*^{-/-};*p53*^{-/-} (n=50) and *nf1a*^{+/-};*nf1b*^{-/-};*p53*^{-/-} (n=66) zebrafish. Tumor-free survival is defined as the time in weeks from date of birth to the date of tumor onset. 25 *nf1a*^{+/-};*nf1b*^{-/-};*p53*^{-/-} fish developed tumors by the age of 36 weeks, while no *nf1b*^{-/-};*p53*^{-/-} fish developed tumors yet. The black arrow indicates one melanoma identified at the age of 17 weeks. The red arrows indicate three high grade gliomas identified at the age of 19 and 27 weeks. (B) 27-week-old *nf1a*^{+/-};*nf1b*^{-/-};*p53*^{-/-} fish with high-grade glioma (arrow). (C) 36-week-old *nf1a*^{+/-};*nf1b*^{-/-};*p53*^{-/-} fish with MPNST (arrow) and a nevi in the tail fin (arrowhead).

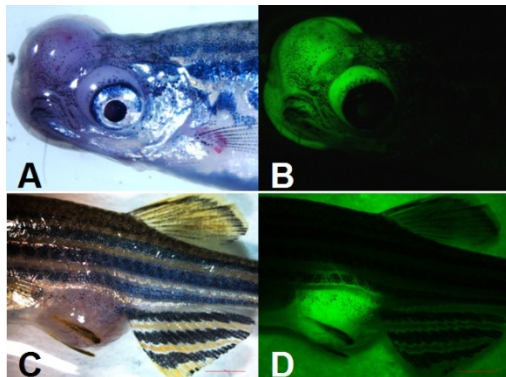
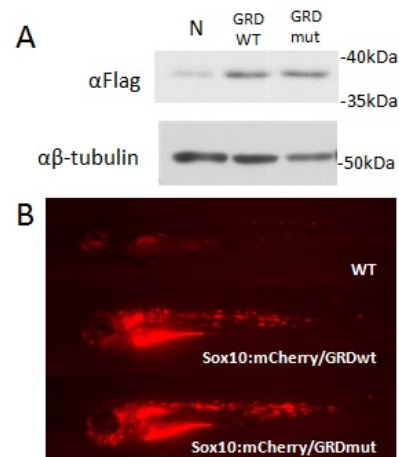


Figure 6. Sox10 is highly expressed in the high-grade gliomas and MPNSTs developed in the *nf1* mutant zebrafish. The initiation and progression of high-grade glioma (A, white light; B, GFP) and MPNST (C, white light; D, GFP) can be monitored in vivo in the *nf1* mutant zebrafish lines using the *sox10:GFP* fluorescent reporter.

Figure 7. Development of stable *nf1* mutant zebrafish lines with expression of the GRD domain of human NF1.

(A) Western blot shows that Flag-tagged GRDwt or GRDmut is expressed in embryos at 5 days after injection. (B) Mosaic expression of *sox10:mCherry*;*sox10:GRD* in injected embryos.



In our original tumor model (Figure 5), the earliest gliomas developed in the *nf1a*^{+/-};*nf1b*^{-/-};*p53*^{-/-} line were observed from 19 weeks, and the earliest MPNSTs were observed after 20 weeks. To improve the model for the *nf1* structure-function analysis using the NF1 constructs, the Look lab has continued with a panel of three independent strategies to further accelerate the tumor onset and increase tumor penetrance over the past three years.

i. Introducing loss of *pten* into the *nf1/p53* mutant lines. Pten (phosphatase and tensin homolog) is one of the most frequently mutated or deleted tumor suppressors in human cancer. Mutations and homozygous deletions of *pten* were found in 36% of glioblastomas (GBM), the most malignant subtype of glioma (5). Loss or decrease of *pten* expression was also detected in a majority of human NF1-associated MPNST lesions (6). There are two orthologues of human *pten* in the zebrafish genome, namely *ptena* and *ptenb* (7). We obtained the loss-of-function *pten* mutant from Dr. Jeroen den Hertog and bred them with our *nf1a*^{+/-};*nf1b*^{-/-};*p53*^{-/-} fish to establish a *nf1a*^{+/-};*nf1b*^{+/-};*p53*^{+/-};*ptena*^{+/-};*ptenb*^{+/-} line. By incrossing the *nf1a*^{+/-};*nf1b*^{+/-};*p53*^{+/-};*ptena*^{+/-};*ptenb*^{+/-} line, we obtained all possible combinational loss of *nf1*, *p53* and *pten* in our zebrafish model. Accelerated formation of tumors associated with neurofibromatosis type 1 was observed in *nf1a*^{+/-};*nf1b*^{-/-};*p53*^{-/-};*ptena*^{+/+};*ptenb*^{-/-} and *nf1a*^{+/-};*nf1b*^{-/-};*p53*^{-/-};*ptena*^{+/-};*ptenb*^{-/-} lines. We are currently analyzing the tumor histology and establishing the *nf1a*^{+/-};*nf1b*^{-/-};*p53*^{-/-};*ptena*^{+/+};*ptenb*^{-/-};*sox10*:GFP and *nf1a*^{+/-};*nf1b*^{-/-};*p53*^{-/-};*ptena*^{+/-};*ptenb*^{-/-};*sox10*:GFP lines for GFP-based tumor watch and the structure-function studies using the NF1 constructs from Aim 1.

ii. Introducing human PDGFR into the *nf1a*^{+/-};*nf1b*^{-/-};*p53*^{-/-} mutant line. PDGFR is frequently mutated in human GBM and MPNST (3-6). To test whether PDGFRA overexpression accelerates the onset of MPNSTs in *nf1* and *p53* deficient zebrafish as an oncogene in MPNST pathogenesis, we cloned the cDNA encoding either wild-type PDGFRA or constitutively activated PDGFRA under the control of the zebrafish *sox10* neural crest-specific promoter. These constructs were co-injected with *sox10*:mCherry into fertilized eggs of *nf1a*^{+/-};*nf1b*^{-/-};*p53*^{e7/e7} zebrafish and the mosaic progeny were monitored for MPNST onset and also outbred at 3 months of age to establish stable transgenic lines. Both wild type and constitutively activated PDGFRA injected zebrafish developed tumors much more frequently than mCherry control *nf1a*^{+/-};*nf1b*^{-/-};*p53*^{e7/e7} zebrafish (Figure 8). The tumors in MPNST prone zebrafish resembled human MPNSTs histologically and expressed high levels of the each of the respective human transgenic PDGFRA proteins by Western blotting. Interestingly, wild-type PDGFRA overexpressers developed MPNST much faster and at higher penetrance than fish transgenic for mutationally activated PDGFRA or control fish. Our results indicate that these high levels of PDGFRA expression are likely pathogenic in the tumor cell growth and survival. Thus, PDGFRA represents an ideal target for treatment with specific tyrosine kinase inhibitors in tumors with either wild-type or mutant PDGFRA expression, and our transgenic zebrafish models are ideal to test the efficacy of PDGFRA inhibitors as well as other small molecule drugs in vivo for activity against MPNST.

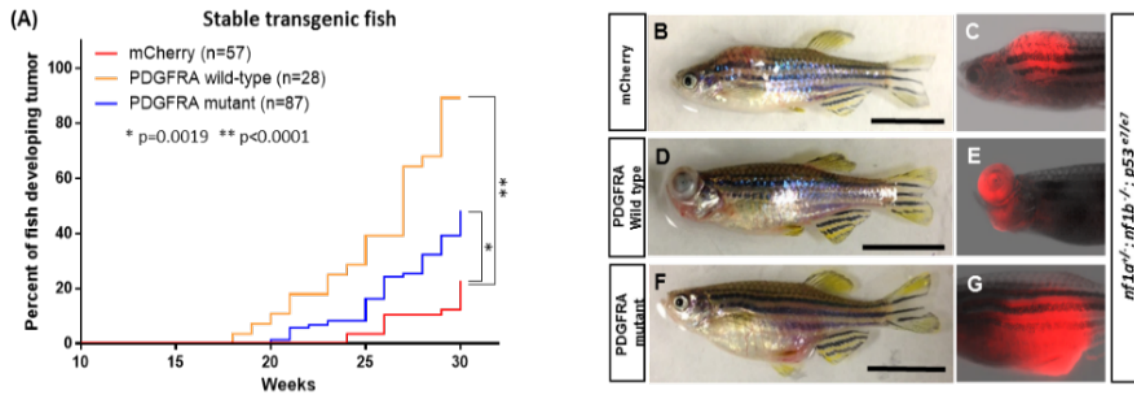


Figure 8. Both wild type and constitutively activated mutant forms of PDGFRA accelerate MPNST tumorigenicity in *nf1* and *p53* deficient fish

(A) Kaplan-Meier analysis of tumorigenesis in PDGFRA overexpressing fish. Onset of MPNSTs in *nf1* and *p53* deficient zebrafish (*nf1a*^{+/-};*nf1b*^{-/-};*p53*^{e7/e7}) with the following DNA constructs: (1) *sox10*:mCherry alone (mCherry, red); (2) *sox10*:PDGFRA wild-type and *sox10*:mCherry (PDGFRA wild-type, yellow); or (3) *sox10*:PDGFRA mutant and *sox10*:mCherry (PDGFRA mutant, blue). Note that wild-type PDGFRA overexpression actually accelerated the onset of MPNSTs more than constitutively activated mutant PDGFRA. (B-G) Example images of the *sox10* promoter driving mCherry positive tumors under different conditions. Transgenic *sox10*:mCherry (B, C), *sox10*:mcherry/PDGFR wild type (D, E), and *sox10*:mcherry/PDGFR CA mutant (F, G) in the *nf1a*^{+/-};*nf1b*^{-/-};*p53*^{e7/e7} background induced tumors which strongly expressed mCherry protein (>30 weeks post fertilization, scale bar=10 mm).

During the past years, in addition to the efforts on acceleration of malignant glioblastomas (CNS) and MPNSTs (PNS) for the in vivo structure-function analysis of NF1, we focused our in vivo structure-function analysis on another type of solid tumor, neuroblastoma. This is because that loss of *nf1* greatly accelerated the onset of neuroblastoma induced by MYCN overexpression, with a penetrance of nearly one hundred percent by 5 weeks in our zebrafish neuroblastoma model (Figure 9). Our results document that loss of *nf1* results in aberrant activation of Ras signaling in MYCN-induced neuroblastoma and promotes both tumor cell survival and proliferation. In vivo structure function analysis with both the wild-type and mutated GRD domain of NF1 revealed that the GAP activity of the GRD domain is required to mediate the tumor suppressor function of *nf1* in MYCN-induced neuroblastoma tumorigenesis. Thus the selection for NF1 mutations in neuroblastoma is largely mediated through the Ras pathway, despite the fact that the GRD domain represents only ~330 amino acids of the 2818 amino acid NF1 protein. Our results in the zebrafish model are particularly significant in light of the previously incompletely appreciated essential role of aberrant RAS-MAPK signaling in high-risk neuroblastoma, as a very recent multi-investigator international study led by Drs G. Schleiermacher, J. Molenaar and J. Maris showed that 80% of relapsed neuroblastomas have mutations predicted to activate RAS-MAPK signaling, including homozygous loss of the NF1 gene, that in many cases were not detected in primary tumors (10). Our faithful zebrafish tumor models with loss of *nf1* that we have established are ideal for small molecule drug screens, conducted in zebrafish embryos, to identify new drugs for NF1-deficient high-grade gliomas, MPNSTs and neuroblastomas.

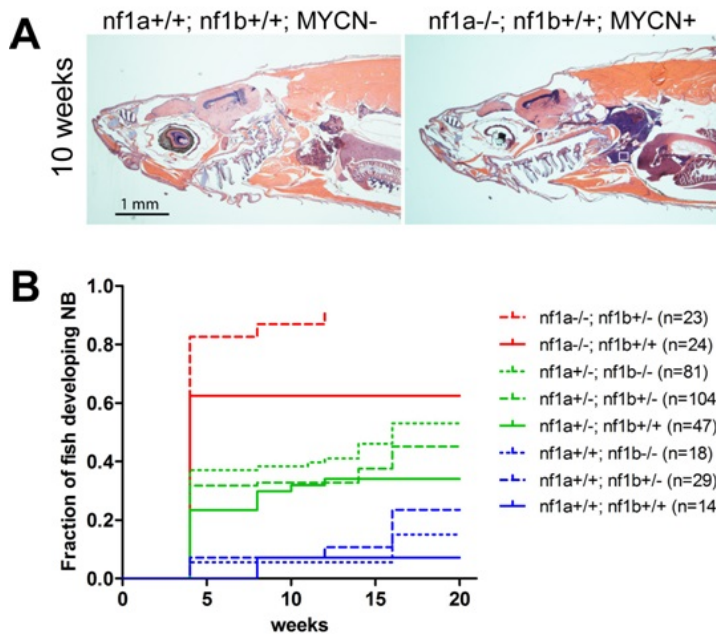


Figure 9. Loss of *nf1* accelerates disease onset and increases the penetrance of *MYCN*-induced neuroblastoma *in vivo*

(A) H&E-stained sagittal sections of a $nf1a^{+/+}; nf1b^{+/+}; GFP$ fish (left) and a $nf1a^{-/-}; nf1b^{+/-}; GFP; MYCN$ fish (right) at 10 weeks of age. Transgenic fish lines without *MYCN* transgene did not develop neuroblastoma, regardless of the mutational status of *nf1*. (B) Cumulative frequency of neuroblastoma in *MYCN* transgenic zebrafish with all of the eight *nf1* genotypes resulted from the breeding the $nf1a^{+/-}; nf1b^{+/-}; MYCN$ line with the $nf1a^{+/-}; nf1b^{+/-}$ zebrafish line.

KEY RESEARCH ACCOMPLISHMENTS

- Characterization of learning defects in *nf1* mutant zebrafish
- Characterization of memory defects in *nf1* mutant zebrafish
- Preparation of NF1 constructs for the structure-function analysis
- Generation of stable zebrafish lines expressing NF1 constructs for the structure-function analysis
- Generation of *nf1/p53/pten* mutant zebrafish
- Generation of zebrafish MPNST model with PDGFRA overexpression in the *nf1/p53* compound mutant background
- Generation of zebrafish neuroblastoma model with MYCN overexpression in the *nf1* mutant background
- In vivo structure-function analysis of NF1 in MYCN-induced neuroblastoma
- Preparation of glioma/MPNST models for the structure-function analysis

CONCLUSION

During the past three years, we have continued to further our studies towards meeting the goals set forth in the funded proposal. An exciting phenotype has been identified that is relevant to the human NF1 disease and to the potential development of meaningful therapies. In collaboration with the Granato lab at Penn, the Epstein lab has discovered striking learning and memory defects in mutant fish. Our data provide compelling evidence that neurofibromin regulates learning and memory by distinct molecular pathways in vertebrates and that deficits produced by genetic loss of function are reversible. These findings support the investigation of cAMP signaling enhancers as a companion therapy to Ras inhibition in the treatment of cognitive dysfunction in NF1. In the Look lab, the zebrafish models of the NF1 tumor suppressor linked cancers of MPNST and glioma have been completely updated to make them

optimal for the structure function studies. Three different strategies are being launched to further accelerate the onset of these tumors to increase the precision of the structure function studies to elucidate the mechanism of tumor suppression by NF1. In particular, we established new transgenic lines with overexpression of the receptor tyrosine kinase PDGFRA, which accelerates disease onset and increases the penetrance of MPNST in *nf1/p53* deficient zebrafish. This new MPNST model with accelerated tumor onset will increase the precision of the structure function studies to elucidate the mechanism of tumor suppression by NF1. We also established a faithful model of high-risk neuroblastoma with loss of *nf1*. The very early tumor onset (5 weeks) and high tumor penetrance (~100%) allowed us to successfully perform in vivo structure-function analysis of NF1. Our results demonstrated that the GAP activity of the GRD domain is required to mediate the tumor suppressor function of *nf1* in MYCN-induced neuroblastoma tumorigenesis. Importantly, our faithful zebrafish tumor models with loss of *nf1* are ideal for small molecule drug screens to identify new drugs for NF1-deficient malignancies, and for use in performing genetic screens to identify modulators of these important diseases.

Questions have been raised about the original Statement of Work (SOW) submitted with the grant application in July, 2011. Thus we are reprinting the SOW verbatim here.

Tasks:

1. Aim 1. To fully characterize *nf1a/b* compound null zebrafish and to perform structure-function studies of Nf1 in vivo by performing rescue experiments in *znf1a/b* loss-of-function zebrafish to determine which aspects of the mutant phenotype are regulated by GAP and non-GAP domains (Epstein lab).

Timeline: Year 1-3

Milestones and methods include the use of compound null mutants of Nf1a and zNf1b fish that will be crossed and the single cell embryos co-injected with full-length or partial-length cDNA constructs for human NF1. Resulting embryos will be examined for rescue of mutant phenotypes by direct observation under the microscope and by staining for genes and proteins using in situ hybridization and immunohistochemistry. These lines will be used to perform rescue experiments using cDNA constructs injected into fertilized eggs. This work will be performed primarily in the Epstein lab.

Outcomes and deliverables include identification of novel functional domains within the neurofibromin protein that are capable of rescuing some or all aspects of the mutant phenotypes.

2. Aim 2. To analyze the contributions of Nf1 GAP and other functional domains, based on Nf1 structure-function analysis in Aim 1, to the suppression of malignant glioblastomas (CNS) and MPNSTs (PNS), which we have shown to develop in conjunction with p53 loss (Look lab).

Timeline: Year 1-3

Milestones and methods include the use of compound null mutants of Nf1a and zNf1b fish that are also in a p53 m/m background that will be crossed and the single cell embryos co-injected with full-length or partial-length cDNA constructs for human NF1 driven by the Sox10 promoter together with an mcherry maker gene also driven by the Sox10 promoter. Cohorts of 100 coinjected animals will be observed to document the

onset of malignant tumors of the CNS (GBM) and PNS (MPNST), we will coinject sox10:mcherry plus the sox10:Nf1 mutant cDNAs, to see which protein domains and amino acids of this very large protein are required for tumor suppression. This work will be performed primarily in the Look lab, using Nf1 constructs prepared by the Epstein lab.

Outcomes and deliverables include identification of novel functional domains within the neurofibromin protein that are capable restoring tumor suppressor function and thus blocking the onset of CNS (GBM) and PNS (MPNST) malignant glial tumors in zebrafish lines harboring only one of the four zebrafish nf1 genes as well as mutant p53.

Over the 3 years of the grant, as outlined in the SOW for Aim 1, the Epstein laboratory investigated the function of various domains of the nf1 protein in producing the phenotypes identified in mutant zebrafish embryos. It rapidly became clear that the most relevant phenotype to the human disease involved learning and memory defects that were discovered in the embryos during the first year of these studies. This led to a very detailed study with the Granato lab on these phenotypes. In the end pharmacologic approaches proved more powerful than genetic replacement to differentiate phenotypes downstream of the Ras pathway affected by nf1 loss (memory defects) from those mediated by cyclic AMP and PKA pathways (learning defects). This work was highly successful and led to a landmark publication in Cell Reports in 2014.

In Aim 2, the role of nf1 loss in carcinogenesis was studied using the sox10 promoter was used to drive various genes to study the contributions of the loss of nf1 to MPNST and glioma tumors that arise in the mutant fish. A key finding was that either the wild-type or mutant PDGFR gene dramatically accelerated MPNST onset and penetrance in nf1 deficient fish, implicating this druggable kinase in disease progression. This study has been presented in abstract form and the manuscript will soon be submitted. Surprisingly, overexpression of PDGFR did not accelerate the onset of gliomas, nor did combining nf1 loss with the loss of pten. Thus, we turned to a third tumor type called neuroblastoma, which also frequently harbors mutations of the Ras pathway, including loss of nf1. In this tumor type, we were able to complete the structure function analysis of nf1 by injecting only the GAP domain. Our surprising finding is that the GAP domain is unable to rescue the effects of loss of nf1 on PSNS development, but is still able to rescue the contribution of loss of nf1 to neuroblastoma development in the same tissue. Thus we were able to dissociate the effects of loss of nf1 on normal development and tumorigenesis in the sympathetic nervous system lineage. This work had important implications of therapy, because it clearly implicates the need to target high levels of RAS signaling in neuroblastomas that have lost Nf1. This manuscript has been presented in abstract form and submitted for publication.

Thus, there can be no doubt that we have exceeded all expectations in meeting and completing the objectives outlined in the SOW that was prepared 4 years ago when we proposed this research study.

REPORTABLE OUTCOMES

- Abstract: Zebrafish neurofibromatosis type 1 genes have redundant functions in tumorigenesis and embryonic development. Look AT. 1st Cold Spring Harbor Asia conference on Fishing for Answers: Zebrafish Models of Human Development and Disease. Suzhou, China, 2012.

- Presentation: Zebrafish neurofibromatosis type 1 genes have redundant functions in tumorigenesis and embryonic development. Look AT. 1st Cold Spring Harbor Asia conference on Fishing for Answers: Zebrafish Models of Human Development and Disease. Suzhou, China, 2012.
- Abstract: In vivo Analysis of the Consequences of loss of the NF1 Tumor Suppressor in High-Grade Glioma, Malignant Peripheral Nerve Sheath Tumor (MPNST) and Neuroblastoma. Shuning He. NF Conference 2014. Washington DC, June 7-10 2014.
- Abstract: In vivo Analysis of the Consequences of loss of the NF1 Tumor Suppressor in High-Grade Glioma, Malignant Peripheral Nerve Sheath Tumor (MPNST) and Neuroblastoma. Shuning He. 11th International Conference on Zebrafish Development and Genetics. Madison, WI, June 24-28 2014
- Abstract: In vivo Analysis of the Consequences of loss of the NF1 Tumor Suppressor in High-Grade Glioma, Malignant Peripheral Nerve Sheath Tumor (MPNST) and Neuroblastoma. Shuning He. Zebrafish Disease Models Conference. Madison, WI, June 28- July 1 2014
- Abstract: Platelet-Derived Growth Factor Receptor Alpha (PDGFRA) increases tumorigenicity of the nf1 associated-MPNST in a zebrafish model. Dong Hyuk Ki, Dana-Farber/Harvard Cancer Center Pediatric Hem/Onc retreat 2014, Dedham MA, Oct 9 2014.
- Abstract: Overexpression of Platelet-Derived Growth Factor Receptor Alpha (PDGFRA) Synergizes with Loss of NF1 in the Molecular Pathogenesis of MPNST. Dong Hyuk Ki, NF Conference 2015, Monterey CA, June 6-9 2015.
- Abstract: Overexpression of platelet-derived growth factor receptor alpha (PDGFRA) synergizes with loss of NF1 in the molecular pathogenesis of malignant peripheral nerve sheath tumor (MPNST), Dong Hyuk Ki, Zebrafish Disease Models Conference (ZDM8). Boston, MA, August 24–27, 2015.
- Abstract: A Genome-Editing Approach for the Stepwise Establishment of Zebrafish Models of Pediatric High-Grade Gliomas and MPNSTs. Felix Oppel. Zebrafish Disease Models Conference (ZDM8). Boston, MA, August 24–27, 2015.
- Presentation: Zebrafish neurofibromatosis type 1 genes have redundant functions in tumorigenesis and embryonic development. Look AT. SickKids Research Institute, Toronto, Canada, 2012
- Presentation: Dr. Look presented the Zebrafish Models of Pediatric and Adult High Grade Gliomas on the Neuro-Oncology Multidisciplinary Conference in Dana-Farber Cancer Institute/ Brigham and Women Hospital (January 10, 2014)
- Presentation: Dr. Epstein recently delivered a prestigious keynote address at the Washington University of St. Louis NF Center Research Symposium (May 16, 2014).
- Presentation: Shuning He (Look lab) presented the “In vivo Analysis of the Consequences of loss of the NF1 Tumor Suppressor in High-Grade Glioma, MPNST and Neuroblastoma” in the NF Conference 2015 in Monterey (June 7, 2015)
- Presentation: A Stepwise Genome-Editing Approach Allows the Progressive Modelling of Pediatric High-Grade Gliomas and MPNSTs in Zebrafish. Felix Oppel. European Zebrafish Meeting 2015. Oslo, Norway, June 28–July 02, 2015.
- Presentation: Shuning He (Look lab) presented the “Synergy between Loss of NF1 and Overexpression of MYCN in Neuroblastoma is Mediated through the GAP-related Domain” in the Zebrafish Disease Models Conference (ZDM8) in Boston (August 26, 2015)
- Presentation: Shuning He (Look lab) will present the “Synergy between Loss of NF1 and Overexpression of MYCN in Neuroblastoma is Mediated through the GAP-related

Domain” in the 2nd Zebrafish for Personalized/Precision Medicine (ZPPM) Conference in Toronto, Canada (September 24, 2015)

- Manuscript: Synergy between loss of NF1 and Overexpression of MYCN in Neuroblastoma is mediated through the GAP-related domain. Shuning He, Marc R. Mansour, Dong Hyuk Ki, Mark W. Zimmerman, Hillary M. Layden, Eric D. de Groh, Antonio R. Perez-Atayde, Shizhen Zhu, Jonathan A. Epstein, and A. Thomas Look (submitted)
- Manuscript: Zebrafish neurofibromatosis type 1 genes have redundant functions in tumorigenesis and embryonic development. Shin J, Padmanabhan A, de Groh ED, Lee JS, Haidar S, Dahlberg S, Guo F, He S, Wolman MA, Granato M, Lawson ND, Wolfe SA, Kim SH, Solnica-Krezel L, Kanki JP, Ligon KL, Epstein JA, Look AT. *Disease Model and Mechanism*. 2012 Nov;5(6):881-94.
- Manuscript: Evaluation and application of modularly assembled zinc-finger nucleases in zebrafish. Zhu C, Smith T, McNulty J, Rayla AL, Lakshmanan A, Siekmann AF, Buffardi M, Meng X, Shin J, Padmanabhan A, Cifuentes D, Giraldez AJ, Look AT, Epstein JA, Lawson ND, Wolfe SA. *Development* 138(20): 4555-64, 2011.
- Manuscript: Wolman MA, de Groh ED, McBride SM, Jongens TA, Granato M, Epstein JA. Modulation of cAMP and ras signaling pathways improves distinct behavioral deficits in a zebrafish model of neurofibromatosis type 1. *Cell reports*. 2014;8(5):1265-70
- Employment or research opportunities applied for and/or received based on experience/training supported by this award: Jimann Shin (Ph.D.) entered a post-doc training program in Lila Solnica-Krezel Lab, Washington University in St. Louis.
- Employment or research opportunities applied for and/or received based on experience/training supported by this award: Arun Padmanabhan received MD/PhD degree from the Univ. of Pennsylvania, 2013
- Employment or research opportunities applied for and/or received based on experience/training supported by this award: Arun Padmanabhan, who performed critical work for this project, has accepted a position as a medical resident at the Massachusetts General Hospital and is highly likely to continue in a career as a physician-scientist. This grant and project played a major role in shaping his career and in providing the training necessary to obtain one of the most coveted medical residency positions in the country.
- Employment or research opportunities applied for and/or received based on experience/training supported by this award: Dr. Dong Hyuk Ki was recruited from Development biology of Stony Brook University to the Look lab to learn about neurofibromatosis type I and to carry out the studies on new pathways for targeted therapy of NF1-associated MPNST through in vivo studies in the zebrafish model system, based on this award.
- Employment or research opportunities applied for and/or received based on experience/training supported by this award: Eric de Groh, PhD, who was supported as a postdoc from this award, obtained a job as a medical writer at Medpace in Cincinnati Ohio.

REFERENCES

1. J. Karamchandani, T. Nielsen, M. van de Rijn, R. West, Sox10 and S100 in the diagnosis of soft-tissue neoplasms. *Appl Immunohistochem Mol Morphol* **20**, 445 (October 1, 2012)
2. J. Shin *et al.*, Zebrafish neurofibromatosis type 1 genes have redundant functions in tumorigenesis and embryonic development. *Dis. Model. Mech.* **5**, 881 (November 1, 2012)
3. Comprehensive genomic characterization defines human glioblastoma genes and core pathways. *Nature* **455**, 1061 (Oct 23, 2008)
4. R. G. W. Verhaak *et al.*, Integrated Genomic Analysis Identifies Clinically Relevant Subtypes of Glioblastoma Characterized by Abnormalities in PDGFRA, IDH1, EGFR, and NF1. *Cancer Cell* **17**, 98 (2010)
5. S. Carroll, N. Ratner, How does the Schwann cell lineage form tumors in NF1? *Glia* **56**, 1590 (November 1, 2008)
6. F. Perrone *et al.*, PDGFRA, PDGFRB, EGFR, and downstream signaling activation in malignant peripheral nerve sheath tumor. *Neuro Oncology* **11**, 725 (December 1, 2009)
7. J. Schwartzenuber *et al.*, Driver mutations in histone H3.3 and chromatin remodelling genes in paediatric glioblastoma. *Nature* **482**, 226 (February 9, 2012)
8. L. Cong *et al.*, Multiplex Genome Engineering Using CRISPR/Cas Systems. *Science* **339**, 819 (February 15, 2013)
9. W. Y. Hwang *et al.*, Efficient genome editing in zebrafish using a CRISPR-Cas system. *Nat Biotech* **31**, 227 (2013)
10. Eleveld *et al.*, Relapsed neuroblastomas show frequent RAS-MAPK pathway mutations. *Nat Genet.* 2015 Aug;47(8)

APPENDICES

Attach all appendices that contain information that supplements, clarifies or supports the text. Examples include original copies of journal articles, reprints of manuscripts and abstracts, a curriculum vitae, study questionnaires, and surveys, etc.

Journal Articles:

(1) Zhu et al, *Development* 138, 4555-4564 (2011)

(2) Shin et al, *Disease Models & Mechanisms* 5, 881-894 (2012)

(3) Wolman et al, *Cell Reports* 8, 1265-1270 (2014)

Development 138, 4555-4564 (2011) doi:10.1242/dev.066779
 © 2011. Published by The Company of Biologists Ltd

Evaluation and application of modularly assembled zinc-finger nucleases in zebrafish

Cong Zhu^{1,*}, Tom Smith^{1,*}, Joseph McNulty¹, Amy L. Rayla¹, Abirami Lakshmanan¹, Arndt F. Siekmann^{1,†}, Matthew Buffardi¹, Xiangdong Meng^{1,‡}, Jimann Shin², Arun Padmanabhan³, Daniel Cifuentes⁴, Antonio J. Giraldez⁴, A. Thomas Look², Jonathan A. Epstein³, Nathan D. Lawson^{1,§} and Scot A. Wolfe^{1,5,§}

SUMMARY

Zinc-finger nucleases (ZFNs) allow targeted gene inactivation in a wide range of model organisms. However, construction of target-specific ZFNs is technically challenging. Here, we evaluate a straightforward modular assembly-based approach for ZFN construction and gene inactivation in zebrafish. From an archive of 27 different zinc-finger modules, we assembled more than 70 different zinc-finger cassettes and evaluated their specificity using a bacterial one-hybrid assay. In parallel, we constructed ZFNs from these cassettes and tested their ability to induce lesions in zebrafish embryos. We found that the majority of zinc-finger proteins assembled from these modules have favorable specificities and nearly one-third of modular ZFNs generated lesions at their targets in the zebrafish genome. To facilitate the application of ZFNs within the zebrafish community we constructed a public database of sites in the zebrafish genome that can be targeted using this archive. Importantly, we generated new germline mutations in eight different genes, confirming that this is a viable platform for heritable gene inactivation in vertebrates. Characterization of one of these mutants, *gata2a*, revealed an unexpected role for this transcription factor in vascular development. This work provides a resource to allow targeted germline gene inactivation in zebrafish and highlights the benefit of a definitive reverse genetic strategy to reveal gene function.

KEY WORDS: *gata2*, Vascular development, Zebrafish, Zinc-finger nuclease

INTRODUCTION

The attributes of the zebrafish have established it as a powerful model for the study of vertebrate development. The accessibility of its externally fertilized embryos allows numerous manipulations, and the transparency of the zebrafish embryo permits direct serial visualization of biological processes in vivo (Beis and Stainier, 2006). These characteristics have enabled forward genetic screens for mutants affecting a wide range of developmental processes (Patton and Zon, 2001). However, the size of the zebrafish genome, the relatively long generation time, and the expense of maintaining large populations preclude forward genetic screening to saturation. Consequently, mutants exist for only a small fraction of zebrafish genes. Although modified antisense oligonucleotides can achieve targeted gene knockdown during embryogenesis (Nasevicius and Ekker, 2000), this technology is problematic with regard to persistence, specificity and penetrance (Robu et al., 2007; Eisen

and Smith, 2008). Thus, definitive reverse genetic strategies are required, especially for the study of later developmental processes, analysis of adult physiology, and for the establishment of disease models.

Zinc-finger nucleases (ZFNs) are chimeric fusions between a zinc-finger protein (ZFP) and the nuclease domain of FokI (Urnov et al., 2010). ZFNs have been employed to achieve heritable targeted gene disruption in the genomes of numerous plant and animal species, including zebrafish (Bibikova et al., 2002; Beumer et al., 2008; Doyon et al., 2008; Meng et al., 2008; Foley et al., 2009; Geurts et al., 2009; Cui et al., 2010; Mashimo et al., 2010; Meyer et al., 2010; Takasu et al., 2010). Gene disruption is achieved through imprecise repair of a ZFN-induced double-strand break within the coding sequence of a target gene (Urnov et al., 2010). ZFNs have also been utilized to achieve tailor-made genomic alterations in animal genomes through stimulation of homology-directed repair from an exogenous donor DNA (Beumer et al., 2008; Cui et al., 2010; Meyer et al., 2010). Although off-target lesions in the genome can result from ZFN treatment, their frequency is significantly lower than at the target site and their location can be predicted based on ZFN specificity (Meng et al., 2008; Perez et al., 2008; Gupta et al., 2011). Together, these characteristics make ZFNs an ideal tool to facilitate reverse genetic studies in zebrafish and other organisms.

Despite their utility, the widespread implementation of ZFNs is hindered by the difficulty in creating highly specific ZFPs. Two general approaches have been employed for this purpose: selection-based methods, which identify ZFPs with a desired specificity from randomized libraries, and assembly-based methods, which utilize archives of predefined zinc fingers to construct ZFPs with a desired specificity. Each approach is hampered by limitations. Selection-based approaches (Greisman and Pabo, 1997; Isalan et al., 1998;

¹Program in Gene Function and Expression, University of Massachusetts Medical School, Worcester, MA 01605, USA. ²Department of Pediatric Oncology, Dana-Farber Cancer Institute, Harvard Medical School, Boston, MA 02115, USA.

³Department of Cell and Developmental Biology, Perelman School of Medicine at the University of Pennsylvania, Philadelphia, PA 19104-6058, USA. ⁴Department of Genetics, Yale University School of Medicine, New Haven, CT 06510, USA.

⁵Department of Biochemistry and Molecular Pharmacology, University of Massachusetts Medical School, Worcester, MA 01605, USA.

*These authors contributed equally to this work

[†]Present address: Max-Planck Institute for Molecular Biomedicine, Laboratory for Cardiovascular Patterning, Roentgenstr. 20, 48149 Muenster, Germany

[‡]Present address: Bio-Rad Laboratories, Gene Expression Division, 2000 Alfred Noble Drive, Hercules, CA 94547, USA

[§]Authors for correspondence (nathan.lawson@umassmed.edu; scot.wolfe@umassmed.edu)

Maeder et al., 2008; Meng et al., 2008), although effective in generating specific ZFPs, can be time-consuming and technically challenging (Kim et al., 2010). Assembly-based approaches are more straightforward (Carroll et al., 2006; Kim et al., 2009) but are dependent on the quality of the available zinc-finger archive and the difficulty in predicting context-dependent effects between neighboring zinc fingers (Desjarlais and Berg, 1993; Greisman and Pabo, 1997; Wolfe et al., 1999). Although assembly-based, or modular, ZFNs have suffered from relatively low success rates (Ramirez et al., 2008), continued characterization of available archives and investigation of context dependence (Carroll et al., 2006; Kim et al., 2009; Sander et al., 2009), along with the generation of new archives with expanded specificity, will make this a more viable approach.

In this study we evaluated an assembly-based approach for creating ZFNs for targeted gene disruption in the zebrafish genome. We constructed an archive of ZFP modules recognizing 27 different triplet sequences and characterized the DNA-binding specificity for three-finger ZFP cassettes assembled from this archive. In parallel, we tested ZFNs constructed from these ZFPs for their ability to induce both somatic and germline lesions in zebrafish embryos. To facilitate the application of this technology in the zebrafish community, we developed a publicly accessible database that assists users in modular ZFN construction using our archive. Finally, we characterized the phenotypes in zebrafish embryos bearing a ZFN-induced deletion in the *gata2a* gene, revealing its role in vascular morphogenesis.

MATERIALS AND METHODS

Fish lines

Zebrafish were handled according to established protocols (Westerfield, 1993) and in accordance with Institutional Animal Care and Use Committee (IACUC) guidelines of participating institutions (University of Massachusetts Medical School, University of Pennsylvania, Dana Farber Cancer Institute and Yale University). The *Tg(kdrl:egfp)^{aj116}* line has been described elsewhere (Choi et al., 2007).

Construction of a modular zinc-finger archive

An archive of zinc-finger modules originating from multiple sources (see Table S1 in the supplementary material and Results) was constructed by subcloning ZFPs into either a pBluescript or pCS2 vector using standard methods. Clones were sequence verified and arrayed into a 96-well plate to generate an address for each module. Plasmids from the archive are available through addgene.org.

Modular assembly of ZFNs

To assemble three-finger ZFPs we first separately amplified modules for each of the three finger positions from plasmid templates by PCR. Distinct primer pairs were used to amplify modules for each position (fingers 1, 2 and 3) (see Table S2 in the supplementary material). PCR was performed using Advantage HF2 polymerase (Clontech) and 20 ng plasmid template. Finger 1 modules were amplified as follows: 94°C for 2 minutes, followed by 20-30 cycles of 94°C for 30 seconds, 60°C for 30 seconds and 68°C for 20 seconds, with a final extension of 68°C for 5 minutes. For finger 2 or 3 modules: 94°C for 2 minutes, then 20-30 cycles of 94°C for 30 seconds, 57°C for 30 seconds and 68°C for 20 seconds, with a final extension of 68°C for 5 minutes. All initial PCR products were gel purified. Three-finger cassettes were constructed by overlapping PCR using 30 ng of each finger module in a 50 µl reaction with Advantage HF2 polymerase. The first five cycles were performed without primers: 94°C for 2 minutes, followed by five cycles of 94°C for 30 seconds, 55°C for 30 seconds and 68°C for 1 minute. We added 2 µl of 10 µM F1 forward and F3 reverse primer and performed the following steps: 24 cycles of 94°C for 15 seconds, 60°C for 30 seconds, 68°C for 1 minute, with a final extension of 68°C for 5 minutes. Final PCR products were gel purified, digested with *Acc65I* and *BamHI* and cloned into

the pCS2 nuclease backbone in frame with the EL/KK heterodimeric variants of FokI (Miller et al., 2007), such that the 5' ZFP was fused to the EL nuclease and the 3' ZFP was fused to the KK nuclease. In several cases, DD/RR nuclease variants (Miller et al., 2007; Szczepek et al., 2007) were used. All constructs were sequence verified.

ZFN injections into zebrafish embryos

Synthesis and injection of ZFN mRNAs, dose optimization (see Table S3 in the supplementary material) and establishment and identification of germline lesions were performed as previously described (Meng et al., 2008; Gupta et al., 2011).

Bacterial one-hybrid binding site selections

Sequence-verified ZFP cassettes were cloned into the 1352-UV2 expression vector using *Acc65I* and *BamHI*. Bacterial one-hybrid (BIH) binding site selections were typically carried out at 5 mM 3-amino-1,2,4-triazole (3-AT), 10 µM IPTG and in the absence of uracil as previously described (Noyes et al., 2008; Gupta et al., 2011). For some ZFPs, lower stringency was required to achieve sufficient enrichment of recognition sequences above background.

Illumina library preparation of BIH-selected binding sites

Preparation of selected binding sites for deep sequencing was performed as described (Gupta et al., 2011), except that amplicons were digested with either *EcoRI* or *NotI* prior to ligation of bar-coded adapters for the identification of sequences associated with each ZFP (see Table S2 in the supplementary material).

Evaluation of the DNA-binding specificity of each ZFP and individual zinc-finger modules

Recognition motifs within the population of unique 28 bp sequences recovered from each binding site selection were identified using MEME (Bailey and Elkan, 1994). Position weight matrices (PWMs) were generated using the Log-Odds method (Hertz and Stormo, 1999) from the aligned sequences within the most statistically significant motif, weighting each sequence based on the number of counts within the Illumina dataset using the formula:

$$S = \sum_{i=1}^9 \log_2 \frac{f_{b,i}}{p_{b,i}}, \quad (1)$$

where S is the PWM score over the 9 bp target site s , b, i is the identity of base b at position i , $f_{b,i}$ is the normalized frequency of occurrence of base b at position i , and $p_{b,i}$ is the probability of observing the same base at the same position in a background model, which is assumed to be an equal distribution. Each ZFP was evaluated by calculating the score for its target site from its derived PWM. Each individual finger module was evaluated by calculating the score for its corresponding 3 bp recognition element (assuming canonical recognition) from this PWM. When data were available for multiple identical modules at identical positions, the scores for these modules were averaged for an overall assessment of the quality of the finger module. Modules with (average) scores that were two standard deviations below the average score of all modules at that position (i.e. finger 1, finger 2 or finger 3) were considered 'questionable' and flagged.

Analysis of somatic lesion frequency

Somatic lesion frequency was determined by Illumina sequencing as previously described (run #1) (Meng et al., 2008; Gupta et al., 2011). A second round of sequencing was performed for a subset of ZFNs from an independent set of injections (run #2). To avoid cross-contamination with samples from the first analysis, a unique pair of PCR primers was designed for each target site that would not amplify the PCR products from the first trial. These primers encoded the Illumina P1 and P2 sequences within each primer pair (see Table S2 in the supplementary material). In this case, PCR products for each ZFN target site were gel purified and amplified using Illumina genomic DNA primers (1.1 and 2.1). The PCR products for each target were then pooled at equal molar ratio, sequenced at 7 pM on a HiSeq 2000 (Illumina), and analyzed in a manner identical to run #1.

Calculation of the occupancy probability for a ZFN pair at its target site

The probability of a ZFP occupying its 9 bp target site was calculated using statistical thermodynamic free energy derived from a modified PWM score based on its B1H-determined DNA-binding specificity:

$$\Delta G = -RT \cdot \left(\sum_{i=1}^9 \ln \frac{f_{b,i}}{p_{b,i}} \right), \quad (2)$$

where $f_{b,i}$ and $p_{b,i}$ are defined as in (1), $R=0.001987$ kcal/(mol.K) and $T=301.5K$ (28.5°C).

All 9mers within the zebrafish genome (Zv8) were extracted considering both strands then the free energy of binding each 9mer by each ZFP was calculated using the scoring function shown in formula (2). These energies were then used to calculate the probability (P) for on-target binding by the ZFP within the zebrafish genome using:

$$P = \frac{e^{-\frac{\Delta G_s}{RT}}}{\sum_{i=1}^l n_i e^{-\frac{\Delta G_{s,i}}{RT}}}, \quad (3)$$

where ΔG_s is the free energy of binding to the 9mer matching the desired ZFP target site, $\Delta G_{s,i}$ is the free energy of binding of the i th 9mer, n_i is the occurrence of the i th 9mer in the genome, and l is total number of 9mers. A threshold for $\Delta G_{s,i}$ was set such that $\Delta G_{s,i} - \Delta G_s \leq 4.0$ to simulate the non-specific binding affinity of each ZFP. The occupancy probability of each ZFN pair was calculated as the product of the occupancy probabilities of the two ZFPs (3' ZFP and 5' ZFP).

Sequence and statistical analyses

All sequence analyses, PWM score calculations, ZFP occupancy calculations and lesion frequency calculations were performed using customized Perl scripts. All statistical analyses, plots and DNA-binding logos were generated using R (<http://www.r-project.org>).

Analysis of *gata2a*^{um27} mutant embryos

For phenotypic analysis, embryos were obtained from individual incrosses of heterozygous carriers. To analyze vascular development, *gata2a*^{um27} was crossed into the *Tg(kdrl:egfp)^{jal116}* background. Vascular morphology and circulatory function were observed by confocal microscopy, confocal microangiography and video microscopy as described elsewhere (Covassin et al., 2006); Quantum Dots were from Invitrogen. Whole-mount in situ hybridization was performed as previously described using antisense riboprobes against *kdrl*, *hey2*, *efnb2a*, *vegfaa*, *flt4*, *tall1* and *gata1* (Lawson et al., 2001; Hart et al., 2007). Following phenotypic analysis or in situ hybridization, DNA was isolated from selected individual embryos as described elsewhere (Roman et al., 2002). The presence of the 10 bp *um27* deletion was determined by PCR amplification (see Table S2 in the supplementary material for primer sequences), followed by gel electrophoresis or analysis on a QiaXL system (Qiagen). A rescue construct was made by amplifying the *gata2a* coding sequence by PCR using primers containing the Gateway attB1 and attB2 sites (see Table S2 in the supplementary material), followed by BP cloning into pDONR221 (Invitrogen). The resulting plasmid, pME-*gata2a*, was used in an LR reaction with pCSDest (Villefranc et al., 2007) to generate pCS*gata2a*, which was linearized with *NotI* and used as a template to synthesize mRNA. Embryos derived from crosses between *gata2a*^{um27} heterozygous carriers were injected at the 1-cell stage with 200 pg *gata2a* mRNA, or a comparable amount of *mcherry* mRNA, and were scored for the presence or absence of trunk circulation at 48 to 55 hours post-fertilization (hpf). Following phenotypic scoring, embryos were genotyped as above.

RESULTS

Overall rationale and experimental approach

To assess ZFNs constructed via modular assembly, we developed the following approach (see Fig. S1 in the supplementary material). We generated a collection of plasmids encoding zinc-finger modules recognizing 27 different triplet sequences. In parallel, we constructed

a database of sites within zebrafish protein-coding genes (Zv7) that could be targeted by ZFNs assembled from this archive. From this database, we chose target genes and generated the corresponding ZFP cassettes. We characterized the specificity of these ZFP cassettes and determined their function in ZFNs by assessing their ability to induce somatic and germline lesions in vivo. Finally, we created zebrafish bearing a truncation allele in *gata2a* and characterized the phenotypes associated with this mutation.

A zinc-finger archive for modular assembly

We compiled an archive of zinc fingers recognizing 27 different triplet sequences in the three finger positions of the Zif268 backbone that can be rapidly assembled by PCR into three-finger ZFPs (see Table S1 in the supplementary material). This archive comprises modules from previously defined finger archives (Segal et al., 1999; Liu et al., 2002; Carroll et al., 2006) or that have been designed based on previously described recognition principles (Isalan et al., 1998; Segal et al., 1999; Wolfe et al., 1999; Dreier et al., 2001; Dreier et al., 2005). We also generated 14 new modules by bacterial one-hybrid (B1H) selection (Meng et al., 2008). In some cases, distinct recognition helices were utilized at different finger positions for a common triplet for the B1H-generated fingers. In general, the archive was focused around GNN recognition elements (see Table S1 in the supplementary material) because of their reliable functional properties (Ramirez et al., 2008). Nine HNG modules with a preference for either G or T at the neighboring 3' position due to an RSD motif at positions -1, 1 and 2 of the recognition helix were included as they should synergistically recognize a composite sequence (NNGGNN) with GNN modules. Finally, AGA and TGT modules were included to expand the set of triplets that could be specified.

Target gene selection

We identified zebrafish genes that could be targeted using ZFNs constructed from the modular archive. In this analysis, each ZFN monomer consists of a three-finger cassette recognizing a 9 bp sequence. Therefore, we searched all coding exons (including the 10 bp flanking each exon) for potential ZFN sites that constitute adjacent, appropriately oriented 9 bp recognition sites compatible with our archive and separated by a 5 or 6 bp gap. Nearly 75% of all annotated zebrafish protein coding genes contained accessible ZFN sites. To generally assess the archive, targets sites were chosen in more than thirty genes (see Table S4 in the supplementary material) by four different laboratories, in which the corresponding ZFNs were constructed. The target genes are involved in multiple biological processes and are located randomly on 19 different chromosomes throughout the zebrafish genome. We restricted target sites to those that should yield a loss-of-function allele (i.e. those in the 5' half of the coding sequence or in a known functional domain) in the event of a ZFN-induced lesion. We gave preference to targets in which a restriction enzyme site overlapped the sequence gap between the ZFP binding sites to allow straightforward lesion identification in founder fish.

Binding specificity of modularly assembled ZFPs

To assess the recognition properties of three-finger ZFPs, we determined their DNA-binding specificities by interrogating each ZFP against a 28 bp randomized library using the B1H system (Noyes et al., 2008). The majority of selections (56 out of 76; see Table S5 in the supplementary material) were successful (i.e. yielded a significant increase in colonies over background) under standard stringency (5 mM or 10 mM 3-AT). Selections were successful for

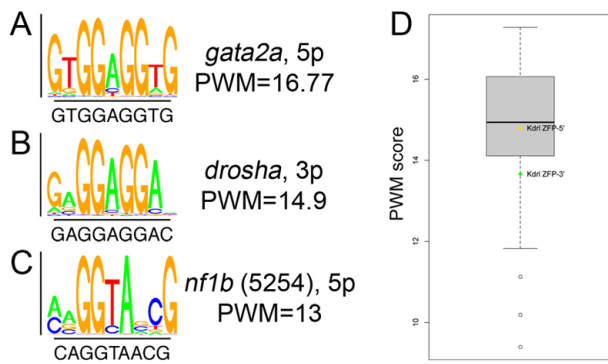


Fig. 1. DNA-binding specificity of modular zinc-finger proteins (ZFPs). (A-C) Sequence logos and position weight matrix (PWM) scores determined for 5' (5p) or 3' (3p) target sites for zebrafish (A) *gata2a*, (B) *drosha* and (C) *nf1b*. (D) Box plot depicting meta-analysis of PWM scores for each target site across all ZFPs for which bacterial one-hybrid (B1H) selections were successful. PWM scores for the previously described *kdrl* ZFPs are shown for reference. Whiskers indicate the largest (smallest) datum still within 1.5 interquartile range (IQR) of the upper (lower) quartile, where outliers are indicated as open circles.

19 of the remaining 20 ZFPs at lower stringency (≤ 2.5 mM 3-AT). For each ZFP a recognition motif (sequence logo) (Schneider and Stephens, 1990) and position weight matrix (PWM) were generated based on binding sites recovered following selection. In general, determined recognition motifs resembled the desired target motif, although there was variability in the overall quality of the PWM score of the target site across all ZFPs (see Fig. S2 in the supplementary material). For example, the 5p ZFP targeting *gata2a* properly specified all 9 bp and displayed among the highest PWM scores, suggesting excellent specificity for its target (Fig. 1A). Most ZFPs exhibited more modest specificity for their target, similar to the *drosha* (*rmasen* – Zebrafish Information Network) 3p ZFP (Fig. 1B), whereas several displayed weaker preference, such as the *nf1b* 5p (Fig. 1C). Overall, the distribution of PWM scores for the modular ZFP cassettes was similar to the engineered ZFPs successfully used to target the zebrafish *kdrl* locus (Fig. 1D) (Meng et al., 2008; Gupta et al., 2011), indicating that the ZFPs constructed using this archive generally display good recognition properties.

We further analyzed the BIH binding site selection data to assess the quality of individual modules, allowing us to identify those with poor or context-dependent specificity. Overall, most modules displayed a strong preference for their recognition triplet based on individually derived PWM scores (Fig. 2A), although modules at fingers 1 and 3 display lower median scores than those at finger 2.

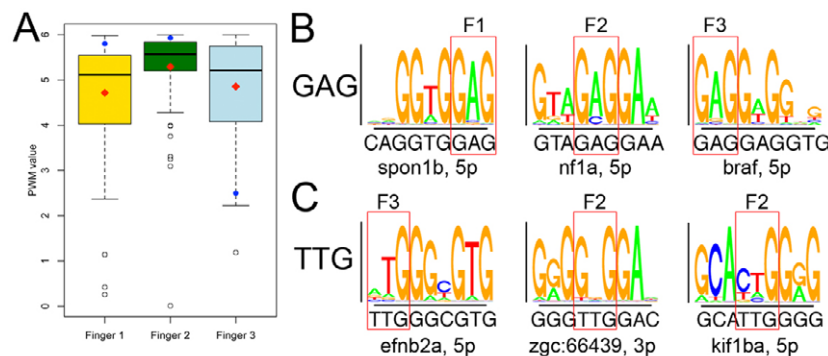


Fig. 2. Assessing the quality and behavior of individual ZFP modules. (A) Box plot depicting meta-analysis of PWM values for individual ZFP modules in each of the three positions in the Zif268 backbone. 5p (red diamonds) and 3p (blue circles) scores for fingers in the *kdrl* ZFPs are shown for reference. Whiskers indicate the largest (smallest) datum still within 1.5 interquartile range (IQR) of the upper (lower) quartile, where outliers are indicated as open circles. (B) Sequence logos for ZFP monomers recognizing GAG in each finger position. (C) Sequence logos for ZFPs containing TTG modules at the indicated finger position.

This is likely to be due to fraying effects at the edges of the protein-DNA complex that reduce the specificity of the determinants at these positions (Choo, 1998). Comparison of PWM values across all individual modules revealed that those targeting purine-rich triplets were among the most robust, regardless of their finger position. For example, the GAG module consistently displayed excellent specificity in multiple finger positions in most ZFPs (Fig. 2B), as did modules targeting GAT, GGG and GGT (see Tables S5 and S6 in the supplementary material). We also identified four modules within the archive that displayed poor specificity at a specific position or in a context-dependent manner. For example, the TTG module displays context-dependent alterations in specificity. We originally utilized the TTG module at finger 3 in ZFPs targeting the zebrafish *kdrl* locus, where it displays moderate preference (NtG) for its triplet (Meng et al., 2008; Gupta et al., 2011), similar to the *efn2a* 5p ZFP in this study (Fig. 2C). However, when it is placed at the finger 2 position adjacent to a C-terminal module bearing an RSD motif at positions -1, 1 and 2, the specificity shifts to a strong preference for a GNG binding site [Fig. 2C, *zgc:66439* (*clec14a* – Zebrafish Information Network), 3p ZFP]. This dramatic alteration in specificity is not observed when the neighboring C-terminal module lacks an RSD motif (Fig. 2C, *kif1b*, 5p ZFP). Overall, the majority of analyzed modules have favorable recognition properties in multiple contexts, although several might specify incorrect triplets in particular contexts.

In vivo activity of modular ZFNs

We evaluated the ability of ZFNs constructed from our modular archive to induce lesions at a target site within the zebrafish genome. Twenty-nine pairs of ZFNs targeting 28 genes (see Table S7 in the supplementary material) were constructed from 76 ZFPs described above (see Table S5 in the supplementary material) by fusing them to engineered heterodimeric FokI nuclease domains (Miller et al., 2007; Szczepek et al., 2007). We assessed lesion frequency by deep sequencing the target region in normal embryos at 24 hpf following injection of mRNAs encoding ZFNs at an optimal dose (see Table S3 in the supplementary material). Eight of the 29 ZFNs displayed lesions frequencies of 1% or more in at least one set of injections (see Table S7 in the supplementary material). The previously characterized *kdrl* ZFNs were injected as a positive control and generated an in vivo lesion frequency of ~7%, similar to our previous observations using Illumina sequencing (Gupta et al., 2011).

Germline transmission of ZFN-induced mutant alleles

Deep sequencing is likely to underestimate the frequency of ZFN-induced lesions because of short read lengths, and assessment of somatic lesions in embryos may not reflect the frequency of

Table 1. Somatic lesion frequency and germline transmission rate of ZFN-induced mutagenic alleles

ZFN ID	Gene	Somatic lesion frequency (%)	Frequency of founders (%)
ZFNv1_68779	<i>chd5</i>	<0.5	0
ZFNv1_53751	<i>kif1b</i>	<0.5	0
ZFNv1_27773	<i>braf</i>	>1	0
ZFNv1_5254	<i>nf1b</i>	ND	1.3
ZFNv1_5253	<i>nf1b</i>	~1	3
ZFNv1_87654	<i>gata2a</i>	~1	4
ZFNv1_19302	<i>nf1a</i>	<0.5	5.5
ZFNv1_94061	<i>ago2</i>	<0.5	6.5
ZFNv1_83611	<i>cxcr4a</i>	~1	10
ZFNv1_37185	<i>numb-like</i>	~1	13
ZFNv1_53765	<i>kif1b</i>	1-2	18
ZFNv1_25601	<i>gata3</i>	>1	25

ND, not determined.

germline transmission. Therefore, we determined the ability of 12 ZFNs targeting 11 genes to generate founder fish bearing germline lesions at the desired target site (Table 1). For most ZFNs that induced appreciable somatic lesion frequencies, we identified founder fish that transmitted mutant alleles through their germline and did so at a higher frequency than the somatic lesion rate (Table 1). Overall, there was a moderate correlation between the somatic lesion frequency and the founder rate ($R^2=0.71$). Notably, for two different ZFNs [*ago2* (*efj2c2* – Zebrafish Information Network) and *nf1a*], we were able to obtain founders despite lesion rates below 1% in somatic cells. Conversely, embryos injected with ZFNs targeting *braf* failed to yield founders even with a somatic lesion frequency greater than 1% (Table 1, see Table S7 in the supplementary material).

Correlations between ZFP specificity and ZFN activity

We next investigated potential correlations between the recognition properties of the ZFPs and the activity of the ZFNs in vivo. This analysis could provide a basis for estimating the likelihood of success of ZFNs generated from this archive. Surprisingly, we did not observe a significant correlation between DNA-binding specificity of the ZFPs and the activity of the respective ZFNs in vivo (Fig. 3A). Specificity alone may not be predictive of activity because genomic sequence is not random and thus activity might depend on the number of favorable binding sites for each ZFP within the genome. Therefore, we estimated the fractional occupancy of each ZFP monomer at its target site based on its DNA-binding specificity and the number of alternative high-affinity binding sites within the zebrafish genome (see Table S7 in the supplementary material). Again, there was no significant difference between the predicted target site occupancy for the active and inactive groups (Fig. 3B).

Although DNA-binding specificity did not appear to definitively predict in vivo ZFN activity, we did observe a strong correlation ($P=0.001$) between the number of GNN subsites within the recognition sequences and active ZFNs (Fig. 3C), consistent with previous observations (Ramirez et al., 2008). One additional prominent element of our module archive is the inclusion of NNG fingers. There are, on average, more NNG fingers in active ZFNs than inactive ZFNs (Fig. 3D), but the difference is not significant ($P=0.36$). Combined, a significant difference ($P=0.019$) exists between the average total number of GNN and NNG fingers in the

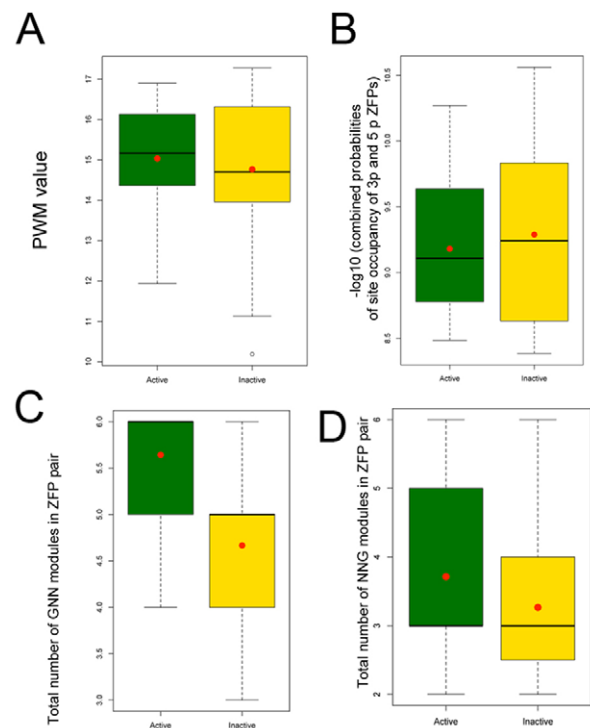


Fig. 3. Correlating ZFP characteristics with in vivo zinc-finger nuclease (ZFN) activity. Box plots depicting (A) PWM score, (B) estimated target site occupancy, (C) number of GNN modules in a ZFN pair and (D) number of NNG modules in a ZFN pair in both active and inactive ZFNs, where red dots indicate the mean of each population. Active ZFNs are those in which somatic lesion frequencies were greater than 0.5% or that successfully generated founders for mutant alleles. Whiskers indicate the largest (smallest) datum still within 1.5 interquartile range (IQR) of the upper (lower) quartile, where outliers are indicated as open circles.

active versus inactive groups of ZFNs, but the majority of the predictive value of this combination is derived from the GNN fingers.

A zebrafish database for modular ZFNs

To facilitate ZFN construction by the zebrafish community, we designed a web-accessible database (pgfe.umassmed.edu/ZFNv1/) that can be used in a standard workflow (see Fig. S3 in the supplementary material), allowing researchers to easily construct ZFNs, generate founder zebrafish bearing targeted lesions, and identify associated phenotypes within 7-12 months. A user can identify ZFN target sites in a gene of interest by entering or uploading an ENSEMBL gene number or RefSeq ID. The resulting output provides a count of ZFN target sites, a gene description and abbreviation, and a link to the locus on the UCSC genome browser (Fig. 4A). The user can view sites within one particular gene or all targets using a sortable list (Fig. 4B) that aids identification of optimal sites based on position (exon rank), presence of a restriction enzyme site in the spacer sequence, or a revised efficacy score. The efficacy score has a maximum of 12 points, where one point is assigned for each guanine at the edge of each recognition triplet (i.e. GNN and NNG fingers), as active ZFNs are enriched for these contacts (see above). The database also notes single-nucleotide polymorphisms in the target site in the reference Tuebingen (Tu) and AB wild-type zebrafish strains that have been

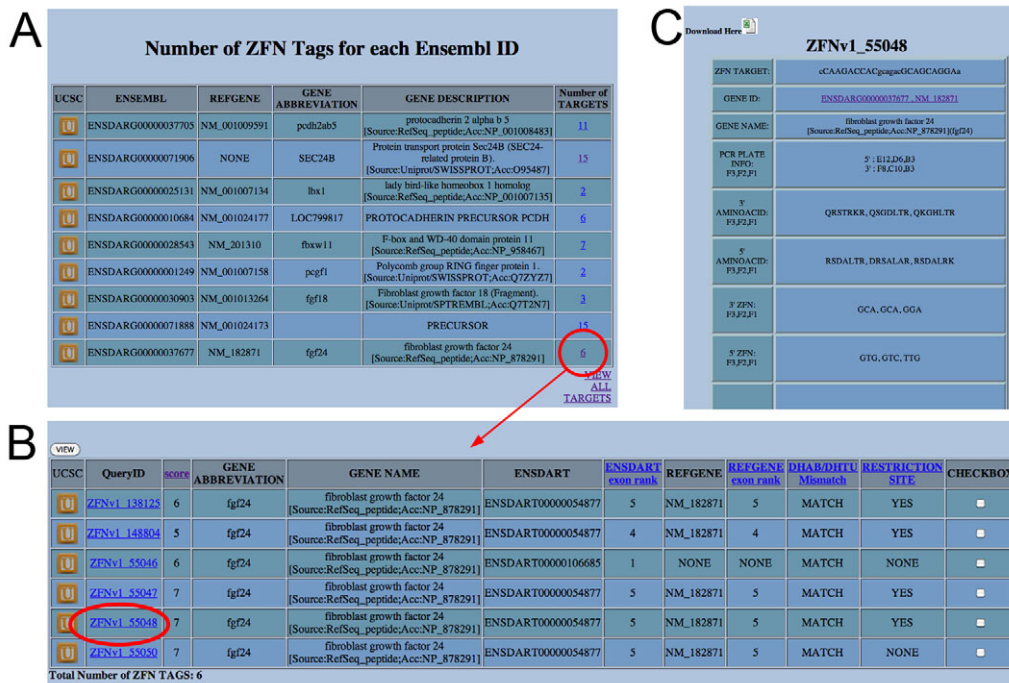


Fig. 4. Screenshots from a modular ZFP/ZFN database. (A) Example output from a search for ZFN target sites. Circle indicates the link to the page shown in B. (B) List of targets in the *fgf24* gene with associated information. Circled number indicates the link to individual target site and ZFN information shown in C. (C) Example output page with individual target site information.

sequenced by the Sanger Center (D. Stemple, personal communication), although we recommend sequencing the target site in wild-type strains other than the hybrid Tu/AB (SAT) reference line.

Once a target site is chosen, the user can click on the ZFN entry (QueryID; see Fig. 4B) for details about each construct (Fig. 4C), such as the target site sequence, the amino acid sequence of the recognition helices for the assembled ZFNs, and clone IDs for each plasmid in the archive (available at addgene.org) to facilitate overlapping PCR of the appropriate modules (see Table S1 in the supplementary material). Alternatively, the DNA sequence of the ZFP cassette is included for direct synthesis. In either case, the inclusion of the amino acid sequence for each entry (Fig. 4C) aids in sequence validation of ZFN-containing plasmids. ZFNs containing modules with poor or context-dependent specificity (see above) are flagged with an asterisk. For lesion detection, we also include restriction sites, when present, within the spacer region separating the ZFP binding sites, along with sequences of flanking primers for PCR amplification. The primer and restriction enzyme information also facilitates easy genotypic analysis of founders and mutant embryos. Data from these pages can be exported into Excel (Microsoft) for easy reference. A query page (<http://pgfe.umassmed.edu/ZFPmodularsearch.html>) is available to identify ZFN sites in sequences not contained within our database.

A novel role for *gata2a* in vascular development

To demonstrate the application of our archive to interrogate gene function and to provide an example of the workflow shown in Fig. S3 in the supplementary material, we investigated defects associated with a ZFN-induced mutation in the *gata2a* gene. *Gata2* is a zinc-finger transcription factor that is essential for definitive hematopoiesis and maintenance of stem cell progenitors in both embryos and adults (Tsai et al., 1994; Rodrigues et al., 2005). *Gata2* has also been implicated in angiogenesis and is associated with early onset coronary artery disease in humans (Connelly et al., 2006; Mammoto et al., 2009), but its role in vascular development

is unknown. As described above, we constructed ZFNs targeting the fourth exon of *gata2a*. The target sequence is upstream of two zinc fingers required for function of the mammalian *Gata2* ortholog (Minegishi et al., 2003) and, therefore, truncation in this region would be expected to generate a null allele (Fig. 5A). Following injection of ZFNs targeting this site, we identified a founder fish bearing a 10 bp deletion allele, referred to as *gata2a^{um27}*, which causes a frameshift to a premature stop codon (Fig. 5A,B).

To identify phenotypes caused by *gata2a* deficiency we observed embryos derived from an incross of *gata2a^{um27}* heterozygous carriers derived from the original founder. At 24 and 48 hpf, all embryos appeared morphologically normal, including normal development of neural tube, notochord and somites (see Fig. S4 in the supplementary material; data not shown). However, ~25% of embryos failed to display trunk blood vessel circulation by 48 hpf (see Movie 1 in the supplementary material, Table 2) whereas the remaining siblings were normal (see Movie 2 in the supplementary material). Genotypic analysis demonstrated that embryos with defective trunk circulation were homozygous for the *um27* deletion, whereas normal embryos were heterozygous or homozygous for the wild-type allele (Fig. 5C, Table 2). Importantly, injection of mRNA encoding wild-type *Gata2a* could rescue trunk circulation in *gata2a^{um27}* mutant embryos (16 out of 26 mutant embryos in two separate experiments) (see Movie 3 in the supplementary material, Fig. 5D,E), whereas injection with *mcherry* mRNA did not (0 out of 13 mutant embryos in two separate experiments) (see Movie 4 in the supplementary material, Fig. 5D,E). Closer inspection of *gata2a^{um27}* mutant embryos revealed the occurrence of pulsating blood cells trapped in the trunk blood vessels and abnormal circulatory connections, or shunts, between the dorsal aorta and posterior cardinal vein (see Movies 1 and 5 in the supplementary material). Despite these defects, mutant embryos displayed a beating heart, the presence of blood cells and circulation through cranial blood vessels (see Movie 6 in the supplementary material), similar to sibling embryos

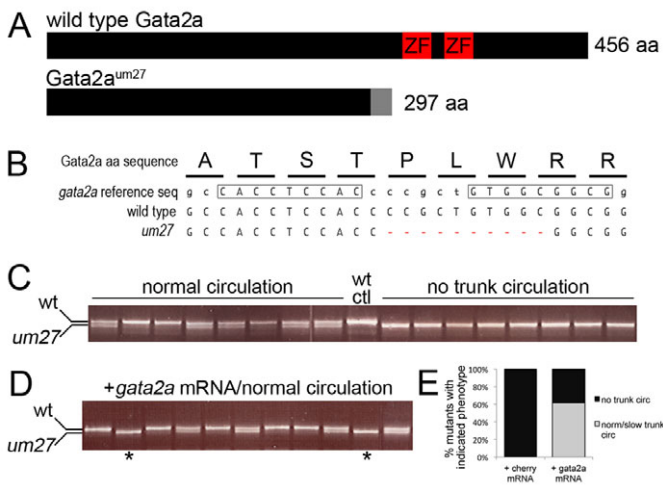


Fig. 5. The ZFN-induced *um27* lesion is a truncation allele of *gata2a*. (A) Location of frameshift caused by the *um27* deletion in the zebrafish *gata2a* gene. ZF, zinc-finger domain. (B) *gata2a* coding and amino acid sequence in the region of the *um27* deletion. ZFN recognition sequences are boxed. (C) Genotype of embryos derived from an incross of *gata2a^{um27}* heterozygous carriers. (D) Genotype of embryos with normal circulation derived from a *gata2a^{um27}* incross injected with 200 pg *gata2a* mRNA. Asterisks denote mutant embryos with normal trunk circulation. (E) Percentage of *gata2a^{um27}* mutant embryos displaying the indicated circulation phenotypes.

with trunk circulation (see Movie 7 in the supplementary material). Together, these observations demonstrate that *gata2a* deficiency leads to a specific defect in circulatory function in embryonic zebrafish.

To further characterize the phenotype caused by loss of *gata2a*, we performed confocal microangiography on wild-type and *gata2a^{um27}* mutant siblings bearing the *Tg(kdrl:egfp)^{la116}* transgene at 50 hpf. Consistent with normal head circulation in *gata2a^{um27}* mutant embryos, we did not note any overt defects in vascular morphology of the cranial vessels when compared with wild-type siblings (Fig. 6A,B). We observed normal formation of arteries and veins within the head, which are fully perfused following angiography (Fig. 6A,B). By contrast, the lateral dorsal aortae in *gata2a^{um27}* mutant embryos are more dilated than in wild-type siblings, although these vessels are perfused, suggesting that lumenization is not affected (Fig. 6C,D). Within the trunk, we

observed specific defects in vascular morphology. Whereas intersegmental vessels appeared largely normal in *gata2a^{um27}* mutant embryos, the dorsal aorta was discontinuous (Fig. 6E). Accordingly, *gata2a^{um27}* mutant trunk vessels were poorly perfused following angiography when compared with their wild-type siblings (Fig. 6E,F). These analyses suggest a specific defect in the morphogenesis of the dorsal aorta in *gata2a^{um27}* mutant embryos, which would be the likely cause of the arteriovenous shunts noted above.

We have previously observed aorta morphogenesis defects and arteriovenous shunts in zebrafish embryos deficient for Notch or Vegf signaling (Lawson et al., 2001; Covassin et al., 2006). In these cases, these defects were associated with loss of arterial endothelial cell identity. However, *gata2a^{um27}* mutant embryos did not display loss of artery markers, such as *efnb2a*, and exhibited normal levels of *vegfaa* expression (data not shown). Similarly, the *hey2* gene, which is also required for proper dorsal aorta morphogenesis (Zhong et al., 2000), was expressed at normal levels in *gata2a^{um27}* mutants (Fig. 7A,B). We also did not observe any significant changes in the expression of blood markers such as *gata1* and *tall* (Fig. 7C,D; data not shown). However, *gata2a^{um27}* mutant embryos displayed a subtle, but consistent, downregulation of *kdrl*, the functional ortholog of *Vegfr2*, when compared with wild-type siblings (Fig. 7E,F). Taken together, our results demonstrate that *gata2a* function is essential for the proper morphogenesis of the dorsal aorta, but may be dispensable for arterial endothelial differentiation.

DISCUSSION

With the increasing characterization of the genomes of model and non-model organisms, there is a broad need for reverse genetic approaches to assess gene function in multiple species. ZFNs allow the direct introduction of targeted germline lesions in vivo, without the need for species-matched embryonic stem cell lines, thus providing a general means to determine gene function. However, the primary limitation hindering the widespread employment of this technology has been the lack of an affordable, simple method for constructing ZFNs that are active in vivo. Modularly assembled ZFNs provide a rapid and effective method for introducing targeted lesions into the genomes of animals. The specificity analysis of our assembled ZFPs indicates that the majority have similar recognition potential to the selected ZFPs incorporated into our *kdrl* ZFNs (Meng et al., 2008; Gupta et al., 2011). Consequently, a sizable fraction (29%) of ZFNs constructed from these modules displayed significant activity ($\geq 1\%$) for the generation of somatic lesions,

Table 2. Linkage of *gata2a^{um27}* to circulatory defects in mutant embryos

Parents	Circulation phenotype	No. embryos	Proportion	<i>gata2a^{um27}</i> genotype		
				+/+	+/-	-/-
A2×A5	Normal	116	0.77	1	10	0
	Head but no trunk	34	0.23	0	0	11
	Normal	59	0.81	3	7	2
	Head but no trunk	14	0.19	1	0	11
A3×A6	Normal	42	0.79	4	7	1
	Head but no trunk	11	0.21	0	0	12
	Normal	67	0.79	3	8	0
	Head but no trunk	18	0.21	0	0	11
Total	Normal	284	0.79	11	32	3
	Head but no trunk	77	0.21	1	0	45

Results are shown for two separate clutches (different days) from each set of parents.

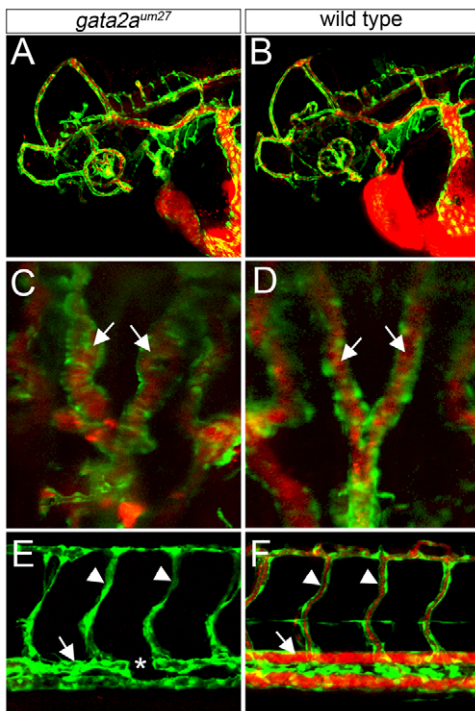


Fig. 6. *gata2a*^{um27} mutant embryos display defects in aorta morphogenesis. Confocal microangiography using Quantum Dots in *Tg(kdrl:egfp)^{la116}* transgenic zebrafish embryos. Endothelial cells are green and vessel perfusion is red. (A,B) Cranial blood vessels in *gata2a*^{um27} mutant (A) and wild-type (B) embryos. Lateral views, anterior to the left, dorsal is up. (C,D) Lateral dorsal aortae (arrows) in *gata2a*^{um27} mutant (C) and wild-type (D) embryos. Dorsal views, anterior is up. (E,F) Trunk blood vessels in *gata2a*^{um27} mutant (E) and wild-type (F) embryos. Lateral views, anterior to the left, dorsal is up. Segmental vessels are indicated by arrowheads and the dorsal aorta by an arrow; the asterisk indicates a region of aorta that failed to form.

establishing the utility of this archive for targeted genome manipulation in complex genomes. This success rate compares favorably with that of other single-finger modular assembly archives for constructing ZFNs (Ramirez et al., 2008; Kim et al., 2009; Kim et al., 2011). Moreover, characterization of DNA-binding specificity provides additional information about the performance of individual modules within this archive and will facilitate its subsequent improvement.

Surprisingly, we did not find a strong correlation between ZFP specificity and in vivo ZFN activity. Previous studies have shown that improvements in DNA-binding specificity can lead to improved ZFN activity (Cornu et al., 2008) and precision (Gupta et al., 2011). It is likely that other factors, such as ZFP affinity, also significantly influence ZFN activity. Whereas the recognition motifs generated using the B1H system provide an estimate of ZFP specificity, our analysis utilized varying stringencies to achieve enrichment of binding sites, possibly bypassing variations that could reflect differences in affinity. That said, seven of eight ZFNs that contained at least one ZFP that displayed low activity in the B1H system (i.e. binding site selections required a stringency below 5 mM 3-AT) displayed low somatic lesion rates (<0.5%). This correlation is consistent with studies utilizing the bacterial two-hybrid system, in which highly active ZFPs often perform well in ZFNs (Ramirez et al., 2008; Lam et al., 2011). Thus, a more

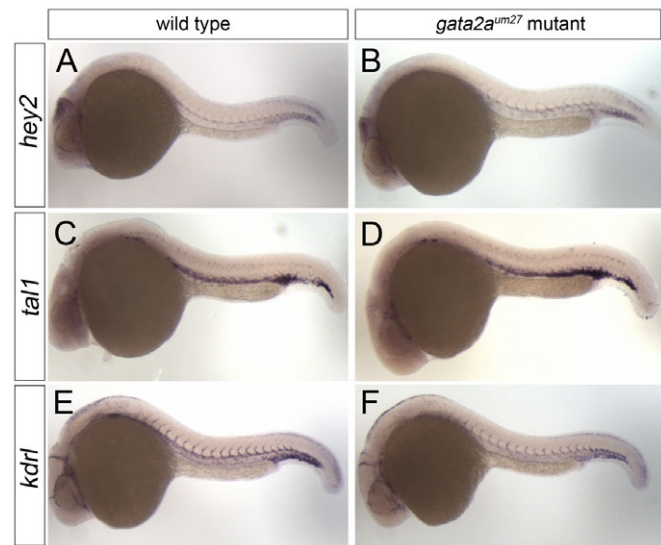


Fig. 7. *gata2a*^{um27} mutant embryos show reduced *kdrl* expression but normal artery and blood differentiation. (A-F) Whole-mount in situ hybridization at 24 hpf using antisense riboprobes against *hey2* (A,B), *tal1* (C,D) and *kdrl* (E,F) in genotypically wild-type zebrafish embryos (A,C,E) and those homozygous for the *um27* deletion (B,D,F). Lateral views, anterior to the left, dorsal is up.

refined analysis of ZFP affinity might provide additional insights into the behavior of our archive. Additionally, ZFN activity could be affected by properties of the endogenous target sequence (e.g. chromatin architecture or DNA methylation status) that could interfere with nuclease recognition or function.

We did observe significantly higher rates of ZFN activity as a function of the number of GNN fingers, consistent with previous observations (Ramirez et al., 2008), and a slight increase in the average number of NNG fingers in the active versus inactive ZFN population. In both sets of modules, arginine-guanine interactions, which can contribute dramatically to binding affinity and specificity (Elrod-Erickson and Pabo, 1999), appear to be critical linchpins for the formation of active ZFN complexes. Consequently, this information is incorporated into a simple scoring function for evaluating our ZFNs that notes the number of these contacts. Consistent with the importance of arginine-guanine interactions, their preservation is a defining feature of active off-target sites for *kdrl* ZFNs in zebrafish (Gupta et al., 2011). Clearly, the presence of a large number of arginine-guanine interactions is not required for the construction of active ZFNs (Hockemeyer et al., 2009), but these particular examples employed larger numbers of fingers, which might compensate for the absence of these favorable interactions.

A limitation of the modular assembly approach highlighted by our analysis is position or context-dependent specificity of individual modules. In other studies, this problem has been partially mitigated by the creation of extensive archives of selected two-finger modules that allow the assembly of multiple ZFPs against a single target site. For example, Sangamo BioSciences employs a proprietary archive of two-finger modules with origins in context-dependent selection for ZFN assembly (Isalan and Choo, 2001). Recently, the Zinc Finger Consortium reported the selection and construction of an archive of two-finger modules, in which three-finger proteins are created from the assembly of overlapping

two-finger modules (CoDA) (Sander et al., 2011). By reducing context-dependent effects both methods are anticipated to improve the success rate for the assembly of functional ZFPs over those assembled from single-finger archives. For the Zinc Finger Consortium-based CoDA ZFPs this has been directly demonstrated on a large scale, in which ~50% of ZFNs were active in vivo (Sander et al., 2011), although only ZFPs that performed well in a bacterial two-hybrid assay were used for in vivo testing in this case. Taking this prefiltering into account, the in vivo efficacy of ZFNs from our archive compares favorably to the CoDA approach. Furthermore, our archive is capable of targeting genomic sequences that are not accessible using CoDA because of differences in the recognition sequences of modules between these archives. Finally, the detailed characterization of ZFPs constructed from our archive allowed us to identify context-dependent or otherwise poorly performing modules, facilitating future improvements to our collection. Taken together, we believe that our archive and the associated computational resources will provide a viable and accessible platform for the generation of gene knockouts in zebrafish, as well as in other organisms.

A number of studies have now described ZFNs that are capable of producing somatic lesions in zebrafish embryos. However, only a handful of new mutants have been generated and there is a paucity of data concerning germline transmission of ZFN-induced alleles. To date, the modular archive described here has been used to generate eight new zebrafish mutants. Significantly, several of these new lines have been used to reveal novel aspects of microRNA biogenesis and vascular development (Siekman et al., 2009; Cifuentes et al., 2010), whereas others, such as *nfla* and *nflb*, will serve as important disease models (Padmanabhan et al., 2009; Lee et al., 2010). Equally importantly, our archive has been used to independently generate these mutant lines in four separate laboratories, suggesting that this approach can be easily implemented within the research community at large to create zebrafish lines bearing mutations in genes of interest.

Among the new mutants that we have generated is a truncation in the *gata2a* gene. We observed that *gata2a*-deficient embryos displayed defects in the formation of the dorsal aorta, yet the remainder of the vascular system is remarkably unaffected. This phenotype is reminiscent of embryos lacking Vegf or Notch signaling components and is often attributed to the loss of properly specified artery and vein endothelial identity (Lawson et al., 2001; Covassin et al., 2006). However, we did not observe obvious loss of artery marker gene expression. These results are somewhat surprising and suggest that vascular morphogenesis and endothelial differentiation might be uncoupled at some point downstream of Vegf. Alternatively, the phenotype of *gata2a^{um27}* mutant embryos might reflect a defect in endothelial mechanosensation that affects morphogenesis independently of differentiation. Indeed, we do not observe any major changes in vascular morphology until the onset of circulation, although *kdrl* expression is slightly downregulated at 24 hpf, prior to blood flow. In addition, GATA2 has recently been implicated in the induction of *VEGFR2* in human endothelial cells in response to increased extracellular matrix stiffening (Mammoto et al., 2009), suggesting a role for this transcription factor in mediating endothelial mechanosensation. In any case, our observations reveal an unexpected and previously undescribed role for *gata2a* in artery morphogenesis. Importantly, the *gata2a^{um27}* mutant generated using modular ZFNs now provides an important tool to further characterize the observed vascular phenotype and to identify relevant target genes that are required for vascular morphogenesis or function.

Acknowledgements

We thank Craig Ceol, Stefania Nicoli and Fatma Kok for critical reading of the manuscript, John Polli for excellent fish care, and Derek Stemple for providing the Tu and AB genome sequences.

Funding

This work was funded by grants from the NIH National Heart, Lung, and Blood Institute to S.A.W. and N.D.L. (R01 HL093766) and to N.D.L. (R01 HL079266) and from the Department of Defense to A.T.L. and J.A.E. (DOD, NF050175), and from the National Institute of General Medical Sciences to A.J.G. (R01 GM081602). Deposited in PMC for release after 12 months.

Competing interests statement

The authors declare no competing financial interests.

Supplementary material

Supplementary material for this article is available at <http://dev.biologists.org/lookup/suppl/doi:10.1242/dev.066779/-DC1>

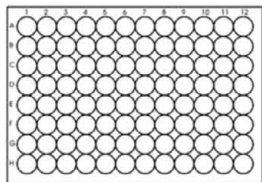
References

- Bailey, T. L. and Elkan, C. (1994). Fitting a mixture model by expectation maximization to discover motifs in biopolymers. *Proc. Int. Conf. Intell. Syst. Mol. Biol.* **2**, 28-36.
- Beis, D. and Stainier, D. Y. (2006). In vivo cell biology: following the zebrafish trend. *Trends Cell Biol.* **16**, 105-112.
- Beumer, K. J., Trautman, J. K., Bozas, A., Liu, J. L., Rutter, J., Gall, J. G. and Carroll, D. (2008). Efficient gene targeting in *Drosophila* by direct embryo injection with zinc-finger nucleases. *Proc. Natl. Acad. Sci. USA* **105**, 19821-19826.
- Bibikova, M., Golic, M., Golic, K. G. and Carroll, D. (2002). Targeted chromosomal cleavage and mutagenesis in *Drosophila* using zinc-finger nucleases. *Genetics* **161**, 1169-1175.
- Carroll, D., Morton, J. J., Beumer, K. J. and Segal, D. J. (2006). Design, construction and in vitro testing of zinc finger nucleases. *Nat. Protoc.* **1**, 1329-1341.
- Choi, J., Dong, L., Ahn, J., Dao, D., Hammerschmidt, M. and Chen, J. N. (2007). FoxH1 negatively modulates flk1 gene expression and vascular formation in zebrafish. *Dev. Biol.* **304**, 735-744.
- Choo, Y. (1998). End effects in DNA recognition by zinc finger arrays. *Nucleic Acids Res.* **26**, 554-557.
- Cifuentes, D., Xue, H., Taylor, D. W., Patnode, H., Mishima, Y., Cheloufi, S., Ma, E., Mane, S., Hannon, G. J., Lawson, N. D. et al. (2010). A novel miRNA processing pathway independent of Dicer requires Argonaute2 catalytic activity. *Science* **328**, 1694-1698.
- Connelly, J. J., Wang, T., Cox, J. E., Haynes, C., Wang, L., Shah, S. H., Crosslin, D. R., Hale, A. B., Nelson, S., Crossman, D. C. et al. (2006). GATA2 is associated with familial early-onset coronary artery disease. *PLoS Genet.* **2**, e139.
- Cornu, T. I., Thibodeau-Beganny, S., Guhl, E., Alwin, S., Eichinger, M., Jung, J. K. and Cathomen, T. (2008). DNA-binding specificity is a major determinant of the activity and toxicity of zinc-finger nucleases. *Mol. Ther.* **16**, 352-358.
- Covassin, L. D., Villefranc, J. A., Kacergis, M. C., Weinstein, B. M. and Lawson, N. D. (2006). Distinct genetic interactions between multiple Vegf receptors are required for development of different blood vessel types in zebrafish. *Proc. Natl. Acad. Sci. USA* **103**, 6554-6559.
- Cui, X., Ji, D., Fisher, D. A., Wu, Y., Briner, D. M. and Weinstein, E. J. (2010). Targeted integration in rat and mouse embryos with zinc-finger nucleases. *Nat. Biotechnol.* **29**, 64-67.
- Desjarlais, J. R. and Berg, J. M. (1993). Use of a zinc-finger consensus sequence framework and specificity rules to design specific DNA binding proteins. *Proc. Natl. Acad. Sci. USA* **90**, 2256-2260.
- Doyon, Y., McCommon, J. M., Miller, J. C., Faraji, F., Ngo, C., Katibah, G. E., Amora, R., Hocking, T. D., Zhang, L., Rebar, E. J. et al. (2008). Heritable targeted gene disruption in zebrafish using designed zinc-finger nucleases. *Nat. Biotechnol.* **26**, 702-708.
- Dreier, B., Beerli, R. R., Segal, D. J., Flippin, J. D. and Barbas, C. F., 3rd (2001). Development of zinc finger domains for recognition of the 5'-ANN-3' family of DNA sequences and their use in the construction of artificial transcription factor. *J. Biol. Chem.* **276**, 29466-29478.
- Dreier, B., Fuller, R. P., Segal, D. J., Lund, C. V., Blancfort, P., Huber, A., Koksche, B. and Barbas, C. F., 3rd (2005). Development of zinc finger domains for recognition of the 5'-CNN-3' family DNA sequences and their use in the construction of artificial transcription factors. *J. Biol. Chem.* **280**, 35588-35597.
- Eisen, J. S. and Smith, J. C. (2008). Controlling morpholino experiments: don't stop making antisense. *Development* **135**, 1735-1743.
- Elrod-Erickson, M. and Pabo, C. O. (1999). Binding studies with mutants of Zif268. Contribution of individual side chains to binding affinity and specificity in the Zif268 zinc finger-DNA complex. *J. Biol. Chem.* **274**, 19281-19285.

- Foley, J. E., Yeh, J. R., Maeder, M. L., Reyon, D., Sander, J. D., Peterson, R. T. and Joung, J. K. (2009). Rapid mutation of endogenous zebrafish genes using zinc finger nucleases made by Oligomerized Pool ENgineering (OPEN). *PLoS ONE* **4**, e4348.
- Geurts, A. M., Cost, G. J., Freyvert, Y., Zeitler, B., Miller, J. C., Choi, V. M., Jenkins, S. S., Wood, A., Cui, X., Meng, X. et al. (2009). Knockout rats via embryo microinjection of zinc-finger nucleases. *Science* **325**, 433.
- Greisman, H. A. and Pabo, C. O. (1997). A general strategy for selecting high-affinity zinc finger proteins for diverse DNA target sites. *Science* **275**, 657-661.
- Gupta, A., Meng, X., Zhu, L. J., Lawson, N. D. and Wolfe, S. A. (2011). Zinc finger protein-dependent and -independent contributions to the in vivo off-target activity of zinc finger nucleases. *Nucleic Acids Res.* **39**, 381-392.
- Hart, D. O., Raha, T., Lawson, N. D. and Green, M. R. (2007). Initiation of zebrafish haematopoiesis by the TATA-box-binding protein-related factor Trf3'. *Nature* **450**, 1082-1085.
- Hertz, G. Z. and Stormo, G. D. (1999). Identifying DNA and protein patterns with statistically significant alignments of multiple sequences. *Bioinformatics* **15**, 563-577.
- Hockemeyer, D., Soldner, F., Beard, C., Gao, Q., Mitalipova, M., DeKaveler, R. C., Katibah, G. E., Amora, R., Boydston, E. A., Zeitler, B. et al. (2009). Efficient targeting of expressed and silent genes in human ESCs and iPSCs using zinc-finger nucleases. *Nat. Biotechnol.* **27**, 851-857.
- Isalan, M. and Choo, Y. (2001). Rapid, high-throughput engineering of sequence-specific zinc finger DNA-binding proteins. *Methods Enzymol.* **340**, 593-609.
- Isalan, M., Klug, A. and Choo, Y. (1998). Comprehensive DNA recognition through concerted interactions from adjacent zinc fingers. *Biochemistry* **37**, 12026-12033.
- Kim, H. J., Lee, H. J., Kim, H., Cho, S. W. and Kim, J. S. (2009). Targeted genome editing in human cells with zinc finger nucleases constructed via modular assembly. *Genome Res.* **19**, 1279-1288.
- Kim, S., Kim, E. J. and Kim, J. S. (2010). Construction of combinatorial libraries that encode zinc finger-based transcription factors. *Methods Mol. Biol.* **649**, 133-147.
- Kim, S., Lee, M. J., Kim, H., Kang, M. and Kim, J.-S. (2011). Preassembled zinc-finger arrays for rapid construction of ZFNs. *Nat. Methods* **8**, 7-7.
- Lam, K. N., van Bakel, H., Cote, A. G., van der Ven, A. and Hughes, T. R. (2011). Sequence specificity is obtained from the majority of modular C2H2 zinc-finger arrays. *Nucleic Acids Res.* **39**, 4680-4690.
- Lawson, N. D., Scheer, N., Pham, V. N., Kim, C. H., Chitnis, A. B., Campos-Ortega, J. A. and Weinstein, B. M. (2001). Notch signaling is required for arterial-venous differentiation during embryonic vascular development. *Development* **128**, 3675-3683.
- Lee, J. S., Padmanabhan, A., Shin, J., Zhu, S., Guo, F., Kanki, J. P., Epstein, J. A. and Look, A. T. (2010). Oligodendrocyte progenitor cell numbers and migration are regulated by the zebrafish orthologs of the NF1 tumor suppressor gene. *Hum. Mol. Genet.* **19**, 4643-4653.
- Liu, Q., Xia, Z., Zhong, X. and Case, C. C. (2002). Validated zinc finger protein designs for all 16 GNN DNA triplet targets. *J. Biol. Chem.* **277**, 3850-3856.
- Maeder, M. L., Thibodeau-Beganny, S., Osiak, A., Wright, D. A., Anthony, R. M., Eichinger, M., Jiang, T., Foley, J. E., Winfrey, R. J., Townsend, J. A. et al. (2008). Rapid 'open-source' engineering of customized zinc-finger nucleases for highly efficient gene modification. *Mol. Cell* **31**, 294-301.
- Mammoto, A., Connor, K. M., Mammoto, T., Yung, C. W., Huh, D., Aderman, C. M., Mostoslavsky, G., Smith, L. E. and Ingber, D. E. (2009). A mechanosensitive transcriptional mechanism that controls angiogenesis. *Nature* **457**, 1103-1108.
- Mashimo, T., Takizawa, A., Voigt, B., Yoshimi, K., Hiai, H., Kuramoto, T. and Serikawa, T. (2010). Generation of knockout rats with X-linked severe combined immunodeficiency (X-SCID) using zinc-finger nucleases. *PLoS ONE* **5**, e8870.
- Meng, X., Noyes, M. B., Zhu, L. J., Lawson, N. D. and Wolfe, S. A. (2008). Targeted gene inactivation in zebrafish using engineered zinc-finger nucleases. *Nat. Biotechnol.* **26**, 695-701.
- Meyer, M., de Angelis, M. H., Wurst, W. and Kuhn, R. (2010). Gene targeting by homologous recombination in mouse zygotes mediated by zinc-finger nucleases. *Proc. Natl. Acad. Sci. USA* **107**, 15022-15026.
- Miller, J. C., Holmes, M. C., Wang, J., Guschin, D. Y., Lee, Y. L., Rupniewski, I., Beausejour, C. M., Waite, A. J., Wang, N. S., Kim, K. A. et al. (2007). An improved zinc-finger nuclease architecture for highly specific genome editing. *Nat. Biotechnol.* **25**, 778-785.
- Minegishi, N., Suzuki, N., Yokomizo, T., Pan, X., Fujimoto, T., Takahashi, S., Hara, T., Miyajima, A., Nishikawa, S. and Yamamoto, M. (2003). Expression and domain-specific function of GATA-2 during differentiation of the hematopoietic precursor cells in midgestation mouse embryos. *Blood* **102**, 896-905.
- Nasevicius, A. and Ekker, S. C. (2000). Effective targeted gene 'knockdown' in zebrafish. *Nat. Genet.* **26**, 216-220.
- Noyes, M. B., Meng, X., Wakabayashi, A., Sinha, S., Brodsky, M. H. and Wolfe, S. A. (2008). A systematic characterization of factors that regulate *Drosophila* segmentation via a bacterial one-hybrid system. *Nucleic Acids Res.* **36**, 2547-2560.
- Padmanabhan, A., Lee, J. S., Ismat, F. A., Lu, M. M., Lawson, N. D., Kanki, J. P., Look, A. T. and Epstein, J. A. (2009). Cardiac and vascular functions of the zebrafish orthologues of the type I neurofibromatosis gene NF1. *Proc. Natl. Acad. Sci. USA* **106**, 22305-22310.
- Patton, E. E. and Zon, L. I. (2001). The art and design of genetic screens: zebrafish. *Nat. Rev. Genet.* **2**, 956-966.
- Perez, E. E., Wang, J., Miller, J. C., Jouvenot, Y., Kim, K. A., Liu, O., Wang, N., Lee, G., Bartsevich, V. V., Lee, Y. L. et al. (2008). Establishment of HIV-1 resistance in CD4+ T cells by genome editing using zinc-finger nucleases. *Nat. Biotechnol.* **26**, 808-816.
- Ramirez, C. L., Foley, J. E., Wright, D. A., Muller-Lerch, F., Rahman, S. H., Cornu, T. I., Winfrey, R. J., Sander, J. D., Fu, F., Townsend, J. A. et al. (2008). Unexpected failure rates for modular assembly of engineered zinc fingers. *Nat. Methods* **5**, 374-375.
- Robu, M. E., Larson, J. D., Nasevicius, A., Beiraghi, S., Brenner, C., Farber, S. A. and Ekker, S. C. (2007). p53 activation by knockdown technologies. *PLoS Genet.* **3**, e78.
- Rodrigues, N. P., Janzen, V., Forkert, R., Dombkowski, D. M., Boyd, A. S., Orkin, S. H., Enver, T., Vyas, P. and Scadden, D. T. (2005). Haploinsufficiency of GATA-2 perturbs adult hematopoietic stem-cell homeostasis. *Blood* **106**, 477-484.
- Roman, B. L., Pham, V. N., Lawson, N. D., Kulik, M., Childs, S., Lekven, A. C., Garrity, D. M., Moon, R. T., Fishman, M. C., Lechleider, R. J. et al. (2002). Disruption of *acvr1l* increases endothelial cell number in zebrafish cranial vessels. *Development* **129**, 3009-3019.
- Sander, J. D., Zaback, P., Joung, J. K., Voytas, D. F. and Dobbs, D. (2009). An affinity-based scoring scheme for predicting DNA-binding activities of modularly assembled zinc-finger proteins. *Nucleic Acids Res.* **37**, 506-515.
- Sander, J. D., Dahlborg, E. J., Goodwin, M. J., Cade, L., Zhang, F., Cifuentes, D., Curtin, S. J., Blackburn, J. S., Thibodeau-Beganny, S., Qi, Y. et al. (2011). Selection-free zinc-finger-nuclease engineering by context-dependent assembly (CoDA). *Nat. Methods* **8**, 67-69.
- Schneider, T. D. and Stephens, R. M. (1990). Sequence logos: a new way to display consensus sequences. *Nucleic Acids Res.* **18**, 6097-6100.
- Segal, D. J., Dreier, B., Beerli, R. R. and Barbas, C. F., 3rd (1999). Toward controlling gene expression at will: selection and design of zinc finger domains recognizing each of the 5'-GNN-3' DNA target sequences. *Proc. Natl. Acad. Sci. USA* **96**, 2758-2763.
- Siekman, A. F., Standley, C., Fogarty, K. E., Wolfe, S. A. and Lawson, N. D. (2009). Chemokine signaling guides regional patterning of the first embryonic artery. *Genes Dev.* **23**, 2272-2277.
- Szczepek, M., Brondani, V., Buchel, J., Serrano, L., Segal, D. J. and Cathomen, T. (2007). Structure-based redesign of the dimerization interface reduces the toxicity of zinc-finger nucleases. *Nat. Biotechnol.* **25**, 786-793.
- Takasu, Y., Kobayashi, I., Beumer, K., Uchino, K., Sezutsu, H., Sajwan, S., Carroll, D., Tamura, T. and Zurovec, M. (2010). Targeted mutagenesis in the silkworm *Bombyx mori* using zinc finger nuclease mRNA injection. *Insect Biochem. Mol. Biol.* **40**, 759-765.
- Tsai, F. Y., Keller, G., Kuo, F. C., Weiss, M., Chen, J., Rosenblatt, M., Alt, F. W. and Orkin, S. H. (1994). An early haematopoietic defect in mice lacking the transcription factor GATA-2. *Nature* **371**, 221-226.
- Urnov, F. D., Rebar, E. J., Holmes, M. C., Zhang, H. S. and Gregory, P. D. (2010). Genome editing with engineered zinc finger nucleases. *Nat. Rev. Genet.* **11**, 636-646.
- Villefranc, J. A., Amigo, J. and Lawson, N. D. (2007). Gateway compatible vectors for analysis of gene function in the zebrafish. *Dev. Dyn.* **236**, 3077-3087.
- Westerfield, M. (1993). *The Zebrafish Book*. Eugene, OR: University of Oregon Press.
- Wolfe, S. A., Greisman, H. A., Ramm, E. I. and Pabo, C. O. (1999). Analysis of zinc fingers optimized via phage display: evaluating the utility of a recognition code. *J. Mol. Biol.* **285**, 1917-1934.
- Zhong, T. P., Rosenberg, M., Mohideen, M. A., Weinstein, B. and Fishman, M. C. (2000). girdlock, an HLH gene required for assembly of the aorta in zebrafish. *Science* **287**, 1820-1824.

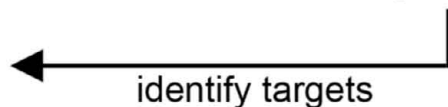
Assemble ZFP archive

- collection of ZFPs recognizing 27 triplet sequences in each of 3 finger positions



Construct target database

- database of ZFN targets in the zebrafish genome (Zv7)
- assembled using our corresponding archive



construct 3-finger ZFP cassettes by overlapping PCR

subclone into p1352

Determine binding specificity

- bacterial 1-hybrid analysis of ZFPs

subclone into pCS2-EL/KK

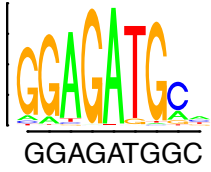
Determine in vivo activity

- inject ZFN mRNAs into 1-cell zebrafish embryos
- assess somatic lesion frequency

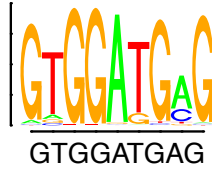
Assess Germline Transmission

- identify founder fish bearing mutagenic alleles for selected ZFN targets

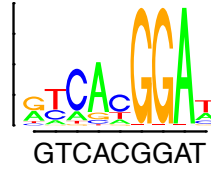
ago2-3p



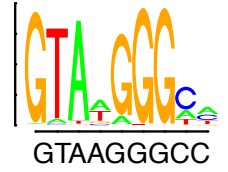
ago2-5p



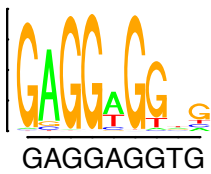
arhgef-3p



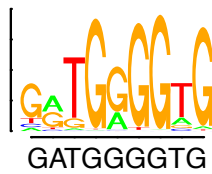
arhgef-5p



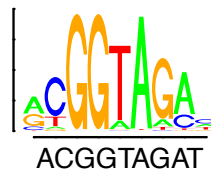
braf-3p



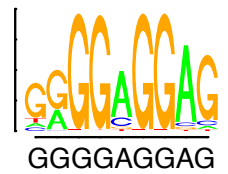
braf-5p



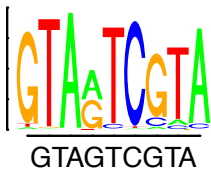
cdkn1b-3p



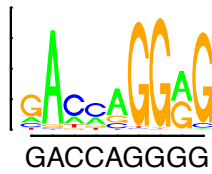
chd5-3p



chd5-5p



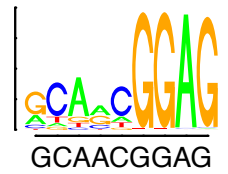
col181a-3p



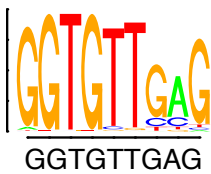
col181a-5p



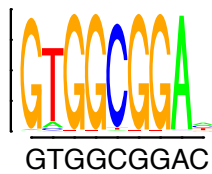
cxcl12b-3p



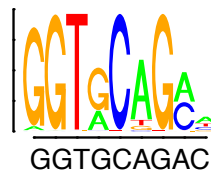
cxcl12b-5p



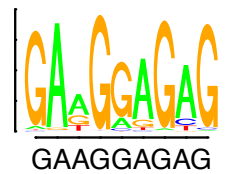
cxcr4a-3p



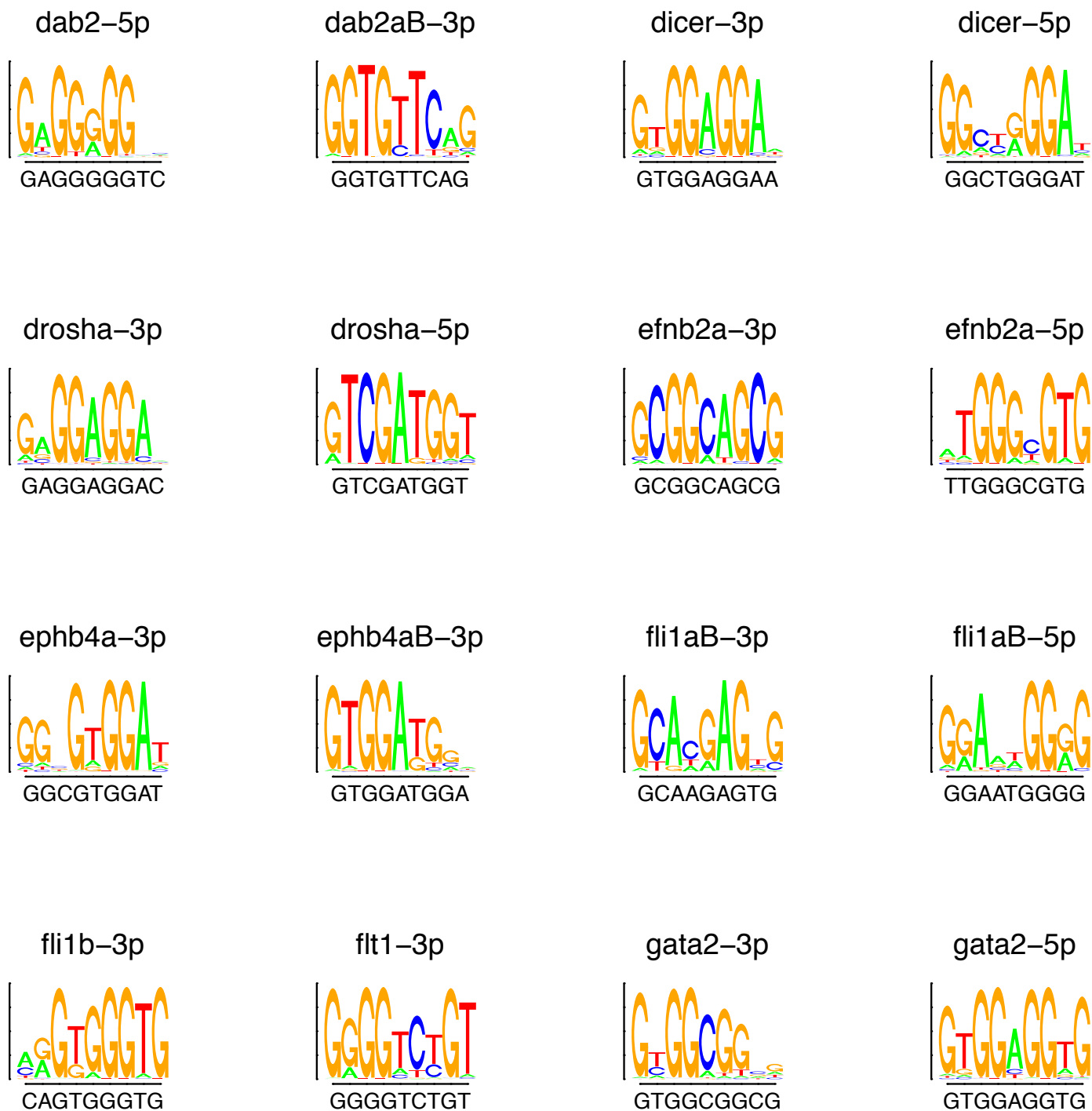
cxcr4a-5p



dab2-3p

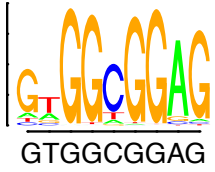


Supplementary Figure 2

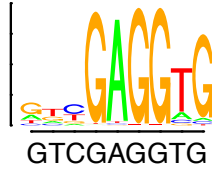


Supplementary Figure 2, continued

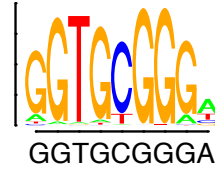
gata3-3p



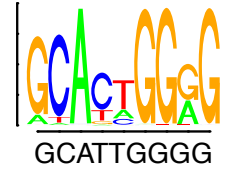
gata3-5p



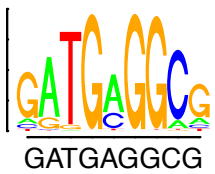
kif1ba-53751-3p



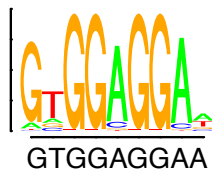
kif1ba-53751-5p



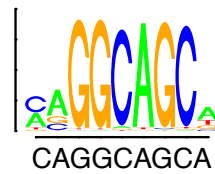
kif1bbeta-53765-3p



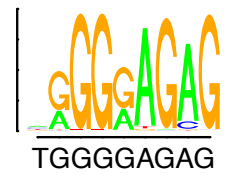
kif1bbeta-53765-5p



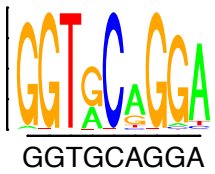
klf2a-3p



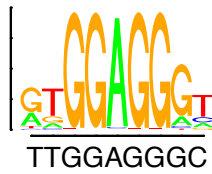
klf2a-5p



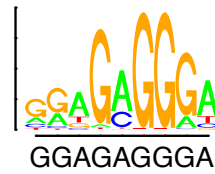
micall2-3p



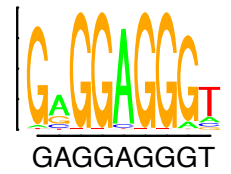
micall2-5p



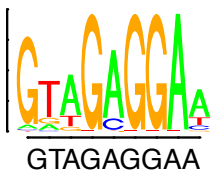
nCHD5-3p



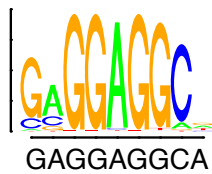
nf1a-3p



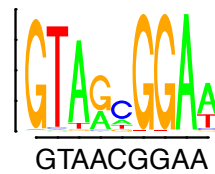
nf1a-5p



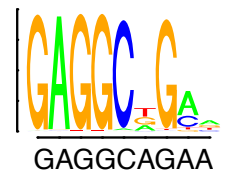
nf1b_5253-3p



nf1b_5253-5p



nf1b_5254-3p

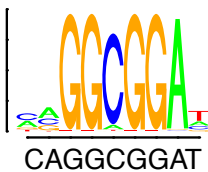


Supplementary Figure 2, continued

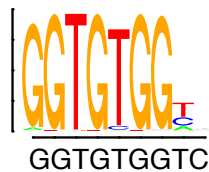
nf1b_5254-5p



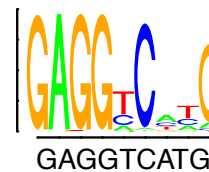
numb_like-3p



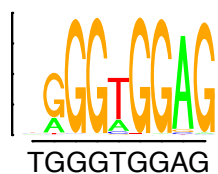
numb_like-5p



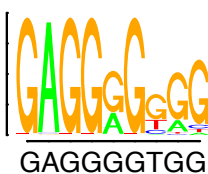
pdgrfb2-3p



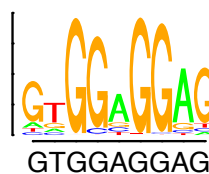
per2-3p



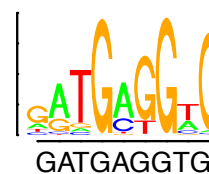
per2-5p



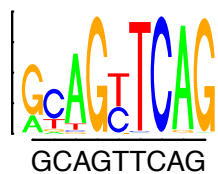
ptpru-3p



ptpru-5p



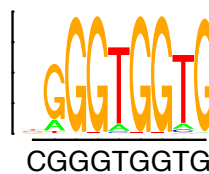
Q0P4B5DANREB-3p



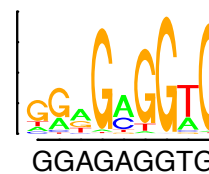
sbno2-3p



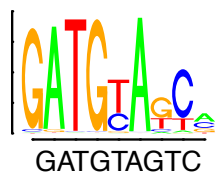
sbno2-5p



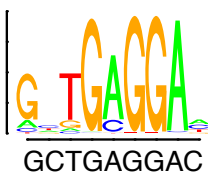
sgk-3p



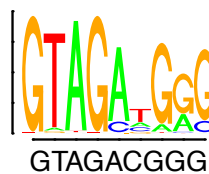
sgk-5p



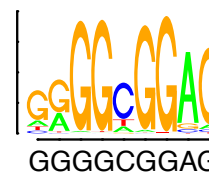
smox-3p



smox-5p

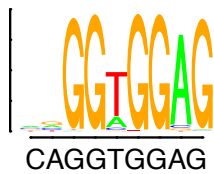


spon1b-3p

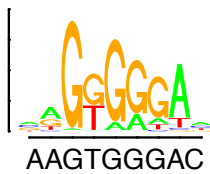


Supplementary Figure 2, continued

spon1b-5p



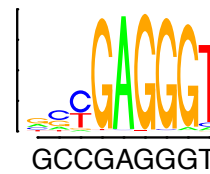
tie1-3p



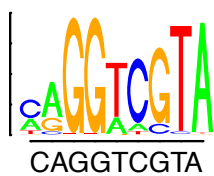
tie1-5p



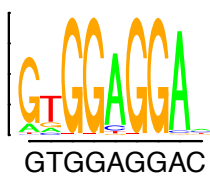
trbp-3p



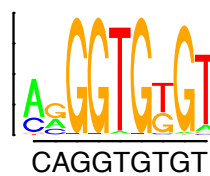
trbp-5p



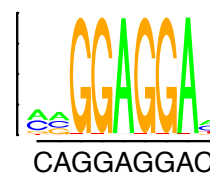
vsg1-3p



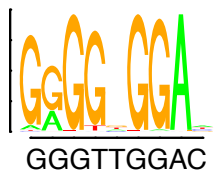
yrk-3p



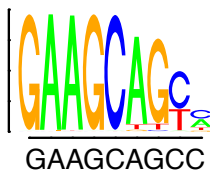
yrk-5p



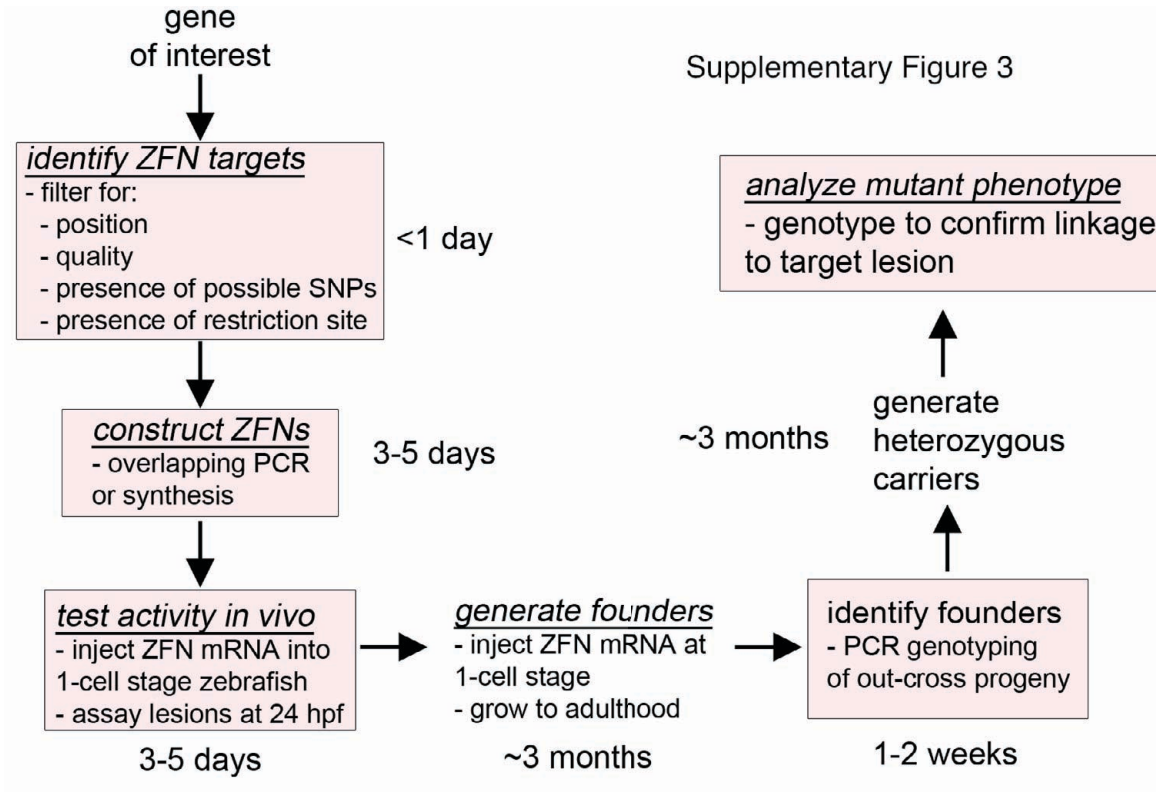
zgc66439-3p



zgc66439-5p

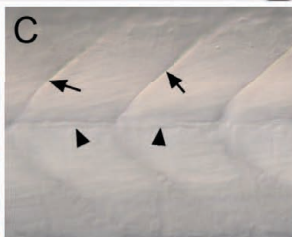
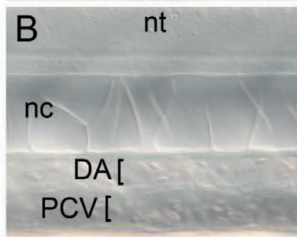


Supplementary Figure 2, continued

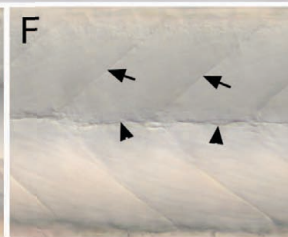
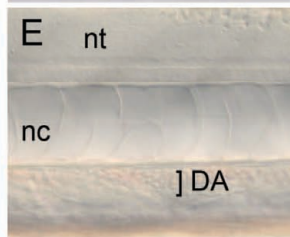
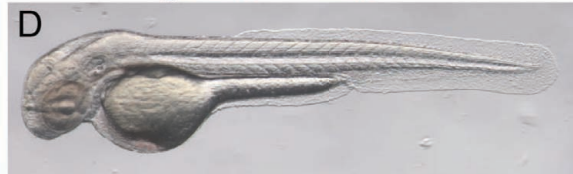


Supplementary Figure 4

wild type sibling



gata2a^{um27} mutant



Zebrafish neurofibromatosis type 1 genes have redundant functions in tumorigenesis and embryonic development

Jimann Shin^{1,*‡}, Arun Padmanabhan^{2,‡}, Eric D. de Groh^{2,‡}, Jeong-Soo Lee^{1,§}, Sam Haidar³, Suzanne Dahlberg¹, Feng Guo¹, Shuning He¹, Marc A. Wolman², Michael Granato², Nathan D. Lawson⁴, Scot A. Wolfe⁴, Seok-Hyung Kim⁵, Lilianna Solnica-Krezel⁶, John P. Kanki¹, Keith L. Ligon³, Jonathan A. Epstein^{2,¶} and A. Thomas Look^{1,¶}

SUMMARY

Neurofibromatosis type 1 (NF1) is a common, dominantly inherited genetic disorder that results from mutations in the *neurofibromin 1 (NF1)* gene. Affected individuals demonstrate abnormalities in neural-crest-derived tissues that include hyperpigmented skin lesions and benign peripheral nerve sheath tumors. NF1 patients also have a predisposition to malignancies including juvenile myelomonocytic leukemia (JMML), optic glioma, glioblastoma, schwannoma and malignant peripheral nerve sheath tumors (MPNSTs). In an effort to better define the molecular and cellular determinants of NF1 disease pathogenesis in vivo, we employed targeted mutagenesis strategies to generate zebrafish harboring stable germline mutations in *nf1a* and *nf1b*, orthologues of *NF1*. Animals homozygous for loss-of-function alleles of *nf1a* or *nf1b* alone are phenotypically normal and viable. Homozygous loss of both alleles in combination generates larval phenotypes that resemble aspects of the human disease and results in larval lethality between 7 and 10 days post fertilization. *nf1*-null larvae demonstrate significant central and peripheral nervous system defects. These include aberrant proliferation and differentiation of oligodendrocyte progenitor cells (OPCs), dysmorphic myelin sheaths and hyperplasia of Schwann cells. Loss of *nf1* contributes to tumorigenesis as demonstrated by an accelerated onset and increased penetrance of high-grade gliomas and MPNSTs in adult *nf1a*^{+/-}; *nf1b*^{-/-}; *p53*^{z7/e7} animals. *nf1*-null larvae also demonstrate significant motor and learning defects. Importantly, we identify and quantitatively analyze a novel melanophore phenotype in *nf1*-null larvae, providing the first animal model of the pathognomonic pigmentation lesions of NF1. Together, these findings support a role for *nf1a* and *nf1b* as potent tumor suppressor genes that also function in the development of both central and peripheral glial cells as well as melanophores in zebrafish.

INTRODUCTION

Type 1 neurofibromatosis (NF1) is an autosomal dominant inherited genetic disorder characterized by pigmented birthmarks known as café-au-lait spots, cutaneous and plexiform

neurofibromas arising in the glial cells of the peripheral nervous system (PNS), optic pathway gliomas, cardiovascular abnormalities and learning defects (Williams et al., 2009). The disease results from mutations in the *NF1* gene, encoding the large protein neurofibromin, which contains a GTPase-activating protein-related domain (GRD) capable of inactivating the *RAS* proto-oncogene (Cawthon et al., 1990; Viskochil et al., 1990; Wallace et al., 1990). Thus, *NF1* loss results in aberrant activation of Ras signaling, which may predispose NF1 patients to a variety of cancers (Cichowski and Jacks, 2001). Heterozygous *Nf1* mutant mice develop pheochromocytoma and myeloid leukemia, whereas the conditional loss of *Nf1* in a *p53*-deficient background results in highly penetrant malignant astrocytoma formation (Jacks et al., 1994; Zhu et al., 2005a; Powers et al., 2007). Furthermore, two recent reports have identified *NF1* mutations in approximately 15-23% of human glioblastoma patients (Parsons et al., 2008; The Cancer Genome Atlas Research Network, 2008). Although these studies demonstrate a strong link between *NF1* function and high-grade glioma, the crucial signaling pathways governing the development of tumorigenesis remain to be elucidated. An animal model facilitating the rapid interrogation of epistatic and functional relationships within signaling pathways would serve as a valuable tool for probing the pathology underlying NF1-induced cell transformation.

We recently developed a zebrafish model of *NF1* deficiency using antisense morpholino oligonucleotides to produce transient gene knockdown (Padmanabhan et al., 2009; Lee et al., 2010). Two

¹Department of Pediatric Oncology, Dana-Farber Cancer Institute, and Children's Hospital Boston, Harvard Medical School, Boston, MA 02115, USA

²Department of Cell and Developmental Biology, Penn Cardiovascular Institute, and the Institute for Regenerative Medicine, Perelman School of Medicine at the University of Pennsylvania, Philadelphia, PA 19104, USA

³Department of Medical Oncology, Center for Molecular Oncologic Pathology, Dana-Farber Cancer Institute, Harvard Medical School, Boston, MA 02215, USA

⁴Program in Gene Function and Expression, University of Massachusetts Medical School, Worcester, MA 06105, USA

⁵Department of Neurology, Vanderbilt University School of Medicine, Nashville, TN 37232, USA

⁶Department of Developmental Biology, Washington University School of Medicine in St Louis, St Louis, MO 63110, USA

*Present address: Department of Developmental Biology, Washington University School of Medicine in St Louis, St Louis, MO 63110, USA

‡These authors contributed equally to this work

§Present address: Aging Research Center, Korea Research Institute of Bioscience and Biotechnology, Daejeon 305-806, Korea

¶Authors for correspondence (epsteinj@mail.med.upenn.edu; thomas_look@dfci.harvard.edu)

Received 2 March 2012; Accepted 14 May 2012

© 2012. Published by The Company of Biologists Ltd
This is an Open Access article distributed under the terms of the Creative Commons Attribution Non-Commercial Share Alike License (<http://creativecommons.org/licenses/by-nc-sa/3.0/>), which permits unrestricted non-commercial use, distribution and reproduction in any medium provided that the original work is properly cited and all further distributions of the work or adaptation are subject to the same Creative Commons License terms.

zebrafish orthologues were identified that are highly homologous to human *NF1* at the amino acid level, sharing approximately 84% identity, including 91-93% identity within the GRD. Both genes maintain syntenic relationships with human *NF1* on chromosome 17q11.2 and are probably the result of the well-described genomic duplication event that occurred early in the evolution of teleosts (Amores et al., 1998). In our previous work with *nf1* morphants, we observed defects in both cardiovascular and nervous system development. However, due to the transient nature of morpholino gene knockdown, the analysis of *nf1*-deficient phenotypes beyond the first 3 days of life was not possible.

We report here the generation of stable mutant *nf1* zebrafish lines, using both zinc finger nuclease (ZFN) and targeting induced local lesions in genomes (TILLING) strategies, and the detailed phenotypic analysis of this new animal model of human NF1. We have successfully generated several independent null alleles of *nf1a* and *nf1b*. Mutant larvae carrying at least one wild-type *nf1a* or *nf1b* allele are viable, fertile and show no obvious phenotypes during early development. By contrast, *nf1a*^{-/-}; *nf1b*^{-/-} larvae exhibit overt pigmentation defects as early as 6 days post fertilization (dpf) and do not survive beyond 10 dpf. Beginning at 4 dpf, *nf1a*^{-/-}; *nf1b*^{-/-} larvae exhibit hyperplasia of oligodendrocyte progenitor cells (OPCs) and Schwann cells, as well as melanophore hypoplasia. Defects resulting from the loss of *nf1* in pigment cell and glial cell lineages mirror those often observed in the tissues of NF1 patients. In a *p53* mutant background (*p53*^{e7/e7}), *nf1a*^{+/-}; *nf1b*^{-/-} fish develop high-grade gliomas and malignant peripheral nerve sheath tumors (MPNSTs), demonstrating a tumor-suppressor function for the zebrafish *nf1* orthologues. Therefore, we have developed and characterized a heritable zebrafish model of NF1 that exhibits clinical hallmarks of the disorder, including nervous system defects and increased susceptibility to tumorigenesis. Furthermore, *nf1* mutant zebrafish represent the first vertebrate model of the pathognomonic pigmentation lesions associated with NF1.

RESULTS

Generation of zebrafish *nf1a* and *nf1b* mutants

We previously identified two zebrafish orthologues of human *NF1*, *nf1a* and *nf1b*, and described the phenotypes that result from their loss of function during early development induced by antisense morpholino oligonucleotides (Padmanabhan et al., 2009; Lee et al., 2010). Although this technology readily permits transient knockdown of gene expression, its efficacy is limited to only the first few days of life. In an effort to gain a better understanding of the roles of *nf1a* and *nf1b* during development, as well as in cancer predisposition, we employed multiple approaches to develop stable lines of zebrafish harboring germline mutations in each of these genes. Using a modular approach (Zhu et al., 2011), zinc finger nucleases (ZFNs) were engineered with binding specificities directed to exon 26 of *nf1a* and exon 17 of *nf1b* (Fig. 1A,B). Paired ZFN mRNAs were injected into zebrafish embryos and independent target-specific mutant alleles for *nf1a* (*nf1a*^{Δ5} and *nf1a*^{Δ8}) and *nf1b* (*nf1b*⁺¹⁰ and *nf1b*^{Δ55}) were identified in the F1 generation (Fig. 1C; supplementary material Fig. S1A-D). Each of these mutations included a deletion and/or insertion within a coding exon that resulted in a frameshift, introducing premature stop codons that would be expected to truncate the neurofibromin protein upstream of the GRD (Fig. 1D,E). In a separate effort, we screened a library

of *N*-ethyl-*N*-nitrosourea (ENU)-mutagenized zebrafish by targeting induced local lesions in genomes (TILLING) (Wienholds et al., 2002) and identified a single founder harboring a nonsense mutation in exon 29 of *nf1a* (*nf1a*^{L1247X}) (Fig. 1C; supplementary material Fig. S1E-G). To confirm that the targeted alleles disrupted production of full-length protein, we performed western blots using an antibody that should recognize both *nf1a* and *nf1b* with extracts prepared from 3 dpf wild-type, *nf1a*^{Δ5/Δ5}; *nf1b*^{+/+}, *nf1a*^{+/+}; *nf1b*^{+10/+10} and *nf1a*^{Δ5/Δ5}; *nf1b*^{+10/+10} larvae (Fig. 1F). We observed a complete loss of Nf1 signal in the double-homozygous null extracts. We detected only low levels of protein expression in *nf1a*^{Δ5/Δ5}; *nf1b*^{+/+} mutant extracts as compared with wild-type or *nf1a*^{+/+}; *nf1b*^{+10/+10} mutant extracts, which might reflect differences in expression levels of the two orthologues at 3 dpf. However, we cannot rule out the possibility that the neurofibromin antibody we used recognizes the two proteins with different affinities. We generated separate zebrafish lines with distinct null alleles of both *nf1a* and *nf1b* to provide evidence that the observed phenotypes were in fact due to *nf1* loss and did not involve any spurious passenger mutations specific to the isolation of any individual *nf1* mutant line (supplementary material Fig. S2). Because our data indicate that these various null alleles are equivalent, we refer to them without individual allelic designations henceforth (*nf1a*^{-/-} and *nf1b*^{-/-}).

Mutants carrying at least one wild-type allele of either *nf1a* or *nf1b* are viable and fertile. However, when crossing parental genotypes that would be expected to yield *nf1a*^{-/-}; *nf1b*^{-/-} progeny, none were observed in the adult population. To investigate this further, we performed quantitative survival studies. At 7 dpf, *nf1a*^{-/-}; *nf1b*^{-/-} larvae began to die, with none surviving beyond 10 dpf, although 100% of wild-type larvae survived to 10 dpf (Fig. 1G). Furthermore, 100% survival at 10 dpf was also observed in *nf1a*^{-/-}; *nf1b*^{+/+} (*n*=26), *nf1a*^{+/+}; *nf1b*^{-/-} (*n*=22), *nf1a*^{-/-}; *nf1b*^{+/-} (*n*=28) and *nf1a*^{+/-}; *nf1b*^{-/-} (*n*=24) larvae. The swim bladders of *nf1a*^{-/-}; *nf1b*^{-/-} larvae were frequently observed to be underinflated. However, *nf1a*^{-/-}; *nf1b*^{-/-} larvae maintained the ability to both consume and transit live paramecia, suggesting that premature death was not the result of starvation (supplementary material Fig. S3). Additionally, an incompletely penetrant valvular insufficiency phenotype was appreciated in *nf1a*^{-/-}; *nf1b*^{-/-} larvae, as well as in those harboring only a single wild-type *nf1* allele (*nf1a*^{+/-}; *nf1b*^{-/-} and *nf1a*^{-/-}; *nf1b*^{+/-}) (supplementary material Movies 1-3).

OPC and Schwann cell hyperplasia in *nf1a*^{-/-}; *nf1b*^{-/-} larvae

We previously described OPC hyperplasia after *nf1a* and *nf1b* morpholino knockdown in the context of a homozygous *p53* mutant background (Lee et al., 2010). To examine *nf1a* and *nf1b* function in OPCs and other tissues beyond the first few days of life, we crossed several cell-type-specific zebrafish reporter lines into *nf1a/nf1b* mutant backgrounds. At 2 dpf, *olig2* expression appeared normal in Tg(*olig2:GFP*); *nf1a*^{-/-}; *nf1b*^{-/-} embryos, as assessed by both whole-mount in situ hybridization analysis of endogenous *olig2* mRNA expression and GFP expression (supplementary material Fig. S4A-D). We also evaluated *nf1* loss in Tg(*sox10:GFP*) embryos. This transgene drives GFP expression in specified ventral spinal cord OPCs, but not the neighboring motoneurons that arise from a common progenitor cell, as well as in Schwann cells of the posterior lateral line nerve (PLLn). At 2 dpf, similar numbers of *sox10:GFP*-positive OPCs were detected

in the dorsal and ventral spinal cord of wild-type and *nf1a*^{-/-}; *nf1b*^{-/-} embryos (supplementary material Fig. S4E,F). Examination of *nf1*-null PNS Schwann cells at 2 dpf showed no effect on the number of *sox10*:GFP-expressing cells associated with the PLLN,

which innervate skin mechanosensory neuromast cells (supplementary material Fig. S4G,H).

However, *nf1a*^{-/-}; *nf1b*^{-/-} larvae exhibited increased numbers of OPCs at 4 dpf compared with controls, as evidenced by an excess

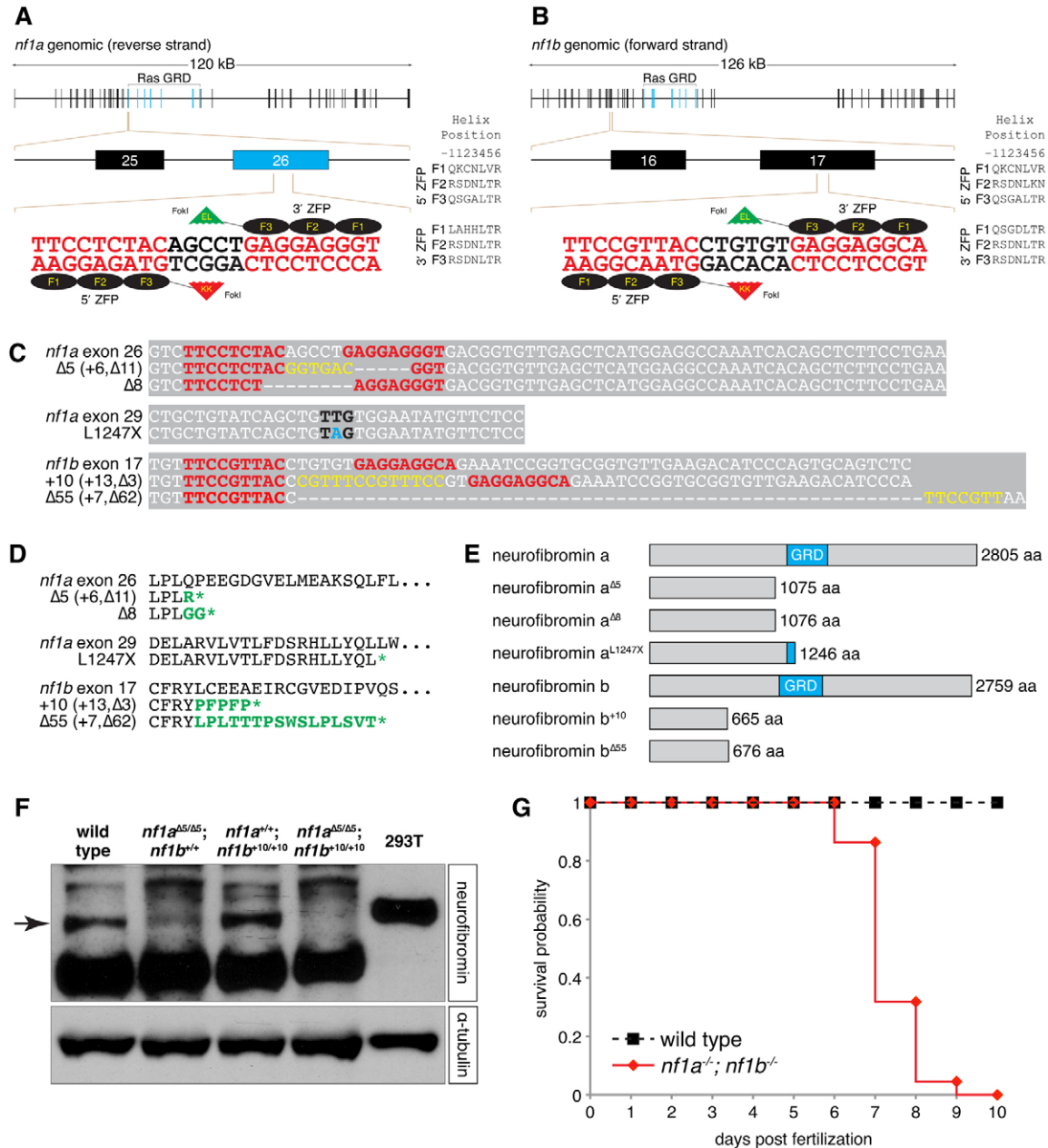


Fig. 1. ZFN and TILLING strategies generate null alleles of zebrafish *nf1a* and *nf1b*. (A,B) Scheme of site targeted for ZFN-mediated cleavage in exon 26 of *nf1a* and exon 17 of *nf1b*. (C) Alignments of nucleotide sequences from wild-type and mutant *nf1a* and *nf1b* alleles. ZFN target sites appear in red. Yellow bases represent insertions that arise from repair of ZFN-induced mutagenic lesions. Black bases correspond to the mutated codon in the *nf1a*^{L1247X} allele generated by a TILLING strategy, with the mutated base appearing in blue. (D) ZFN-induced mutagenic lesions in *nf1a* and *nf1b* produce frameshift mutations that lead to truncated protein products following short regions of altered translation, which are indicated in green. The nonsense mutation in the *nf1a*^{L1247X} allele generated by a TILLING strategy also appears in green. (E) The truncated protein products predicted by the ZFN- and TILLING-induced mutant *nf1a/nf1b* alleles all harbor complete or partial loss of the neurofibromin GAP-related domain (GRD). (F) Western blot analysis for neurofibromin in protein lysates from 3 dpf wild-type, *nf1a*^{Δ5/Δ5}; *nf1b*^{+10/+10}, *nf1a*^{+10/+10}; *nf1b*^{+10/+10} and *nf1a*^{Δ5/Δ5}; *nf1b*^{+10/+10} zebrafish larvae (100 μg each) or 293T cells (25 μg) demonstrates absence of Nf1 protein in *nf1a*^{-/-}; *nf1b*^{-/-} larvae. Equal loading was confirmed by stripping the membrane and reprobing for α-tubulin. (G) Kaplan-Meier survival analysis demonstrates that 100% of *nf1a*^{-/-}; *nf1b*^{-/-} larvae (*n*=22) die by 10 dpf as compared with 0% of wild-type larvae (*n*=27).

of dorsally migrated *olig2*:GFP-positive OPCs (Fig. 2A,B) along with increased numbers of both dorsally and ventrally positioned *sox10*:GFP-positive OPCs (Fig. 2C,D), consistent with our analyses of *nf1* morphants at 3 dpf (Lee et al., 2010). In addition, we observed an increase in *sox10*:GFP-positive Schwann cells associated with the PLLn (Fig. 2E,F). This increase in PLLn Schwann cell number was not associated with altered proliferation of these cells (supplementary material Fig. S5A-F). To assess the roles of *nf1a* and *nf1b* in the developing radial glial cells of the spinal cord, *nf1a/nf1b* mutants were crossed into the Tg(*gfap*:GFP) line, which expresses GFP from the glial fibrillary acidic protein (*gfap*) promoter. At 4 dpf, *nf1a*^{-/-}; *nf1b*^{-/-} larvae harboring a *gfap*:GFP transgene demonstrated no readily discernible differences in *gfap*:GFP-positive spinal cord radial glial cells as compared with wild-type larvae (supplementary material Fig. S4I,J). However, *gfap* expression in the extensive processes of radial glial cells precludes precise quantification and might obscure subtle differences.

To determine whether neuronal numbers increased in concert with OPCs in *nf1a/nf1b* mutant larvae, we used anti-HuC/D and anti-SOX10 antibodies (see Methods) to discriminate between *olig2*:GFP-positive neurons and OPCs, respectively. No difference between the number of *olig2*:GFP-positive and HuC/D-positive neurons was appreciable in 4 dpf spinal cord sections from wild-type and *nf1a*^{-/-}; *nf1b*^{-/-} larvae (Fig. 2G,H, green and magenta; Fig. 2K). However, the numbers of *olig2*:GFP-positive and Sox10-positive OPCs (Fig. 2G,H, arrowheads; Fig. 2L) and PLLn Schwann cells (Fig. 2I,J,M) were significantly increased at 4 dpf in *nf1a*^{-/-}; *nf1b*^{-/-} larvae relative to wild-type controls. OPC cell numbers continued to increase in *nf1a*^{-/-}; *nf1b*^{-/-} larvae at 8 dpf, as reflected by increased numbers of dorsally localizing *olig2*:GFP-positive OPCs as well as both dorsally and ventrally localizing *sox10*:GFP-positive OPCs (supplementary material Fig. S4M-P). Increased numbers of *sox10*:GFP-expressing PLLn Schwann cells were also evident in *nf1a*^{-/-}; *nf1b*^{-/-} larvae at 8 dpf (supplementary material Fig. S4Q,R). Thus, loss of *nf1a* and *nf1b* does not affect the specification of OPCs at 2 dpf, but instead promotes the progressive expansion of OPCs without a concomitant increase in neuronal cell numbers. Furthermore, *nf1a/nf1b* loss triggers Schwann cell hyperplasia beginning at 4 dpf.

Immunohistochemical analysis using the Zrf1 antibody, which labels Gfap in zebrafish, showed coexpression with GFP expressed from the *gfap*:GFP transgene and revealed a similar pattern of expression in wild-type and *nf1a*^{-/-}; *nf1b*^{-/-} larvae at 4 dpf (supplementary material Fig. S6A,B). Zebrafish radial glial cells also express brain lipid-binding protein (Blbp), and immunohistochemical analysis of wild-type and *nf1a*^{-/-}; *nf1b*^{-/-} spinal cords with an anti-BLBP antibody at 4 dpf revealed an obvious decrease in Blbp expression in the *gfap*:GFP-positive radial glia of *nf1a*^{-/-}; *nf1b*^{-/-} larvae (supplementary material Fig. S6C,D). These results suggest that although *gfap*:GFP-positive radial glial cells in *nf1a*^{-/-}; *nf1b*^{-/-} larvae appear normal in number, they fail to express appropriate levels of Blbp indicating a defect in gliogenesis. An additional abnormality of gliogenesis was observed at 8 dpf as a disruption in the regular segmental pattern of glial process outgrowth in Tg(*gfap*:GFP); *nf1a*^{-/-}; *nf1b*^{-/-} larvae (supplementary material Fig. S4K,L).

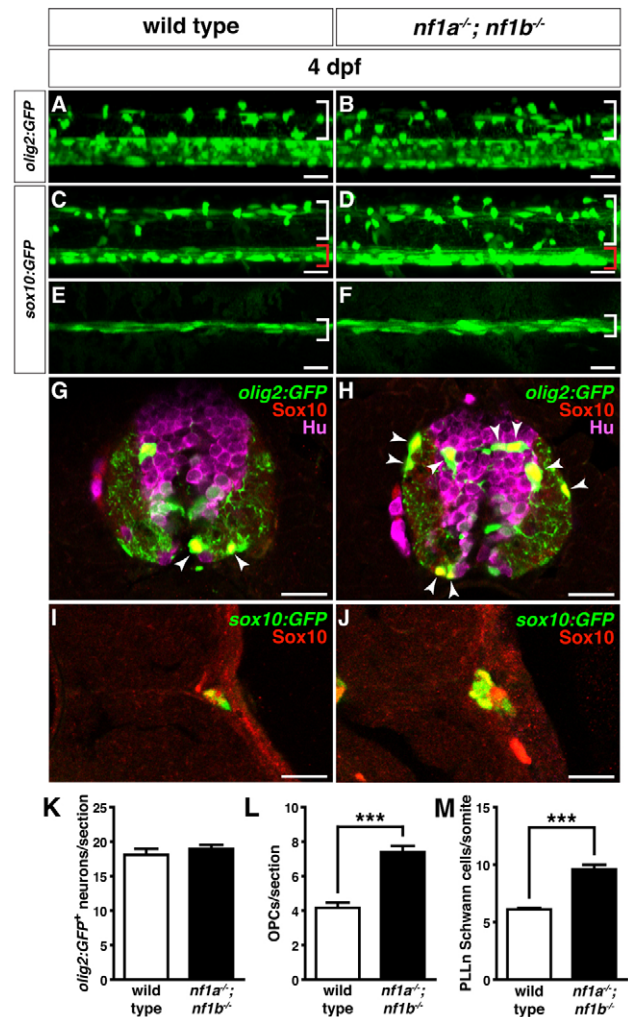


Fig. 2. Loss of *nf1a* and *nf1b* causes hyperplasia of OPCs and Schwann cells. (A,B) Confocal images of spinal cords in *nf1a*^{-/-}; *nf1b*^{-/-}; Tg(*olig2*:GFP) larvae (B) demonstrate increased numbers of dorsally migrating (white brackets) *olig2*:GFP-positive OPCs as compared with wild-type; Tg(*olig2*:GFP) larvae (A) at 4 dpf. (C,D) Confocal images of spinal cord in *nf1a*^{-/-}; *nf1b*^{-/-}; Tg(*sox10*:GFP) larvae (D) demonstrate increased numbers of both dorsally (white brackets) and ventrally (red brackets) positioned *sox10*:GFP-positive OPCs as compared with wild-type; Tg(*sox10*:GFP) larvae (C) at 4 dpf. (E,F) *nf1a*^{-/-}; *nf1b*^{-/-}; Tg(*sox10*:GFP) larvae (F) show an increased number of *sox10*:GFP-positive Schwann cells associated with the peripheral lateral line nerve (PLLn; white brackets) as compared with wild-type; Tg(*sox10*:GFP) larvae (E) at 4 dpf. (G,H) Neuronal numbers (*olig2*:GFP- [green], HuC/D- [magenta] positive) do not increase in concert with OPCs (*olig2*:GFP- [green], Sox10- [red] positive; arrowheads) in transverse sections through the spinal cord of *nf1a*^{-/-}; *nf1b*^{-/-}; Tg(*olig2*:GFP) larvae (H) as compared with wild-type; Tg(*olig2*:GFP) larvae (G) at 4 dpf. (I,J) Increased numbers of PLLn Schwann cells (*sox10*:GFP- [green], Sox10- [red] positive) are appreciated in transverse sections of *nf1a*^{-/-}; *nf1b*^{-/-}; Tg(*sox10*:GFP) larvae (J) as compared with wild-type; Tg(*sox10*:GFP) larvae (I) at 4 dpf. (K,L) Quantification of neurons (*olig2*:GFP-, HuC/D-positive cells) (K) and OPCs (*olig2*:GFP-, Sox10-positive cells) (L) from transverse sections through the spinal cord of wild-type; Tg(*olig2*:GFP) and *nf1a*^{-/-}; *nf1b*^{-/-}; Tg(*olig2*:GFP) larvae at 4 dpf. Values indicate mean + s.e.m. per section ($n=30$ from five each of wild-type and *nf1a*^{-/-}; *nf1b*^{-/-} larvae). (M) Quantification of *sox10*:GFP-positive Schwann cells in the PLLn of wild-type; Tg(*sox10*:GFP) and *nf1a*^{-/-}; *nf1b*^{-/-}; Tg(*sox10*:GFP) larvae at 4 dpf. Values indicate mean + s.e.m. per hemisegment ($n=5$ each for wild-type and *nf1a*^{-/-}; *nf1b*^{-/-} larvae). *** $P<0.001$. Scale bars: 20 μ m.

OPC hyperplasia in *nf1a*^{-/-}; *nf1b*^{-/-} larvae results from increased proliferation

In *nf1a*^{-/-}; *nf1b*^{-/-} larvae, OPC numbers were increased relative to control animals at 4 dpf, but not at 2 dpf, suggesting that *nf1*-null OPCs might proliferate faster during this time period. We assessed OPC proliferation by labeling larvae with BrdU for 12 hours starting at 3.5, 4.5 and 5.5 dpf followed by immunohistochemical analysis of transverse sections through the spinal cord. By 4 dpf and continuing through 6 dpf, the number of *olig2*:GFP-positive and Sox10-positive OPCs in *nf1*-null larvae was significantly increased in comparison with wild-type controls (Fig. 3A-H, arrows; Fig. 3I). Mutant larvae further exhibited significantly increased numbers of *olig2*:GFP⁻, Sox10⁻ and BrdU-positive OPCs at 4 and 5 dpf as compared with controls, indicating that neurofibromin normally suppresses the proliferation of OPCs during this period of development (Fig. 3A-H, arrowheads; Fig. 3J). There was little detectable BrdU incorporation at 6 dpf in either mutant or control populations.

Myelination is aberrant in *nf1a*^{-/-}; *nf1b*^{-/-} larvae

We evaluated the ability of *nf1a*^{-/-}; *nf1b*^{-/-} OPCs to differentiate appropriately by examining the gene expression levels of proteolipid protein 1a (*plp1a*) and myelin basic protein (*mbp*), markers of differentiated oligodendrocytes, in wild-type and mutant larvae at 5 dpf. In *nf1*-null larvae, fewer *plp1a*-positive cells were detected in the midbrain and hindbrain regions (Fig. 4A,B) as well as along the dorsal and ventral spinal cords (Fig. 4C,D) as compared with controls. Central nervous system (CNS)

expression of *mbp*, on the other hand, was indistinguishable between wild-type and *nf1a*^{-/-}; *nf1b*^{-/-} larvae at 5 dpf (supplementary material Fig. S7). However, *mbp* expression was elevated in Schwann cells of the PLLn in *nf1a*^{-/-}; *nf1b*^{-/-} larvae as compared with controls (Fig. 4E,F, arrowheads). These data are consistent with perturbed oligodendrocyte differentiation in the CNS as well as in PNS Schwann cells associated with the PLLn of *nf1a*^{-/-}; *nf1b*^{-/-} larvae.

We went on to examine the ultrastructure of myelinated CNS axons in control and *nf1*-null larvae by transmission electron microscopy (TEM). At 8 dpf, oligodendritic myelin sheaths were tightly wrapped around CNS axons in the ventral spinal cord of wild-type larvae (Fig. 4G,I). By contrast, *nf1a*^{-/-}; *nf1b*^{-/-} axons were loosely encircled by multiple lamellae rather than by compact myelin sheaths, indicating that neurofibromin is required for the normal formation of the concentric layers of oligodendrocyte membranes that enwrap neuronal axons of the CNS to promote neural conduction (Fig. 4H,J).

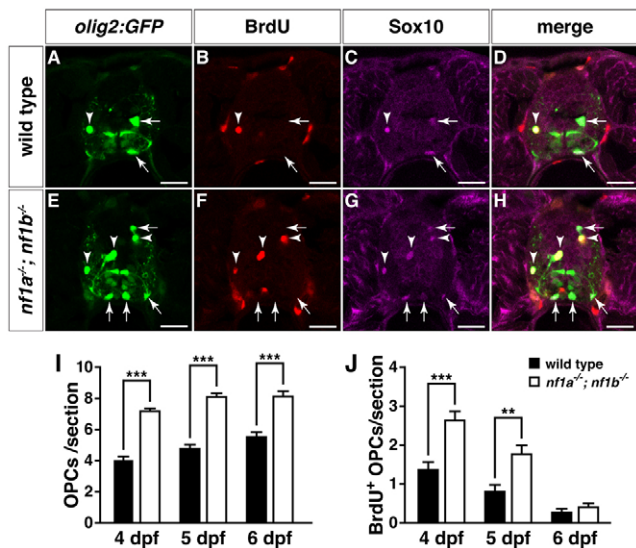


Fig. 3. Increased proliferation drives OPC hyperplasia in *nf1a*^{-/-}; *nf1b*^{-/-} larvae. (A-H) Transverse spinal cord sections of wild-type; Tg(*olig2*:GFP) (A-D) and *nf1a*^{-/-}; *nf1b*^{-/-}; Tg(*olig2*:GFP) larvae (E-H) labeled with anti-BrdU antibody (B,F, red) or anti-SOX10 antibody (C,G, magenta) at 4 dpf. Arrows indicate BrdU-negative, Tg(*olig2*:GFP)⁻, Sox10-positive OPCs. Arrowheads indicate BrdU-positive, Tg(*olig2*:GFP)⁻, Sox10-positive OPCs. (I,J) Quantification of total (I) and BrdU-positive OPCs (J) from transverse spinal cord sections of wild-type; Tg(*olig2*:GFP) and *nf1a*^{-/-}; *nf1b*^{-/-}; Tg(*olig2*:GFP) larvae at 4, 5 and 6 dpf. Values indicate mean + s.e.m. per section ($n=30$ from five each of wild-type and *nf1a*^{-/-}; *nf1b*^{-/-} larvae). *** $P<0.01$; **** $P<0.001$. Scale bars: 20 μ m.

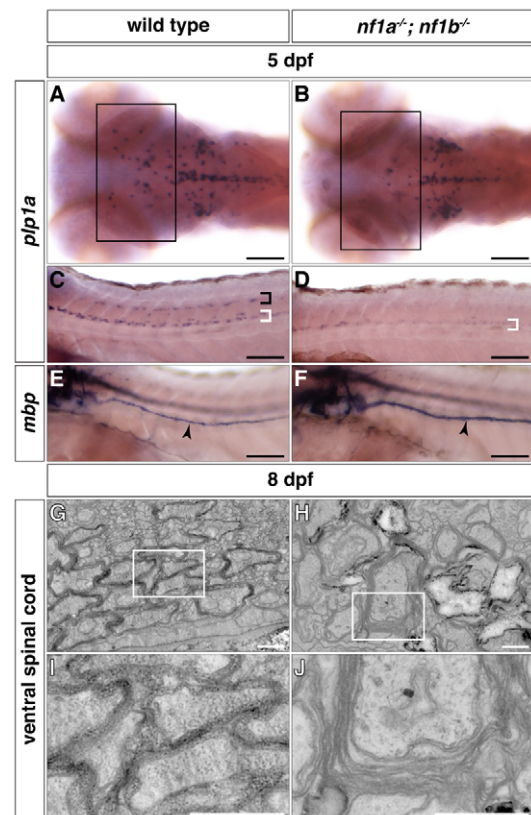


Fig. 4. *nf1a*^{-/-}; *nf1b*^{-/-} larvae exhibit myelination defects. (A-D) *plp1a* expression is decreased in glial cells of the midbrain and hindbrain regions (A,B, boxes) as well as the dorsal (black bracket) and ventral (white brackets) spinal cord of *nf1a*^{-/-}; *nf1b*^{-/-} larvae (B,D) as compared to wild-type larvae (A,C) by whole-mount in situ hybridization at 5 dpf. (E,F) *mbp* expression is elevated in Schwann cells of the PLLn (arrowheads) of *nf1a*^{-/-}; *nf1b*^{-/-} larvae (F) as compared to wild-type larvae (E) by whole-mount in situ hybridization at 5 dpf. (G-J) Transverse sections through the ventral spinal cord *nf1a*^{-/-}; *nf1b*^{-/-} larvae (H, boxed region magnified in J) demonstrate defects in formation of compact myelin sheaths as compared with wild-type larvae (G, boxed region magnified in I) at 8 dpf. Scale bars: 100 μ m (A-F) and 0.5 μ m (G-J).

Loss of *nf1a* and *nf1b* causes upregulation of Ras signaling in the spinal cord

Given the well-described role of neurofibromin as a negative regulator of Ras, we hypothesized that *nf1* loss in our mutants would lead to activation of downstream effector pathways. Western blot analysis of whole larvae extracts revealed an upregulation of phosphorylated ERK1 and ERK2 (pERK1/2) in *nf1a*^{-/-}; *nf1b*^{-/-} larvae at 3 dpf, whereas levels in *nf1a*^{-/-}; *nf1b*^{+/+} and *nf1a*^{+/-}; *nf1b*^{-/-} larvae remained unchanged (Fig. 5A). These data are consistent with the absence of functioning neurofibromin protein in *nf1a*^{-/-}; *nf1b*^{-/-} larvae and support functional redundancy between *nf1a* and *nf1b*. We next assessed the activation of Ras effector pathways in the spinal cords of wild-type, *nf1a*^{+/-}; *nf1b*^{-/-}, *nf1a*^{-/-}; *nf1b*^{+/+} and *nf1a*^{-/-}; *nf1b*^{-/-} animals by immunohistochemical analysis of transverse larval sections. Antibodies directed against HuC/D, pERK1/2, and phosphorylated S6 (pS6) were used to label neurons and assess activation of ERK and mTOR signaling pathways, respectively (Fig. 5B-Q). Although pERK1/2 staining was only minimally observed in a few neurons and portions of spinal cord white matter at 4 dpf in wild-type larvae (Fig. 5B,N), a striking upregulation of pERK1/2 was detected in *nf1a*^{-/-}; *nf1b*^{-/-} larvae (Fig. 5E,Q). Increased ERK signaling was also noted at 3 dpf in spinal cord neurons and white matter of *nf1a*^{-/-}; *nf1b*^{-/-} larvae, but was absent at 2 dpf (supplementary material Fig. S8). Although pS6 signaling was evident in multiple spinal cord neurons, we observed no differences in these cells between wild-type and *nf1* mutant animals at 2, 3 or 4 dpf (supplementary material Fig. S8Ae-Ah, Be-Bh; Fig. 5F-I). These data suggest that activation of mTOR signaling (as assessed by S6 phosphorylation) is not altered, at least in the spinal cord following *nf1* loss.

nf1 and *p53* cooperate to accelerate zebrafish tumorigenesis in vivo

Mammalian *NF1* has been shown to be a potent tumor suppressor; however, we did not identify any tumors over 18 months of observation in adult zebrafish homozygous for either mutant *nf1* allele alone (*nf1a*^{-/-}; *nf1b*^{+/+} or *nf1a*^{+/-}; *nf1b*^{-/-}) or in combination with heterozygous loss of the remaining allele (*nf1a*^{+/-}; *nf1b*^{-/-} or *nf1a*^{-/-}; *nf1b*^{+/-}). Loss of p53 has been shown to cooperate with NF1 (Cichowski et al., 1999; Vogel et al., 1999) as well as other mutations that activate Ras signaling (Eliyahu et al., 1984; Parada et al., 1984; Kemp et al., 1994; Tanaka et al., 1994; Hundley et al., 1997) in mammalian tumorigenesis, so we next bred *p53* mutant zebrafish into an *nf1*-mutant background to generate *nf1a*^{+/-}; *nf1b*^{-/-}; *p53*^{e7/e7} fish. These animals were incrossed to derive *nf1a*^{+/+}; *nf1b*^{-/-}; *p53*^{e7/e7} and *nf1a*^{+/-}; *nf1b*^{-/-}; *p53*^{e7/e7} fish, which were subsequently monitored carefully for tumorigenesis. At 31 weeks post fertilization (wpf), *nf1a*^{+/-}; *nf1b*^{-/-}; *p53*^{e7/e7} fish began to develop tumors with high penetrance although only one *nf1a*^{+/+}; *nf1b*^{-/-}; *p53*^{e7/e7} fish developed a tumor at 44 wpf (Fig. 6A). At 45 wpf, tumor penetrance was higher in *nf1a*^{+/-}; *nf1b*^{-/-}; *p53*^{e7/e7} fish (24/39; 62%) than in *nf1a*^{+/+}; *nf1b*^{-/-}; *p53*^{e7/e7} fish (1/14; 7%). We have previously reported that *p53*^{e7/e7} fish with wild-type *nf1* alleles develop MPNSTs. These tumors did not begin to develop until 41 weeks of age, which was similar to the results with *nf1a*^{+/+}; *nf1b*^{-/-}; *p53*^{e7/e7} animals (Fig. 6A). Furthermore, the penetrance of tumors in *p53*-null animals was only 28% by 66 wpf (Berghmans et al., 2005). Thus, the combined loss of *p53* and 3 of 4 *nf1* alleles in

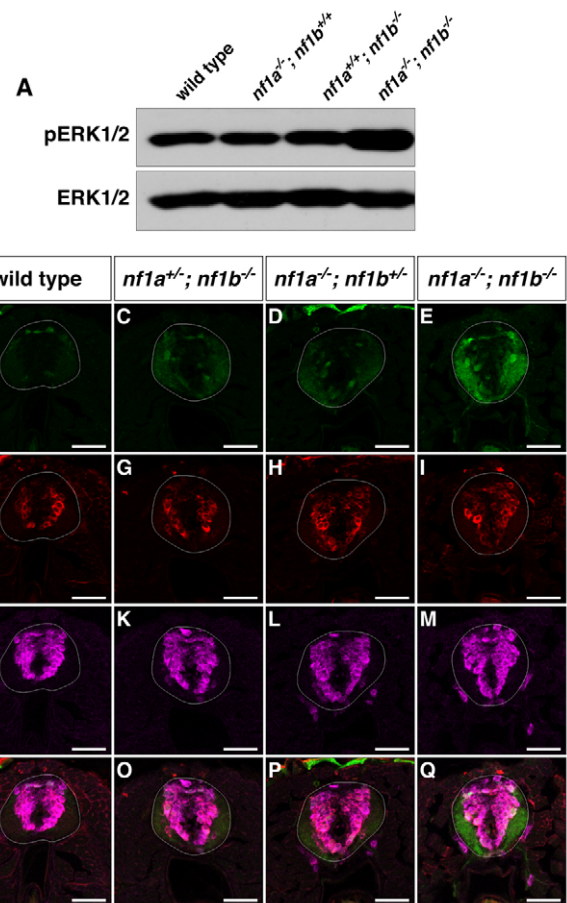


Fig. 5. *nf1a/nf1b* mutants exhibit upregulation of pERK1/2. (A) Western blot analysis for pERK1/2 in protein lysates prepared from wild-type, *nf1a*^{-/-}; *nf1b*^{+/+}, *nf1a*^{+/-}; *nf1b*^{-/-} and *nf1a*^{-/-}; *nf1b*^{-/-} larvae (100 µg) reveals increased pERK1/2 levels in *nf1a*^{-/-}; *nf1b*^{-/-} larvae as compared with wild-type, *nf1a*^{+/-}; *nf1b*^{+/+} and *nf1a*^{+/-}; *nf1b*^{-/-} larvae at 3 dpf. Equal loading was confirmed by stripping the membrane and reprobing for total ERK1/2. (B-Q) Transverse spinal cord sections of wild-type (B,F,J,N), *nf1a*^{+/-}; *nf1b*^{-/-} (C,G,K,O), *nf1a*^{-/-}; *nf1b*^{+/+} (D,H,L,P) and *nf1a*^{-/-}; *nf1b*^{-/-} (E,I,M,Q) larvae labeled with anti-pERK1/2 antibody (B-E, green), anti-pS6 antibody (F-I, red), or anti-HuC/D antibody (J-M, magenta) demonstrate marked upregulation of pERK1/2 in *nf1a*^{-/-}; *nf1b*^{-/-} larvae and intermediate levels of pERK1/2 in larvae harboring a single functioning *nf1* allele as compared with wild-type larvae at 4 dpf ($n=5$ each for wild-type and mutant larvae). Scale bars: 40 µm.

zebrafish markedly accelerates the onset and increases the penetrance of tumors as compared with the loss of *p53* alone or the concomitant loss of *p53* and both alleles of *nf1b*, but with intact *nf1a*.

Tumors in *nf1a*^{+/-}; *nf1b*^{-/-}; *p53*^{e7/e7} fish were observed in the brain ($n=2$), eye ($n=8$), gill ($n=1$), abdomen ($n=8$) and trunk ($n=5$). Brain tumors developed very early (31 and 33 wpf) (Fig. 6A, arrows) and demonstrated features of diffuse high-grade gliomas, whereas all other tumor types were most consistent with MPNSTs (Fig. 6B-G). Histopathologically, the brain tumors were highly cellular and composed of ovoid to rounded cells with marked nuclear pleomorphism and diffuse single cell infiltration of parenchyma, including pre-existing neurons (Fig. 7A-F). Occasional mitoses were

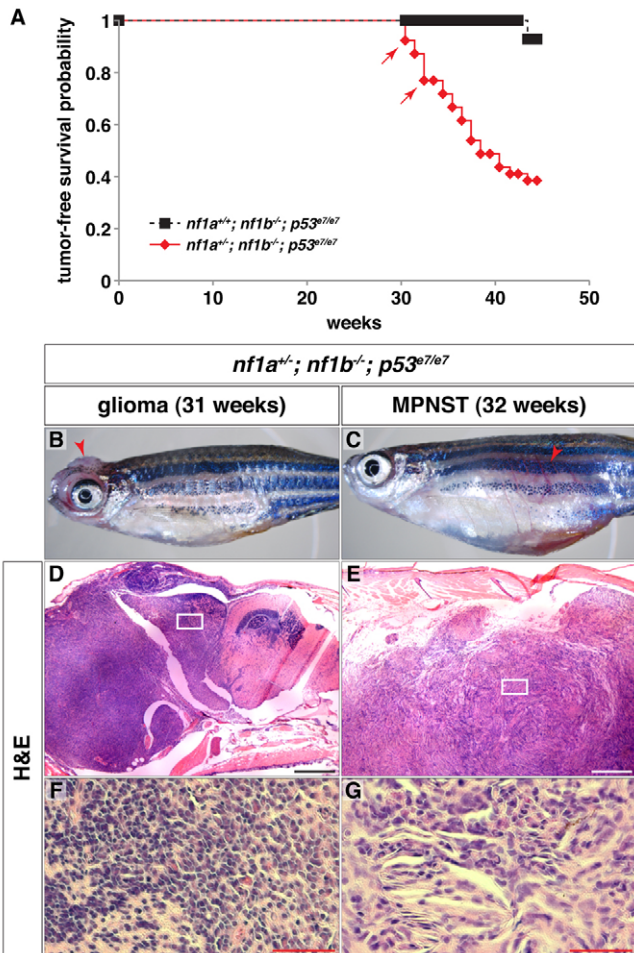


Fig. 6. *nf1a/nf1b* mutants demonstrate increased susceptibility to tumorigenesis in a *p53* mutant background. (A) Kaplan-Meier tumor-free survival analysis for *nf1a*^{+/+};*nf1b*^{-/-};*p53*^{e7/e7} (*n*=39) animals demonstrates significantly decreased survival as compared with *nf1a*^{+/+};*nf1b*^{-/-};*p53*^{e7/e7} (*n*=14) animals (*P*<0.001). Arrows indicate ages at which animals were identified with brain tumors demonstrating features of diffuse high-grade gliomas. (B,C) 31-week-old *nf1a*^{+/+};*nf1b*^{-/-};*p53*^{e7/e7} animal with a high-grade glioma (B, arrowhead) and 32-week-old *nf1a*^{+/+};*nf1b*^{-/-};*p53*^{e7/e7} animal with a malignant peripheral nerve sheath tumor (MPNST) (C, arrowhead). (D-G) H&E staining of sagittal sections through the high-grade optic glioma (D, boxed area magnified in F) or MPNST (E, boxed area magnified in G). Scale bars: 200 μ m (D,E) and 50 μ m (F,G).

identified, but no necrosis or vascular proliferation was detected (Fig. 7G-I). Assessment of tumor lineage by immunohistochemical analysis showed that approximately 80% of tumor cells stained positive for the oligodendroglial marker Sox10, with little staining in matched wild-type tissue (Fig. 7J-L). The presence of a Sox10-negative tumor cell subpopulation is consistent with the level of heterogeneity for oligodendroglial transcription factors, such as Sox10 and Olig2, and is characteristic of astrocytic or mixed gliomas as compared with pure oligodendroglial class tumors (Fig. 7K, arrowhead) (Ligon et al., 2004; Bannykh et al., 2006). Staining for the astrocytic marker Gfap (Fig. 7M-O) highlighted a subpopulation of cells within the tumor with coarse, irregular cytoplasmic

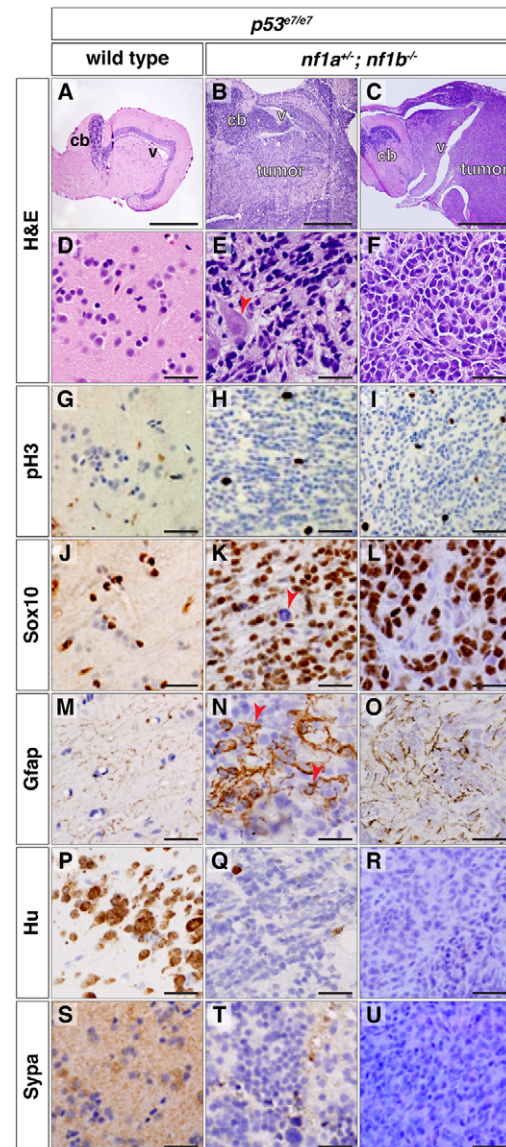


Fig. 7. Tumors from *nf1a*^{+/+};*nf1b*^{-/-};*p53*^{e7/e7} animals express glial markers. (A-F) H&E staining of sagittal sections through *p53*^{e7/e7} brain tissue (A,D) or brain tumors in *nf1a*^{+/+};*nf1b*^{-/-};*p53*^{e7/e7} animals at 31 (B,E) and 33 (C,F) wpf (cb, cerebellum; v, ventricle). The arrowhead in E shows infiltration of a single cell through the parenchyma and around normal neurons. (G-U) Immunohistochemical analyses for phosphorylated histone H3 (G-I, pH3), SRY-box 10 (J-L, Sox10), glial fibrillary acidic protein (M-O, Gfap), HuC/D (P-R, Hu) and synaptophysin (S-U, Sypa) on sagittal sections through *p53*^{e7/e7} brain tissue (G,J,M,P,S) or brain tumors in *nf1a*^{+/+};*nf1b*^{-/-};*p53*^{e7/e7} animals at 31 (H,K,N,Q,T) and 33 (I,L,O,R,U) wpf demonstrate occasional mitoses in tumor tissue (H,I) with most tumor cells staining positive for the oligodendroglial marker Sox10 (K,L), a Sox10-negative subpopulation (K, arrowhead), an astrocytic component (N, arrowheads and O) and the absence of mature neuronal markers HuC/D (Q,R) or synaptophysin (T,U). Scale bars: 450 μ m (A-C) and 20 μ m (D-U).

processes also consistent with the presence of an astrocytic lineage component (Fig. 7N, arrowheads). Tumor cells did not express the mature neuronal markers HuC/D or synaptophysin (Sypa), consistent with their glial origin (Fig. 7P-U).

Immunohistochemical analysis for pERK1/2 and pS6 to assess activation of ERK and mTOR signaling pathways, respectively (supplementary material Fig. S9A-F) revealed increased pERK1/2 staining in the more malignant of these two brain tumors, with normal amounts of pS6 (supplementary material Fig. S9C,D). The more hyperplastic brain tumor showed increased pERK1/2 and pS6 staining (supplementary material Fig. S9E,F). These data demonstrate that some, but not all, brain tumors in *nf1a*^{+/-}; *nf1b*^{-/-}; *p53*^{e7/e7} animals demonstrate hyperactivation of ERK and mTOR pathways, consistent with mouse and human *NF1*-derived MPNSTs and gliomas (Dasgupta et al., 2005; Zhu et al., 2005b). Collectively, these findings suggest that the tumors were high-grade gliomas most closely resembling human anaplastic astrocytoma or anaplastic oligoastrocytoma WHO grade III. Furthermore, MPNSTs (Fig. 6C,E,G) exhibited spindle-shaped tumor cells and extensive necrosis consistent with this tumor type (Ducatman et al., 1986; Wanebo et al., 1993; Hirose et al., 1998). Taken together, we conclude that *nf1a* and *nf1b* mutations cooperate with *p53* loss to generate high-grade gliomas and MPNSTs.

nf1a^{-/-}; *nf1b*^{-/-} larvae show motor and learning deficits

Deficits in motor coordination and cognition, including learning and memory, are characteristic of *NF1* patients and animal models. To examine motor behavior and cognition in *nf1a*^{-/-}; *nf1b*^{-/-} larvae, we performed kinematic analysis of the short-latency C-start (SLC), a highly stereotyped yet modifiable acoustic startle reflex in the zebrafish (Burgess and Granato, 2007a; Wolman et al., 2011). Unlike their siblings, *nf1a*^{-/-}; *nf1b*^{-/-} larvae showed a deficit in short-term SLC habituation when presented with repetitive acoustic stimulation (supplementary material Fig. S10A). Furthermore, *nf1a*^{-/-}; *nf1b*^{-/-} larvae performed kinematically weaker SLC responses, as indicated by decreased head turning angle, maximum angular velocity and distance traveled following delivery of an acoustic stimulus (supplementary material Fig. S10B-D). Taken together, these data support the hypothesis that *nf1a* and *nf1b* function redundantly during zebrafish development and that only one of the four wild-type *nf1* alleles is required for phenotypically normal embryonic development, motor behavior and cognition.

nf1 mutants exhibit melanophore defects

Notably, *nf1* null larvae displayed aberrant lateral stripe pigmentation as compared with wild-type controls at 6 dpf (Fig. 8A-D). This phenotype was first appreciable at 4 dpf and was manifested as a disruption in the uniform pattern of melanophores arranged along the lateral stripes (Fig. 8B,D, brackets). To further investigate this phenotype, we quantified melanophore numbers along the lateral stripes of 3 and 6 dpf wild-type and *nf1a*^{-/-}; *nf1b*^{-/-} larvae. No significant differences in the number of melanophores comprising the 3 dpf lateral stripes were appreciable in any combination of mutant *nf1* alleles as compared with sibling wild-type controls (supplementary material Fig. S11). However, at 6 dpf, *nf1a*^{-/-}; *nf1b*^{-/-} larvae exhibited a significant reduction in the number of lateral stripe melanophores (Fig. 8E). Less severe, but still significant, decreases were also noted in larvae carrying two or three mutant *nf1* alleles (Fig. 8E). No difference in the number of apoptotic cells between wild-type and mutant larvae was discernible at 3 dpf (68.1±11 cells/larva, *n*=12 wild-type versus

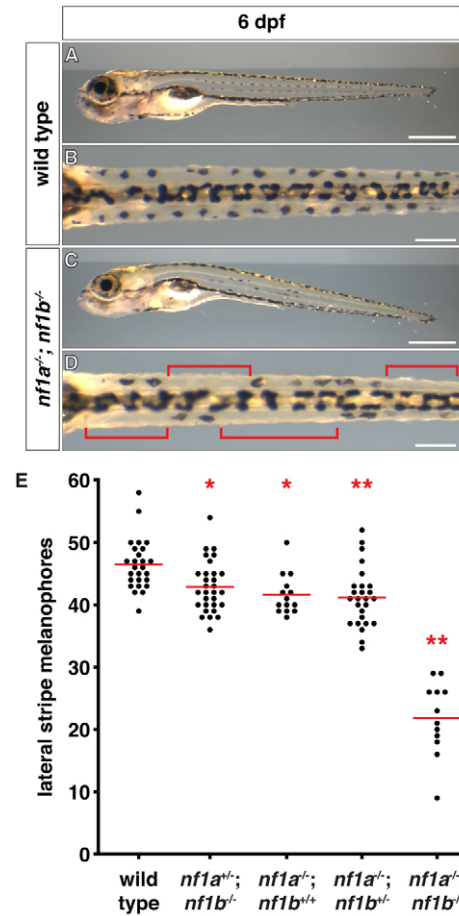


Fig. 8. *nf1* mutants display decreased lateral stripe melanophores.

(A-D) Lateral stripe melanophores of wild-type (A,B) larvae demonstrate a normal uniform pattern that is absent in *nf1a*^{-/-}; *nf1b*^{-/-} larvae (C,D) at 6 dpf. The brackets in D highlight regions where melanophores are absent. (E) Quantification of lateral stripe melanophores from wild-type (*n*=26), *nf1a*^{+/-}; *nf1b*^{-/-} (*n*=30), *nf1a*^{-/-}; *nf1b*^{+/-} (*n*=14), *nf1a*^{-/-}; *nf1b*^{-/-} (*n*=26) and *nf1a*^{-/-}; *nf1b*^{+/-} (*n*=12) larvae at 6 dpf. Each point represents the number of lateral stripe melanophores in an individual embryo and red lines indicate mean values. **P*<0.05, ***P*<0.01. Scale bars: 0.5 mm (A,C) and 150 μm (B,D).

63.8±8.5, *n*=12 mutants; *P*=0.27) (supplementary material Fig. S12A-F). Serial observation of melanophore development in individual *nf1a*^{-/-}; *nf1b*^{-/-} and wild-type larvae revealed a defect of migration or differentiation of regeneration and metamorphic lineage melanophores. At 3 dpf, a time point at which embryonic melanophore development is complete (Hultman et al., 2009), no difference in melanophore number along the lateral stripe was observed (supplementary material Fig. S13A,B,G), indicating that the melanophores develop normally in *nf1* mutants. To assess the regeneration and metamorphic lineage of melanophores, we suppressed melanin synthesis after 3 dpf by treatment with *N*-phenylthiourea (PTU) (Hultman and Johnson, 2010), which allowed us to identify newly formed melanophores by their melanin-negative and pale appearance (supplementary material Fig. S13C,D, red arrows). Removal of PTU at 5 dpf restored melanin synthesis and regeneration and metamorphic melanophores appeared

melanin-positive by 6 dpf (supplementary material Fig. S13E,F, black arrows). The abnormal appearance of the lateral stripes in mutant larvae can be attributed to defects in patterning of regeneration and metamorphic melanophores (supplementary material Fig. S13F,G, brackets), suggesting abnormal migration or differentiation of this lineage. Head melanophore numbers at 6 dpf were not significantly changed in *nf1* mutant larvae and sibling controls (supplementary material Fig. S14). Collectively, these data demonstrate a specific defect in lateral stripe melanophore numbers following *nf1* allele loss, most prominent in the setting of biallelic *nf1a/nf1b* loss. Each *nf1a*^{-/-}; *nf1b*^{-/-} larvae showed a unique pattern of lateral stripe melanophore loss, suggesting a stochastic defect in melanophore differentiation from neural crest, proliferation, migration or survival, rather than a defect specific to any particular somite of the developing embryo and larvae.

DISCUSSION

NF1 is a common tumor-predisposing, autosomal dominant genetic disorder characterized by café-au-lait macules and cutaneous neurofibromas. In addition to these pigmentation defects and tumors of the peripheral nervous system (PNS), NF1 patients demonstrate highly diversified clinical features with multiple tissue types affected. Prominent lesions include optic pathway gliomas, Lisch nodules, skeletal dysplasia, cardiovascular abnormalities, learning defects and various cancers such as leukemia and intestinal tumors (Side et al., 1997; Side et al., 1998; Bahuau et al., 2000; Andersson et al., 2005; Williams et al., 2009). It remains unclear how *NF1* mutations contribute to the diverse symptoms and tissue types affected in patients. Because neurofibromin is a very large protein that is highly conserved evolutionarily, it is likely to have activities related to functional domains other than those affecting Ras signaling. For example, in addition to Ras, neurofibromin can bind to microtubules, syndecan, phospholipids and amyloid precursor protein (Xu and Gutmann, 1997; Hsueh et al., 2001; D'Angelo et al., 2006; De Schepper et al., 2006). Intriguingly, recent studies indicate that neurofibromin might function as a positive regulator of adenylyl cyclase (Guo et al., 2000; Tong et al., 2002; Dasgupta et al., 2003). This function of neurofibromin modulates neuronal differentiation (Hegeudus et al., 2007), suggesting the possibility that cognitive defects in NF1 patients might be related to defects in cAMP signaling rather than activated Ras. Furthermore, the tremendous clinical variability in the phenotypic spectrum seen among families with the same molecular *NF1* lesion posits the role of unlinked modifier loci in regulating the expressivity of disease characteristics (Easton et al., 1993; Sabbagh et al., 2009). Nevertheless, the identification of specific modifier genes and the relative contributions of Ras signaling versus other neurofibromin-regulated pathways for specific phenotypes have yet to be fully elucidated. The zebrafish model that we have developed offers an attractive tool for furthering this analysis because it is amenable to small molecule screens, genetic modifier screens and genetic rescue experiments.

A hallmark feature of human NF1 is the presence of pigmentation defects known as café-au-lait spots. Little is known about the underlying mechanisms responsible for this abnormality, and pigmentation abnormalities in other animal models of NF1 have not been described. In this regard, it is of interest that zebrafish lacking neurofibromin exhibit abnormal patterning of the

melanophores that compose the lateral stripes, a phenotype similar to that following pharmacologic inhibition of the upstream Ras effector ErbB (Hultman et al., 2009; Hultman and Johnson, 2010). This easily observable and quantifiable phenotype offers the opportunity to probe underlying molecular pathways modulated by *nf1* in melanophores.

Several studies employing murine models have previously shown a role for neurofibromin in regulating cell numbers of CNS OPCs and astrocytes as well as PNS Schwann cells and sympathetic neurons (Brannan et al., 1994; Gutmann et al., 1999; Bennett et al., 2003; Zhu et al., 2005b; Hegeudus et al., 2007; Zheng et al., 2008). These are consistent with our findings in *nf1a/nf1b* mutants and indicative of a strong evolutionary conservation of Nf1 function in neural development. Our observation of impaired compact myelin formation and reduced CNS *plp1a* expression with unperturbed CNS and increased PNS *mbp* expression suggests that the differentiation programs of oligodendrocytes and Schwann cells respond differently to Nf1 deficiency. Alternatively, the observed ultrastructural defects in myelinated CNS axons might arise secondary to neuronal defects. The accessibility of the zebrafish embryo to mosaic analysis offers the ability to differentiate between these possibilities. Unlike *Nf1*-deficient mice, however, *nf1a/nf1b* mutant radial glia failed to demonstrate an appreciable increase in *Gfap* expression. Instead, we observed a decrease in *Blbp* expression and irregularities in patterning of *nf1a*^{-/-}; *nf1b*^{-/-} radial glial cells. This discrepancy might reflect species-specific differences in neural tissue as opposed to Nf1 function, because it remains unclear whether zebrafish radial glia-like ependymal cells are functionally equivalent to mammalian astrocytes.

We have previously characterized cardiovascular defects resulting from morpholino knockdown of *nf1a* and *nf1b* in zebrafish (Padmanabhan et al., 2009; Lee et al., 2010). These defects were observed at 48 and 72 hpf and probably resulted from impairment of both maternal and zygotic gene expression. In our stable compound mutants, we observed partially penetrant insufficiency of the atrioventricular valve at 3 dpf along with significant edema and impaired blood circulation associated with irregular heart rates beginning at 5-6 dpf (data not shown). However, we could not determine whether these effects were primary or secondary. It is possible that impaired cardiac function is the cause of death of these larvae. The absence of earlier cardiovascular phenotypes is most probably due to the activity of maternal transcripts (Abrams and Mullins, 2009); confirmation of this interpretation awaits the creation of a maternal zygotic mutation.

Ubiquitous and conditional *Nf1* knockout mice have been generated to investigate the role of neurofibromin in development and tumorigenesis (Cichowski and Jacks, 2001; Le and Parada, 2007). Conditional loss of *Nf1* with *p53* deficiency in mice results in the development of grade III and IV astrocytomas with full penetrance (Zhu et al., 2005a), indicating that *Nf1* mutations are associated not only with low-grade but also high-grade astrocytoma. Indeed, two independent studies have demonstrated that *NF1* mutations are found in about 15-23% of human glioblastoma multiformes (GBMs) (Parsons et al., 2008; The Cancer Genome Atlas Research Network, 2008). Interestingly, we also observed gliomas in zebrafish lacking *nf1* and *p53*. Likewise, MPNSTs are observed in both mouse and zebrafish models. Thus, the relative advantages of murine and zebrafish systems can be

leveraged for future studies aimed at developing therapeutics for these lethal complications of NF1.

In summary, we have developed and characterized zebrafish lines containing specific targeted mutations in *nf1a* and *nf1b*. Compound deficiency of *nf1a* and *nf1b* results in lethality and predisposes to tumor formation. These studies provide a powerful new tool for analysis of neurofibromin function and for the development of therapies for a common human disorder.

METHODS

Zebrafish lines

The *nf1a*^{Δ5}, *nf1a*^{Δ8}, *nf1b*⁺¹⁰ and *nf1b*^{Δ55} mutant alleles were generated by application of modularly assembled ZFNs. The *nf1a*^{L1247X} mutant allele was generated by TILLING. Our *nf1* mutant alleles were crossed into various transgenic lines, including Tg(*gfap:GFP*) (Lam et al., 2009), Tg(*sox10:GFP*) (Thermes et al., 2002; Carney et al., 2006) and Tg(*olig2:GFP*) (Shin et al., 2003), as well as the *p53*^{e7/e7} mutant line (Berghmans et al., 2005). Zebrafish were maintained under standard conditions as previously described (Westerfield, 2000). All experiments involving animals were approved by the Institutional Animal Care and Use Committees of Harvard University and the University of Pennsylvania.

TILLING with screening by CEL-I method

Individual samples from a preconstructed 'live library' of pooled genomic DNA from ENU-mutagenized F1 animals were used as a template for PCR with the following PCR primer pairs: *nf1a*_outer_F, 5'-TGGCAAATAAATGCTGACAGA-3' and *nf1a*_inner_F, 5'-HEX-TTTTTATATCTCATGTTTAGCTCACAA-3'; *nf1a*_outer_R, 5'-AAGTCTTAAATGGCCTGAGTGG-3' and *nf1a*_inner_R, 5'-6FAM-AAATGGCCTGAGTGGTAATAAA-3'. A nested PCR was performed first using the outer primer pair with the following PCR conditions: 94°C for 2 minutes; 30 cycles of 94°C for 30 seconds, 60°C for 40 seconds and 72°C for 1 minute; and 72°C for 5 minutes. Amplification was then performed using the inner primer pair with the following PCR conditions: 94°C for 2 minutes; 25 cycles of 94°C for 30 seconds, 60°C for 40 seconds and 72°C for 1 minute; and 72°C for 5 minutes. PCR products were denatured, allowed to re-anneal, subjected to CEL-I digestion and separated by acrylamide electrophoresis using a LI-COR DNA analyzer. Upon identification of a genomic DNA sample harboring a mutation in the analyzed region, the individual animals comprising that genomic DNA pool were rescreened to identify the appropriate F1 animal harboring the lesion of interest. This F1 animal was then outcrossed to wild-type fish and progeny were selected on the basis of the presence of the desired mutation. A genotyping strategy was developed to identify animals harboring the nonsense allele isolated by our TILLING strategy using the following PCR primers: *nf1a*_stop_PstI_F, 5'-CTCTCTTCGACTCTCGCCATCTGCTGTATCAGCTGC-3' and *nf1a*_stop_R, 5'-GAAGCAGAAGGTCATAATCTTGCTGGCTAGGC-3'. PCR conditions were 95°C for 2 minutes; 32 cycles of 94°C for 30 seconds, 62°C for 30 seconds and 72°C for 30 seconds; and 72°C for 5 minutes. This generates a 134 bp PCR product. The wild-type allele is resistant to PCR digestion by *PstI*, but the mutant allele is not.

Modular assembly of ZFNs

The desired three finger zinc finger proteins (ZFPs) were constructed by a splice overlap extension PCR strategy, with individual finger modules amplified from a archive of ZFPs with defined DNA-binding specificities (Zhu et al., 2011). Three individual fingers (F1, F2 and F3) were amplified using primers specific to their desired backbone position, followed by an overlapping PCR step to place them together into a single ZFP fragment which was cloned, sequence verified and subsequently subcloned in frame with a *FokI* nuclease variant in a pCS2 expression plasmid. The primers for the three backbone positions were as follows: F1 forward, 5'-GCGATGGGTACCCGCCCATATGCTTGC-3' and F1 reverse, 5'-CACTGGAAGGGCTTCTGGCCTGTGTGAATCCGGATGTG-3'; F2 forward, 5'-CATCCGGATTCACACAGGCCAGAA-GCCCTTCCAGTGTGCGCATCTGC-3' and F2 reverse, 5'-ATGTCGCATGCAAAAGGCTTCTCGCCTGTGTGGGTGCGGATGTG-3'; F3 forward, 5'-CGAGAAGCCTTTTGCATGCGACA-3' and F3 reverse, 5'-GCGTAGGATCCACCTGTGTGGATCTTGGTGTG-3'. The PCR conditions for amplifying F1 were 98°C for 2 minutes and 15 cycles of 94°C for 30 seconds, 68°C for 30 seconds and 72°C for 20 seconds. The PCR conditions for F2 and F3 were 98°C for 2 minutes and 20 cycles of 94°C for 30 seconds, 57°C for 30 seconds and 72°C for 30 seconds. The three individual gel-purified PCR products for positions F1, F2 and F3 were combined (15 ng of each) in a PCR using Advantage 2 HiFi polymerase (Clontech) and subjected to the thermal cycling of 94°C for 2 minutes and five cycles of 94°C for 30 seconds, 55°C for 30 seconds and 72°C for 30 seconds. Following this cycling program, F1 forward and F3 reverse primers were added to the reaction and thermal cycling was continued as follows: 25 cycles of 94°C for 15 seconds and 68°C for 30 seconds. This PCR product of approximately 300 bp was gel-purified, cloned, sequence verified and subcloned in frame with the DD/RR or EL/KK *FokI* variants (Miller et al., 2007; Szczepek et al., 2007) with and without the 3'-UTR of *nanos1* (Koprunner et al., 2001).

ZFN mRNA injections and genotyping assays

We utilized protocols similar to those recently described (Zhu et al., 2011). pCS2-based expression plasmids containing our constructed ZFNs were linearized downstream of the SV40 polyadenylation signal and used as templates for in vitro transcription of ZFN mRNAs (Ambion). One-cell fertilized zebrafish embryos were injected with varying amounts of DD/RR or EL/KK *FokI* variant mRNAs. Site-specific ZFN function was verified by a genotyping strategy wherein introduction of mutagenic lesions at the target site leads to loss of a unique endogenous restriction site. This same strategy was later used to genotype F1 animals. For *nf1a* and *nf1b*, PCR was performed using the following primer pairs and PCR conditions: *nf1a* F genotyping primer, 5'-GGTGTGTATGTAATGGGCTCAATG-3'; *nf1a* R genotyping primer, 5'-TACAGTTCCATAAAACCTGACATTTTC-3'; *nf1b* F genotyping primer, 5'-TGCTACCTGCCGGCAGGCTCAG-3'; and *nf1b* R genotyping primer, 5'-ACCTGTGACCATCATGTTACTGACA-3'. PCR conditions for *nf1a* were 94°C for 2 minutes; 35 cycles of 94°C for 30 seconds, 54.8°C for 30 seconds and 72°C for 40 seconds; and 72°C for 5 minutes. PCR conditions for *nf1b* were 94°C for 2 minutes; 35 cycles of 94°C for 30 seconds,

62°C for 30 seconds and 72°C for 40 seconds; and 72°C for 5 minutes. For both *nf1a* and *nf1b*, a 223-bp PCR product was generated. Mutant alleles were resistant to subsequent digestion with *BspCNI* or *DdeI* (*nf1a*) and *BsII* or *EcoNI* (*nf1b*), whereas the wild-type alleles were completely digested. The molecular identities of the various mutant alleles were determined by cloning and sequencing the restriction enzyme-resistant PCR products from individual embryos derived from outcrosses of F1 animals to wild-type fish.

Larval genotyping

A modified fin clip genotyping strategy was utilized to identify larval genotypes prior to sacrifice. Briefly, 2-dpf larvae were anesthetized with tricaine and stereomicroscopic amputation was performed on the caudal fin with an angled dissecting knife (Fine Science Tools, 10056-12). Genomic DNA from fin-clipped tissue samples was prepared by collecting specimens in 1.5 µl of the surrounding medium and dispensing into PCR tubes containing 7.5 µl of 60 mM NaOH, which were incubated at 95°C for 20 minutes followed by 4°C for 5 minutes with the subsequent addition of 1 µl of 1 M Tris-HCl pH 8. Genotyping for *nf1a* or *nf1b* was performed as described with an increase in PCR cycle number to 40. Genomic DNA prepared by this strategy was sufficient for a single genotyping reaction. Thus, parental crosses were selected to ensure all progeny were homozygous for the non-genotyped *nf1* allele (e.g. *nf1a*^{+/-}; *nf1b*^{-/-} incross). This was verified by genotyping the homozygous mutant allele in sibling clutchmates.

Whole-mount in situ hybridization and TUNEL staining, immunohistochemistry and BrdU labeling

Antisense RNA probes were generated for *plp1a* (Park et al., 2002) and *mbp* (Lyons et al., 2005) using a digoxigenin RNA labeling kit (Roche). A previously published protocol (Thisse and Thisse, 2008) was followed with minor modifications. Terminal deoxynucleotidyl transferase dUTP nick-end labeling (TUNEL) staining of larvae was performed using the ApopTag Peroxidase In Situ Apoptosis Detection Kit (EMD Millipore) with minor modifications. Larvae were subsequently blocked in 2% blocking reagent (Roche) for 4 hours at room temperature and incubated overnight in anti-digoxigenin-POD antibody (Roche; 1:500) at 4°C. TUNEL-positive cells were detected using the TSA fluorescein system (PerkinElmer). Apoptotic cells were quantified by counting TUNEL-positive cells between somites 6 and 15. For immunohistochemical analysis of zebrafish larvae, we used mouse anti-BrdU (Developmental Studies Hybridoma Bank G3G4; 1:1000), mouse anti-HuC/D (Invitrogen A-21271; 1:100), mouse anti-pERK1/2 (Sigma; 1:200), mouse anti-Zrf1 (Zebrafish International Resource Center; 1:1000), rabbit anti-BLBP (Millipore AB9558; 1:1000), rabbit anti-pS6 (Cell Signaling 2211; 1:200), and rabbit anti-SOX10 (Park et al., 2005) (a generous gift from Bruce Appel, University of Colorado, Denver, CO; 1:5000) as primary antibodies. For fluorescent detection of antibody labeling, we used anti-mouse and anti-rabbit IgG antibodies conjugated with Alexa Fluor 488, 568 and 647 (Invitrogen; 1:200). Immunohistochemistry of adult zebrafish tumor samples was performed according to a previously published protocol (Ligon et al., 2004). Primary antibodies included anti-pERK1/2 (Cell Signaling 4370; 1:200), anti-pS6 (Cell Signaling 2211; 1:50), anti-phosphorylated histone H3 (Cell Signaling 9706; 1:100), rabbit anti-SOX10 (Park et al., 2005) (1:3000), mouse anti-GFAP

(Sigma G3893; 1:10,000), anti-HuC/D (Invitrogen A-21271; 1:200) and anti-synaptophysin (Millipore MAB5258; 1:1000). Antibody binding was detected using a diaminobenzidine-peroxidase visualization system (EnVision+, Dako). Mayer's hematoxylin was used for counterstaining. For BrdU labeling, embryos were incubated in BrdU solution (10 mM BrdU in 2% DMSO) for 12 hours. After BrdU incubation, embryos were fixed with 4% paraformaldehyde and embedded in 1.5% agarose. Sections from embedded frozen specimens were immersed in 2 M HCl for 15 minutes and processed for immunohistochemistry. Paraffin sectioning followed by hematoxylin and eosin (H&E) staining was performed at the Dana-Farber/Harvard Cancer Center Research Pathology Core.

Behavioral analysis

Startle behavioral experiments were performed on 5-dpf larvae raised as previously described (Burgess and Granato, 2007b). Larvae with underinflated swim bladders were excluded from behavioral testing. Acoustic startle responses were elicited and measured as previously described (Burgess and Granato, 2007a; Wolman et al., 2011), such that larvae could be tracked and analyzed individually. All startle stimuli were 1000 Hz waveforms of 3 milliseconds duration at an intensity of approximately 150 m/second². Stimulus intensity was calculated by measuring the displacement of the testing arena due to vibration. To evaluate short latency C-start (SLC) behavior, images were recorded 30 milliseconds prior to and 90 milliseconds following the delivery of the 3 millisecond acoustic stimulus. To examine acoustic startle larval motor behaviors, we captured video recordings using a MotionPro high-speed camera (Redlake) at 1000 frames per second with 512×512 pixel resolution using a 50 mm macro lens. Behavioral analyses were carried out with the FLOTE software package (Burgess and Granato, 2007b; Burgess and Granato, 2007a). Startle short-term habituation was performed and analyzed as previously described (Wolman et al., 2011). Larvae were genotyped following behavioral testing.

Western blotting

Protein lysates were prepared from 3-dpf wild-type, *nf1a*^{-/-}; *nf1b*^{+/+}, *nf1a*^{+/+}; *nf1b*^{-/-} and *nf1a*^{-/-}; *nf1b*^{-/-} larvae. Briefly, groups of 10-20 larvae with identical genotype were anesthetized with tricaine, deyolked in a solution of ice-cold PBS with 0.1% Tween-20 (PBST), transferred to a pre-chilled microcentrifuge tube containing 5 µl of lysis buffer (150 mM NaCl, 50 mM Tris-HCl pH 8, 5 mM EDTA, 1 mM PMSE, 1% Igepal CA 630, 0.5% sodium deoxycholate, 0.1% SDS and 1× Halt protease inhibitor cocktail (Thermo Fisher Scientific) per larva, sonicated using a Bioruptor (Diagenode) and cleared by centrifugation. Larval (100 µg) and 293T (25 µg) protein lysates were separated by gel electrophoresis, transferred to PVDF membranes and probed overnight at 4°C with the following primary antibodies: anti-neurofibromin (Abcam ab17963; 1:1000), anti- α -tubulin (Sigma T6074; 1:1000), anti-pERK1/2 (Cell Signaling 4377; 1:1000), and anti-ERK1/2 (Cell Signaling 9102; 1:1000). Primary antibody binding was visualized on X-ray film using anti-mouse-HRP (Cell Signaling 7076; 1:10,000) or anti-rabbit-HRP (Cell Signaling 7074; 1:10,000) secondary antibodies along with LumiGLO (Cell Signaling) or SuperSignal West Femto (Thermo Fisher Scientific) chemiluminescent substrates. Each Western blot was performed in three independent replicates with a representative image of one presented.

Quantification of lateral line and head melanophores

Lateral stripe melanophores, including those observed along the horizontal myoseptum, were counted by a blinded observer in live progeny from *nf1a*^{+/-}; *nf1b*^{+/-} incrosses at 3 and 6 dpf. Each discrete melanized region was counted as a single melanophore. Following 6-dpf lateral stripe melanophore quantitation, larvae were immersed in E3 medium containing 5 mg/ml epinephrine (Sigma E4375) for 10 minutes to induce contraction of melanosomes around cell bodies and allow evaluation of head melanophore numbers. Larvae were fixed overnight in 4% paraformaldehyde in PBS at 4°C, washed twice with PBS for 5 minutes, and melanophores anterior to somite one across the crown of the head (supplementary material Fig. S14) were counted. Larvae were subsequently genotyped for *nf1a* and *nf1b*. Data analysis was performed by one-way ANOVA with Dunnett's post-test (GraphPad InStat 3.1a, GraphPad Software).

Serial tracking of lateral line melanophores

Lateral stripe melanophores of live progeny from *nf1a*^{+/-}; *nf1b*^{-/-} or wild-type incrosses were individually imaged at 3 dpf followed by incubation with 0.2 mM *N*-phenylthiourea (PTU, Sigma) to prevent melanin synthesis. At 5 dpf, lateral stripe melanophores were again imaged, after which PTU was washed out. Larvae were reimaged at 6 dpf and subsequently genotyped for *nf1a*. Images were acquired using a Nikon SMZ1500 microscope and NIS-Elements F2.20 software with identical settings. Melanophores in a 200-μm region, corresponding to roughly 12 somites at 3 dpf, were counted at 3 and 6 dpf for each larva. Statistical analysis was performed using a one-tail, unpaired *t*-test (GraphPad Prism 5, GraphPad Software).

Intestinal transit assays

Groups of 5-dpf wild-type and *nf1a*^{-/-}; *nf1b*^{-/-} larvae were placed in individual wells of six-well plates containing feeding medium [4 ml E3, 2 ml paramecia culture and 5 μl of 2-μm yellow-green microspheres (Polysciences 18338)]. Larvae were incubated at 28.5°C for 1 hour followed by several E3 washes. Individual larvae were transferred to 24-well plates and visually assessed for the presence of fluorescent microspheres in the intestinal bulb. Extent of intestinal transit was observed at 2, 4, 6 and 24 hours. Transit was considered to be complete when fluorescence was no longer detectable in the intestinal tract.

Transmission electron microscopy

TEM was carried out at the Harvard Medical School Electron Microscopy Facility. Briefly, embryos were fixed in 2% formaldehyde and 2.5% glutaraldehyde, post-fixed with 1% osmium tetroxide and embedded in epon. Sections were collected in the trunk region of embryos. Images were captured by a Tecnai G² Spirit BioTWIN electron microscope with an AMT 2k CCD camera.

Tumor identification

nf1a^{Δ8/+}; *nf1b*^{+10/+10}; *p53*^{e7/e7} fish were incrossed and progeny were manually evaluated weekly for 45 weeks. Animals identified as having tumors were separated and fin-clipped for genotyping purposes. These samples were subsequently subjected to histological and immunohistochemical analyses as described above for determination of tumor type. At the completion of 45 weeks, all tumor-free fish were genotyped for subsequent statistical analysis.

TRANSLATIONAL IMPACT

Clinical issue

Neurofibromatosis type 1 (NF1) is one of the most commonly inherited human genetic disorders. Despite nearly complete penetrance, the clinical expression of NF1 varies widely, even within families harboring identical mutations at the *NF1* locus. Not surprisingly, few genotype-phenotype relationships have thus far been reported for NF1, suggesting important contributions from unlinked modifier genes and/or environmental factors. However, these observations do not preclude mutations or deletions within the *NF1* locus from influencing pathology. Instead, they highlight the need for better experimental tools to address this important and clinically relevant observation. Additional models of NF1 are needed to begin elucidating these mechanisms using scalable chemical and genetic approaches.

Results

The authors employ zinc finger nucleases and TILLING to isolate null alleles of the two zebrafish orthologues of human *NF1*, *nf1a* and *nf1b*. They report that zebrafish lacking *nf1a* and *nf1b* exhibit valvular insufficiency, defects in learning and behavior and early larval lethality. Larvae carrying a single wild-type allele of either *nf1a* or *nf1b* are viable and fertile, suggesting functional redundancy. The authors also observe hyperplasia and aberrant differentiation in the oligodendrocyte progenitor cells and Schwann cells populating the nervous systems of *nf1*-null larvae. This is accompanied by irregularities in the myelin sheaths surrounding the neuronal axons of the central nervous system. Human *NF1* is a potent tumor-suppressor gene and the authors provide evidence that zebrafish *nf1a* and *nf1b* function similarly: they demonstrate that Ras is hyperactivated in the spinal cords of *nf1*-null larvae, and that the combined loss of *nf1* and *p53* accelerates tumorigenesis. Finally, the authors characterize a melanophore defect resulting from *nf1* loss that disrupts the uniform pigmentation pattern observed along the lateral stripes.

Implications and future directions

Using zebrafish to probe the genetic, epistatic and environmental factors underlying NF1 pathology offers several important advantages over currently available murine models. The low costs and high fecundity of zebrafish coupled with their ability to survive for several days as haploid organisms make them amenable to large-scale genetic screens. Thus, *nf1*-deficient zebrafish should greatly facilitate the identification of modifier genes influencing NF1 pathogenesis. In addition, genetic rescue experiments using specific *NF1* mutations or deletions could clarify the molecular basis of pathology. The feasibility of high-throughput chemical screening using this model should provide additional valuable mechanistic insights and identify lead compounds for future therapeutics. Few treatment options are currently available for individuals affected with NF1, so advances in this area are urgently needed. Importantly, this represents the first animal model that demonstrates pigmentation defects analogous to the pathognomonic café-au-lait spots seen in affected individuals. Therefore, this model will provide a platform for further investigation of one of the most common clinical pathologies associated with NF1.

ACKNOWLEDGEMENTS

We thank members of the Epstein and Look laboratories for helpful discussions, especially Rajan Jain and Nikhil Singh. We are grateful to Jie He for her expert assistance with zebrafish husbandry; Michael Pack and Mary Mullins for thoughtful suggestions; Joshua Abrams, Jesse Isaacman-Beck and Allison Rosenberg for technical instruction; and Thomas Joseph for critical reading of the manuscript.

COMPETING INTERESTS

The authors declare that they do not have any competing or financial interests.

AUTHOR CONTRIBUTIONS

J.S., A.P., E.D.D., M.A.W., J.P.K., N.D.L., S.A.W., K.L.L., J.A.E. and A.T.L. conceived and designed the experiments. J.S., A.P., E.D.D., J.S.L., S.H., S.D., F.G. and M.A.W. performed the experiments. J.S., A.P., E.D.D., J.P.K., K.L.L., J.A.E. and A.T.L. analyzed the data. M.G., N.D.L., S.A.W., S-H.K., L.S-K. and K.L.L. contributed reagents, materials and analysis tools. A.P., J.S., E.D.D., J.P.K., A.T.L. and J.A.E. wrote the paper.

FUNDING

This work was supported by the Department of Defense [grant numbers W81XWH-07-1-0228 and W81XWH-12-1-0125 to J.A.E. and A.T.L.] and the National Institutes of Health [grant numbers R01 HL062974 to J.A.E.; R01 HL093766 to N.D.L. and S.A.W.; T32 HL007843-15 to E.D.D.; and R01 HG002995 to L.S.-K.]. A.T.L. was supported by an Innovator Award from Alex's Lemonade Stand Foundation. A.P. was supported by a fellowship from the Sarnoff Cardiovascular Research Foundation. J.S. was supported by a fellowship from the Dana-Farber Cancer Institute (DFCI) Pediatric Low-Grade Astrocytoma Program, and J.-S.L. was supported by a Young Investigator Award from the Children's Tumor Foundation. This work was also supported by the Vanderbilt University Academic Venture Capital Fund to L.S.-K. as well as the Spain Fund for Regenerative Medicine and the W.W. Smith Endowed Chair to J.A.E.

SUPPLEMENTARY MATERIAL

Supplementary material for this article is available at <http://dmm.biologists.org/lookup/suppl/doi:10.1242/dmm.009779/-/DC1>

REFERENCES

- Abrams, E. W. and Mullins, M. C.** (2009). Early zebrafish development: it's in the maternal genes. *Curr. Opin. Genet. Dev.* **19**, 396-403.
- Amores, A., Force, A., Yan, Y. L., Joly, L., Amemiya, C., Fritz, A., Ho, R. K., Langeland, J., Prince, V., Wang, Y. L. et al.** (1998). Zebrafish hox clusters and vertebrate genome evolution. *Science* **282**, 1711-1714.
- Andersson, J., Sihto, H., Meis-Kindblom, J. M., Joensuu, H., Nupponen, N. and Kindblom, L. G.** (2005). NF1-associated gastrointestinal stromal tumors have unique clinical, phenotypic, and genotypic characteristics. *Am. J. Surg. Pathol.* **29**, 1170-1176.
- Bahuau, M., Laurendeau, I., Pelet, A., Assouline, B., Lamireau, T., Taine, L., Le Bail, B., Vergnes, P., Gallet, S., Vidaud, M. et al.** (2000). Tandem duplication within the neurofibromatosis type 1 gene (NF1) and reciprocal t(15;16)(q26.3;q12.1) translocation in familial association of NF1 with intestinal neuronal dysplasia type B (IND B). *J. Med. Genet.* **37**, 146-150.
- Bannykh, S. I., Stolt, C. C., Kim, J., Perry, A. and Wegner, M.** (2006). Oligodendroglial-specific transcriptional factor SOX10 is ubiquitously expressed in human gliomas. *J. Neurooncol.* **76**, 115-127.
- Bennett, M. R., Rizvi, T. A., Karyala, S., McKinnon, R. D. and Ratner, N.** (2003). Aberrant growth and differentiation of oligodendrocyte progenitors in neurofibromatosis type 1 mutants. *J. Neurosci.* **23**, 7207-7217.
- Berghmans, S., Murphey, R. D., Wienholds, E., Neuberg, D., Kutok, J. L., Fletcher, C. D., Morris, J. P., Liu, T. X., Schulte-Merker, S., Kanki, J. P. et al.** (2005). tp53 mutant zebrafish develop malignant peripheral nerve sheath tumors. *Proc. Natl. Acad. Sci. USA* **102**, 407-412.
- Brannan, C. I., Perkins, A. S., Vogel, K. S., Ratner, N., Nordlund, M. L., Reid, S. W., Buchberg, A. M., Jenkins, N. A., Parada, L. and Copeland, N. G.** (1994). Targeted disruption of the neurofibromatosis type-1 gene leads to developmental abnormalities in heart and various neural crest-derived tissues. *Genes Dev.* **8**, 1019-1029.
- Burgess, H. A. and Granato, M.** (2007a). Sensorimotor gating in larval zebrafish. *J. Neurosci.* **27**, 4984-4994.
- Burgess, H. A. and Granato, M.** (2007b). Modulation of locomotor activity in larval zebrafish during light adaptation. *J. Exp. Biol.* **210**, 2526-2539.
- Carney, T. J., Dutton, K. A., Greenhill, E., Delfino-Machin, M., Dufourcq, P., Blader, P. and Kelsch, R. N.** (2006). A direct role for Sox10 in specification of neural crest-derived sensory neurons. *Development* **133**, 4619-4630.
- Cawthon, R. M., Weiss, R., Xu, G. F., Viskochil, D., Culver, M., Stevens, J., Robertson, M., Dunn, D., Gesteland, R., O'Connell, P. et al.** (1990). A major segment of the neurofibromatosis type 1 gene: cDNA sequence, genomic structure, and point mutations. *Cell* **62**, 193-201.
- Cichowski, K. and Jacks, T.** (2001). NF1 tumor suppressor gene function: narrowing the GAP. *Cell* **104**, 593-604.
- Cichowski, K., Shih, T. S., Schmitt, E., Santiago, S., Reilly, K., McLaughlin, M. E., Bronson, R. T. and Jacks, T.** (1999). Mouse models of tumor development in neurofibromatosis type 1. *Science* **286**, 2172-2176.
- D'Angelo, I., Welti, S., Bonneau, F. and Scheffzek, K.** (2006). A novel bipartite phospholipid-binding module in the neurofibromatosis type 1 protein. *EMBO Rep.* **7**, 174-179.
- Dasgupta, B., Dugan, L. L. and Gutmann, D. H.** (2003). The neurofibromatosis 1 gene product neurofibromin regulates pituitary adenylate cyclase-activating polypeptide-mediated signaling in astrocytes. *J. Neurosci.* **23**, 8949-8954.
- Dasgupta, B., Yi, Y., Chen, D. Y., Weber, J. D. and Gutmann, D. H.** (2005). Proteomic analysis reveals hyperactivation of the mammalian target of rapamycin pathway in neurofibromatosis 1-associated human and mouse brain tumors. *Cancer Res.* **65**, 2755-2760.
- De Schepper, S., Boucneau, J. M., Westbroek, W., Mommaas, M., Onderwater, J., Messiaen, L., Naeyaert, J. M. and Lambert, J. L.** (2006). Neurofibromatosis type 1 protein and amyloid precursor protein interact in normal human melanocytes and colocalize with melanosomes. *J. Invest. Dermatol.* **126**, 653-659.
- Ducatman, B. S., Scheithauer, B. W., Piepgras, D. G., Reiman, H. M. and Ilstrup, D. M.** (1986). Malignant peripheral nerve sheath tumors. A clinicopathologic study of 120 cases. *Cancer* **57**, 2006-2021.
- Easton, D. F., Ponder, M. A., Huson, S. M. and Ponder, B. A.** (1993). An analysis of variation in expression of neurofibromatosis (NF) type 1 (NF1): evidence for modifying genes. *Am. J. Hum. Genet.* **53**, 305-313.
- Eliyahu, D., Raz, A., Gruss, P., Givol, D. and Oren, M.** (1984). Participation of p53 cellular tumour antigen in transformation of normal embryonic cells. *Nature* **312**, 646-649.
- Guo, H. F., Tong, J., Hannan, F., Luo, L. and Zhong, Y.** (2000). A neurofibromatosis-1-regulated pathway is required for learning in *Drosophila*. *Nature* **403**, 895-898.
- Gutmann, D. H., Loehr, A., Zhang, Y., Kim, J., Henkemeyer, M. and Cashen, A.** (1999). Haploinsufficiency for the neurofibromatosis 1 (NF1) tumor suppressor results in increased astrocyte proliferation. *Oncogene* **18**, 4450-4459.
- Hegedus, B., Dasgupta, B., Shin, J. E., Emmett, R. J., Hart-Mahon, E. K., Elghazi, L., Bernal-Mizrachi, E. and Gutmann, D. H.** (2007). Neurofibromatosis-1 regulates neuronal and glial cell differentiation from neuroglial progenitors in vivo by both cAMP- and Ras-dependent mechanisms. *Cell Stem Cell* **1**, 443-457.
- Hirose, T., Scheithauer, B. W. and Sano, T.** (1998). Perineurial malignant peripheral nerve sheath tumor (MPNST): a clinicopathologic, immunohistochemical, and ultrastructural study of seven cases. *Am. J. Surg. Pathol.* **22**, 1368-1378.
- Hsueh, Y. P., Roberts, A. M., Volta, M., Sheng, M. and Roberts, R. G.** (2001). Bipartite interaction between neurofibromatosis type I protein (neurofibromin) and syndecan transmembrane heparan sulfate proteoglycans. *J. Neurosci.* **21**, 3764-3770.
- Hultman, K. A. and Johnson, S. L.** (2010). Differential contribution of direct-developing and stem cell-derived melanocytes to the zebrafish larval pigment pattern. *Dev. Biol.* **337**, 425-431.
- Hultman, K. A., Budi, E. H., Teasley, D. C., Gottlieb, A. Y., Parichy, D. M. and Johnson, S. L.** (2009). Defects in ErbB-dependent establishment of adult melanocyte stem cells reveal independent origins for embryonic and regeneration melanocytes. *PLoS Genet.* **5**, e1000544.
- Hundley, J. E., Koester, S. K., Troyer, D. A., Hilsenbeck, S. G., Subler, M. A. and Windle, J. J.** (1997). Increased tumor proliferation and genomic instability without decreased apoptosis in MMTV-ras mice deficient in p53. *Mol. Cell. Biol.* **17**, 723-731.
- Jacks, T., Shih, T. S., Schmitt, E. M., Bronson, R. T., Bernards, A. and Weinberg, R. A.** (1994). Tumour predisposition in mice heterozygous for a targeted mutation in Nf1. *Nat. Genet.* **7**, 353-361.
- Kemp, C. J., Burns, P. A., Brown, K., Nagase, H. and Balmain, A.** (1994). Transgenic approaches to the analysis of ras and p53 function in multistage carcinogenesis. *Cold Spring Harb. Symp. Quant. Biol.* **59**, 427-434.
- Koprinner, M., Thisse, C., Thisse, B. and Raz, E.** (2001). A zebrafish nanos-related gene is essential for the development of primordial germ cells. *Genes Dev.* **15**, 2877-2885.
- Lam, C. S., Marz, M. and Strahle, U.** (2009). gfp and nestin reporter lines reveal characteristics of neural progenitors in the adult zebrafish brain. *Dev. Dyn.* **238**, 475-486.
- Le, L. Q. and Parada, L. F.** (2007). Tumor microenvironment and neurofibromatosis type I: connecting the GAPs. *Oncogene* **26**, 4609-4616.
- Lee, J. S., Padmanabhan, A., Shin, J., Zhu, S., Guo, F., Kanki, J. P., Epstein, J. A. and Look, A. T.** (2010). Oligodendrocyte progenitor cell numbers and migration are regulated by the zebrafish orthologs of the NF1 tumor suppressor gene. *Hum. Mol. Genet.* **19**, 4643-4653.
- Ligon, K. L., Alberta, J. A., Kho, A. T., Weiss, J., Kwaan, M. R., Nutt, C. L., Louis, D. N., Stiles, C. D. and Rowitch, D. H.** (2004). The oligodendroglial lineage marker OLIG2 is universally expressed in diffuse gliomas. *J. Neuropathol. Exp. Neurol.* **63**, 499-509.
- Lyons, D. A., Pogoda, H. M., Voas, M. G., Woods, I. G., Diamond, B., Nix, R., Arana, N., Jacobs, J. and Talbot, W. S.** (2005). *erbb3* and *erbb2* are essential for schwann cell migration and myelination in zebrafish. *Curr. Biol.* **15**, 513-524.
- Miller, J. C., Holmes, M. C., Wang, J., Guschin, D. Y., Lee, Y. L., Rupniewski, I., Beausejour, C. M., Waite, A. J., Wang, N. S., Kim, K. A. et al.** (2007). An improved zinc-finger nuclease architecture for highly specific genome editing. *Nat. Biotechnol.* **25**, 778-785.
- Padmanabhan, A., Lee, J. S., Ismat, F. A., Lu, M. M., Lawson, N. D., Kanki, J. P., Look, A. T. and Epstein, J. A.** (2009). Cardiac and vascular functions of the zebrafish orthologues of the type I neurofibromatosis gene NF1. *Proc. Natl. Acad. Sci. USA* **106**, 22305-22310.
- Parada, L. F., Land, H., Weinberg, R. A., Wolf, D. and Rotter, V.** (1984). Cooperation between gene encoding p53 tumour antigen and ras in cellular transformation. *Nature* **312**, 649-651.

- Park, H. C., Mehta, A., Richardson, J. S. and Appel, B.** (2002). *olig2* is required for zebrafish primary motor neuron and oligodendrocyte development. *Dev. Biol.* **248**, 356-368.
- Park, H. C., Boyce, J., Shin, J. and Appel, B.** (2005). Oligodendrocyte specification in zebrafish requires notch-regulated cyclin-dependent kinase inhibitor function. *J. Neurosci.* **25**, 6836-6844.
- Parsons, D. W., Jones, S., Zhang, X., Lin, J. C., Leary, R. J., Angenendt, P., Mankoo, P., Carter, H., Siu, I. M., Gallia, G. L. et al.** (2008). An integrated genomic analysis of human glioblastoma multiforme. *Science* **321**, 1807-1812.
- Powers, J. F., Evinger, M. J., Zhi, J., Picard, K. L. and Tischler, A. S.** (2007). Pheochromocytomas in Nf1 knockout mice express a neural progenitor gene expression profile. *Neuroscience* **147**, 928-937.
- Sabbagh, A., Pasmant, E., Laurendeau, I., Parfait, B., Barbarot, S., Guillot, B., Combemale, P., Ferkal, S., Vidaud, M., Aubourg, P. et al.** (2009). Unravelling the genetic basis of variable clinical expression in neurofibromatosis 1. *Hum. Mol. Genet.* **18**, 2768-2778.
- Shin, J., Park, H. C., Topczewska, J. M., Mawdsley, D. J. and Appel, B.** (2003). Neural cell fate analysis in zebrafish using *olig2* BAC transgenics. *Methods Cell Sci.* **25**, 7-14.
- Side, L., Taylor, B., Cayouette, M., Conner, E., Thompson, P., Luce, M. and Shannon, K.** (1997). Homozygous inactivation of the NF1 gene in bone marrow cells from children with neurofibromatosis type 1 and malignant myeloid disorders. *N. Engl. J. Med.* **336**, 1713-1720.
- Side, L. E., Emanuel, P. D., Taylor, B., Franklin, J., Thompson, P., Castleberry, R. P. and Shannon, K. M.** (1998). Mutations of the NF1 gene in children with juvenile myelomonocytic leukemia without clinical evidence of neurofibromatosis, type 1. *Blood* **92**, 267-272.
- Szcepek, M., Brondani, V., Buchel, J., Serrano, L., Segal, D. J. and Cathomen, T.** (2007). Structure-based redesign of the dimerization interface reduces the toxicity of zinc-finger nucleases. *Nat. Biotechnol.* **25**, 786-793.
- Tanaka, M., Omura, K., Watanabe, Y., Oda, Y. and Nakanishi, I.** (1994). Prognostic factors of colorectal cancer: K-ras mutation, overexpression of the p53 protein, and cell proliferative activity. *J. Surg. Oncol.* **57**, 57-64.
- The Cancer Genome Atlas Research Network.** (2008). Comprehensive genomic characterization defines human glioblastoma genes and core pathways. *Nature* **455**, 1061-1068.
- Thermes, V., Grabher, C., Ristoratore, F., Bourrat, F., Choulika, A., Wittbrodt, J. and Joly, J. S.** (2002). I-SceI meganuclease mediates highly efficient transgenesis in fish. *Mech. Dev.* **118**, 91-98.
- Thisse, C. and Thisse, B.** (2008). High-resolution in situ hybridization to whole-mount zebrafish embryos. *Nat. Protoc.* **3**, 59-69.
- Tong, J., Hannan, F., Zhu, Y., Bernard, A. and Zhong, Y.** (2002). Neurofibromin regulates G protein-stimulated adenylyl cyclase activity. *Nat. Neurosci.* **5**, 95-96.
- Viskochil, D., Buchberg, A. M., Xu, G., Cawthon, R. M., Stevens, J., Wolff, R. K., Culver, M., Carey, J. C., Copeland, N. G., Jenkins, N. A. et al.** (1990). Deletions and a translocation interrupt a cloned gene at the neurofibromatosis type 1 locus. *Cell* **62**, 187-192.
- Vogel, K. S., Klesse, L. J., Velasco-Miguel, S., Meyers, K., Rushing, E. J. and Parada, L. F.** (1999). Mouse tumor model for neurofibromatosis type 1. *Science* **286**, 2176-2179.
- Wallace, M. R., Marchuk, D. A., Andersen, L. B., Letcher, R., Odeh, H. M., Saulino, A. M., Fountain, J. W., Breteron, A., Nicholson, J., Mitchell, A. L. et al.** (1990). Type 1 neurofibromatosis gene: identification of a large transcript disrupted in three NF1 patients. *Science* **249**, 181-186.
- Wanebo, J. E., Malik, J. M., Vandenberg, S. R., Wanebo, H. J., Driesen, N. and Persing, J. A.** (1993). Malignant peripheral nerve sheath tumors. A clinicopathologic study of 28 cases. *Cancer* **71**, 1247-1253.
- Westerfield, M.** (2000). *The Zebrafish Book: A Guide for the Laboratory Use of Zebrafish (Danio rerio)* (4th edn). Eugene, OR: University of Oregon Press.
- Wienholds, E., Schulte-Merker, S., Walderich, B. and Plasterk, R. H.** (2002). Target-selected inactivation of the zebrafish *rag1* gene. *Science* **297**, 99-102.
- Williams, V. C., Lucas, J., Babcock, M. A., Gutmann, D. H., Korf, B. and Maria, B. L.** (2009). Neurofibromatosis type 1 revisited. *Pediatrics* **123**, 124-133.
- Wolman, M. A., Jain, R. A., Liss, L. and Granato, M.** (2011). Chemical modulation of memory formation in larval zebrafish. *Proc. Natl. Acad. Sci. USA* **108**, 15468-15473.
- Xu, H. and Gutmann, D. H.** (1997). Mutations in the GAP-related domain impair the ability of neurofibromin to associate with microtubules. *Brain Res.* **759**, 149-152.
- Zheng, H., Chang, L., Patel, N., Yang, J., Lowe, L., Burns, D. K. and Zhu, Y.** (2008). Induction of abnormal proliferation by nonmyelinating schwann cells triggers neurofibroma formation. *Cancer Cell* **13**, 117-128.
- Zhu, Y., Guignard, F., Zhao, D., Liu, L., Burns, D. K., Mason, R. P., Messing, A. and Parada, L. F.** (2005a). Early inactivation of p53 tumor suppressor gene cooperating with NF1 loss induces malignant astrocytoma. *Cancer Cell* **8**, 119-130.
- Zhu, Y., Harada, T., Liu, L., Lush, M. E., Guignard, F., Harada, C., Burns, D. K., Bajenaru, M. L., Gutmann, D. H. and Parada, L. F.** (2005b). Inactivation of NF1 in CNS causes increased glial progenitor proliferation and optic glioma formation. *Development* **132**, 5577-5588.
- Zhu, C., Smith, T., McNulty, J., Rayla, A. L., Lakshmanan, A., Siekmann, A. F., Buffardi, M., Meng, X., Shin, J., Padmanabhan, A. et al.** (2011). Evaluation and application of modularly assembled zinc-finger nucleases in zebrafish. *Development* **138**, 4555-4564.

Modulation of cAMP and Ras Signaling Pathways Improves Distinct Behavioral Deficits in a Zebrafish Model of Neurofibromatosis Type 1

Marc A. Wolman,^{1,3,5} Eric D. de Groh,^{1,3} Sean M. McBride,² Thomas A. Jongens,² Michael Granato,^{1,4} and Jonathan A. Epstein^{1,4,*}

¹Department of Cell and Developmental Biology, Perelman School of Medicine, University of Pennsylvania, Philadelphia, PA 19104, USA

²Department of Genetics, Perelman School of Medicine, University of Pennsylvania, Philadelphia, PA 19104, USA

³Co-first author

⁴Co-senior author

⁵Present address: Department of Zoology, University of Wisconsin, Madison, WI 53706, USA

*Correspondence: epsteinj@upenn.edu

<http://dx.doi.org/10.1016/j.celrep.2014.07.054>

This is an open access article under the CC BY-NC-ND license (<http://creativecommons.org/licenses/by-nc-nd/3.0/>).

SUMMARY

Neurofibromatosis type 1 (NF1) is a common autosomal-dominant disorder associated with attention deficits and learning disabilities. The primary known function of neurofibromin, encoded by the *NF1* gene, is to downregulate Ras activity. We show that *nf1*-deficient zebrafish exhibit learning and memory deficits and that acute pharmacological inhibition of downstream targets of Ras (MAPK and PI3K) restores memory consolidation and recall but not learning. Conversely, acute pharmacological enhancement of cAMP signaling restores learning but not memory. Our data provide compelling evidence that neurofibromin regulates learning and memory by distinct molecular pathways in vertebrates and that deficits produced by genetic loss of function are reversible. These findings support the investigation of cAMP signaling enhancers as a companion therapy to Ras inhibition in the treatment of cognitive dysfunction in NF1.

INTRODUCTION

Neurofibromatosis type 1 (NF1) is associated with a broad range of clinical characteristics, including a predisposition to develop benign and malignant tumors, pigmentation defects, and cognitive deficits (Cichowski and Jacks, 2001). As many as 50%–70% of children with NF1 exhibit attention deficits and learning disabilities that contribute to scholastic underachievement and impaired social development (Hyman et al., 2005, 2006; Levine et al., 2006). Genetic and pharmacological experiments performed in mice and *Drosophila* support a role for the Ras-GTPase activating domain (GRD), which functions to downregulate Ras activity in protein-synthesis-dependent memory (Costa et al., 2002; Cui et al., 2008; Guilding et al., 2007; Ho et al., 2007; Li et al., 2005; Silva et al., 1997). However, cognitive dysfunction

in NF1 has been linked to mutations throughout the *NF1* gene that do not cluster in the region encoding the GRD, leading to the proposal that neurofibromin serves additional cellular functions (Fahsold et al., 2000). Studies performed in *Drosophila* suggest that neurofibromin can also stimulate adenylyl cyclase (AC), cAMP production, and PKA to promote learning and memory (Guo et al., 2000; Hannan et al., 2006; The et al., 1997; Tong et al., 2002). *Nf1*-deficient *Drosophila* brains show reduced cAMP levels, and expression of a C-terminal neurofibromin fragment lacking the GRD is sufficient to rescue learning (Ho et al., 2007; Tong et al., 2002). Similarly, brains of *Nf1*^{+/-} mice exhibit reduced cAMP levels (Brown et al., 2010, 2012; Hegedus et al., 2007) and cAMP regulation of dopaminergic function in the hippocampus is disrupted (Diggs-Andrews et al., 2013). The mechanism by which neurofibromin regulates AC remains controversial, and both Ras-dependent and Ras-independent pathways have been suggested (Guo et al., 1997; Hannan et al., 2006; Tong et al., 2002). Studies in *Drosophila* models of NF1 further argue that the resulting elevation in Ras activity, mediated through the upstream activation of neuronal dAkt, is responsible for observed decreases in cAMP signaling (Gouzi et al., 2011; Walker et al., 2006, 2013). Neurofibromin is also known to modulate both neural and glial development from neuroglial progenitors, and both Ras and cAMP have been implicated (Hegedus et al., 2007). Recent studies suggest that pharmacological activation of the cAMP pathway may enhance cognition in murine models (Jayachandran et al., 2014; Peng et al., 2014; Richter et al., 2013). However, it remains unclear whether NF1-dependent cAMP signaling is critical for learning or memory in vertebrates. Furthermore, the contributions of developmental and structural abnormalities to learning and memory deficits in NF1 have not yet been clearly defined (Armstrong et al., 2012; Karlsgodt et al., 2012; Shilyansky et al., 2010).

RESULTS AND DISCUSSION

We utilized a zebrafish model of NF1 that harbors null alleles in the *NF1* orthologs *nf1a* and *nf1b* (Shin et al., 2012) to evaluate molecular signaling pathways that control NF1-dependent

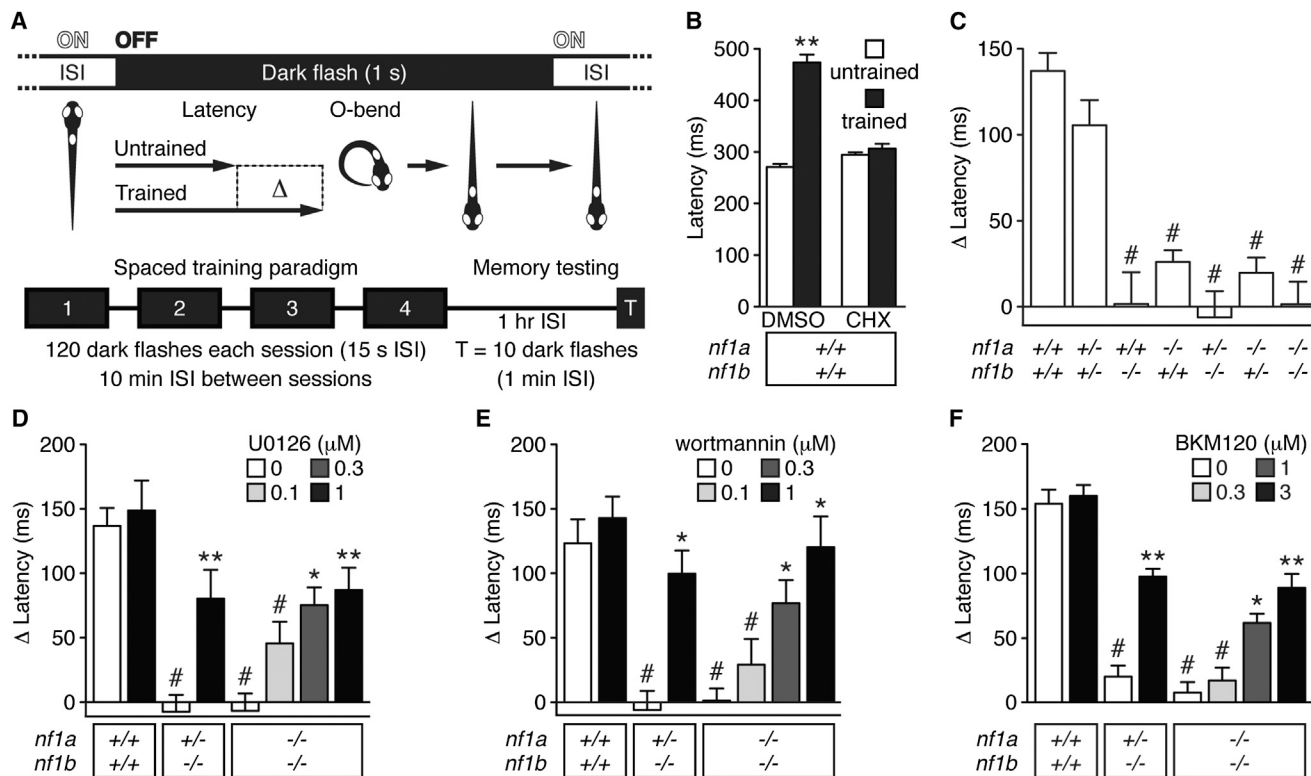


Figure 1. *nf1* Mutant Larvae Exhibit Reduced Memory Recall

(A) Schematic representation of the visual memory assay. ISI, interstimulus interval.

(B–F) Mean O-bend latency (B) or latency change (C–F) 1 hr after spaced training (test) versus untrained controls (n = 26–130 O-bend maneuvers per genotype/ treatment). #p < 0.001 versus wild-type untreated (C) or DMSO-treated (B and D–F) larvae. *p < 0.01, **p < 0.001 versus same genotype, DMSO-treated larvae. One-way ANOVA. Error bars denote SEM.

See also [Figures S2](#) and [S3](#).

learning and memory in vertebrates. Larval zebrafish show a remarkable capacity for behavioral plasticity in response to visual and acoustic stimuli, including habituation (Roberts et al., 2013; Wolman et al., 2011), as evidenced by a progressive decline in responsiveness to repeated, inconsequential stimuli (Thompson and Spencer, 1966). The duration of habituated behavior provides a metric for nonassociative learning (short-term habituation) and memory formation and recall (longer-term, protein-synthesis-dependent habituation). Importantly, habituation reflects a highly conserved form of attention-based learning and memory that is similar to the type of cognition impairment found in NF1 children (Hyman et al., 2005; Isenberg et al., 2013; Levine et al., 2006). We tested 5-day-old larvae for protein-synthesis-dependent visual habituation to evaluate memory formation and recall. After a period of light adaptation, exposing the larvae to a sudden absence of light, termed a dark flash, elicited a highly stereotyped yet habituable reorientation maneuver known as an O-bend (Movie S1; Burgess and Granato, 2007a). Delivering repetitive dark flashes through a spaced training paradigm elicited protein-synthesis-dependent memory formation (Figures 1A and 1B). One hour after training, wild-type larvae showed a near doubling in the latency time period before initiating an O-bend compared with responses prior to training (Figure 1B). Treatment with the protein synthesis

inhibitor cycloheximide (CHX, 10 μM) abolished this increase (Figure 1B), consistent with a requirement for protein synthesis (Beck and Rankin, 1995; Davis and Squire, 1984). Larvae null for *nf1a* or *nf1b* showed impaired memory (Figure 1C). This memory deficit is consistent with cognitive impairment observed in NF1 patients and in other animal models of NF1, and supports the use of *nf1* mutant zebrafish to probe the mechanisms of NF1-dependent cognition.

Memory impairment in *Drosophila* and mouse NF1 models is due at least in part to elevated Ras signaling (Costa et al., 2002; Cui et al., 2008; Hannan et al., 2006; Li et al., 2005). Since *nf1* mutant larvae also show increased Ras activity (Shin et al., 2012), we asked whether acute pharmacological inhibition of the Ras effectors MAPK and PI3K could improve memory recall in *nf1* mutants. Small molecules readily cross the developing blood-brain barrier of larval zebrafish until at least 8 days of age (Fleming et al., 2013), facilitating pharmacogenetic approaches for identifying signaling pathways that underlie biological processes and screening of potential therapeutics for neuropsychiatric disorders such as NF1. We treated wild-type, *nf1a*^{+/-}; *nf1b*^{-/-}, and *nf1a*^{-/-}; *nf1b*^{-/-} larvae with inhibitors of MAPK (U0126) or PI3K (wortmannin, BKM120) for 30 min before and throughout training and testing for memory recall. Each compound improved memory recall in *nf1* mutant larvae in a

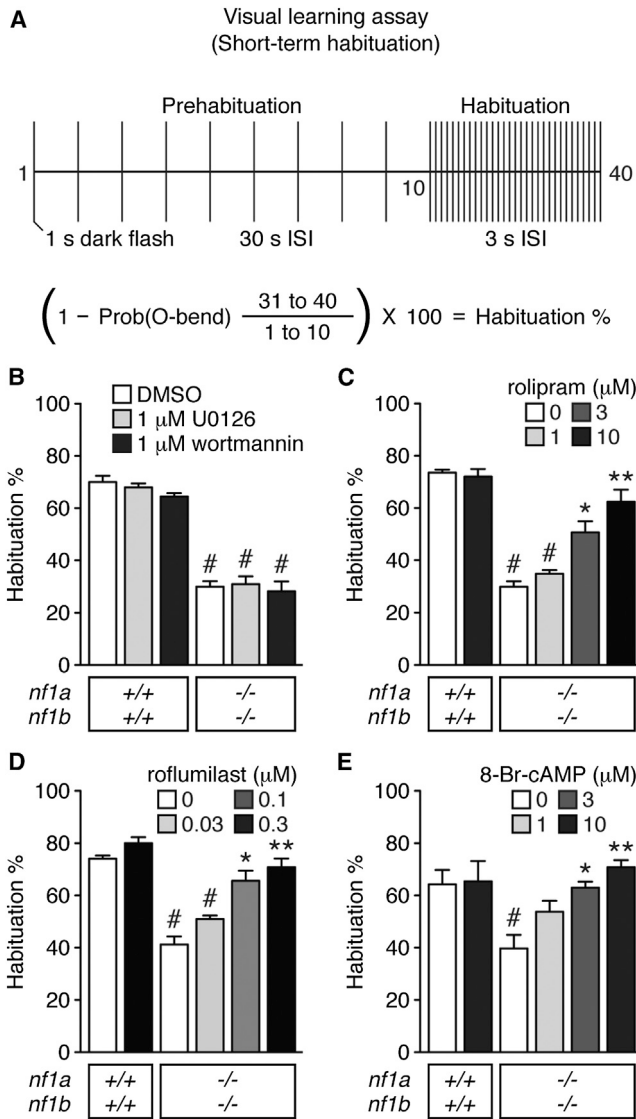


Figure 2. cAMP Signaling Mediates *nf1*-Dependent Visual Learning

(A) Schematic representation of the visual learning assay. (B–E) Mean percentage of habituation to repeated dark-flash stimulation ($n = 3$ groups of 15–20 larvae for all genotype/treatment groups). # $p < 0.001$ versus DMSO-treated wild-type larvae. * $p < 0.01$, ** $p < 0.001$ versus DMSO-treated *nf1a*^{-/-}; *nf1b*^{-/-} larvae. One-way ANOVA. Error bars denote SEM. See also Figures S1 and S3.

dose-dependent manner (Figures 1D–1F). Treatment with 1 μM wortmannin restored memory to wild-type levels, and 1 μM U0126 or 3 μM BKM120 yielded significant memory improvement. Although each of these Ras pathway antagonists exhibits known off-target effects, their different selectivity profiles (Bain et al., 2007; Liao and Laufs, 2005; Maira et al., 2012) suggest that nonspecific effects are unlikely to underlie the observed increase in memory recall. Therefore, these results support a conserved function for the neurofibromin GRD domain in regulation of memory formation through the Ras/MAPK/PI3K signaling pathway.

Learning (the acquisition of information) is critical for establishing memory. We evaluated learning by exposing larvae to dark-flash stimuli delivered at 3 s interstimulus intervals (ISIs) and measuring short-term habituation, as indicated by a reduction in the probability of initiating an O-bend response (Figure 2A). *nf1a*^{-/-}; *nf1b*^{-/-} larvae showed markedly reduced short-term visual (Figure 2B) and acoustic (Figures S1A and S1B; Shin et al., 2012) habituation compared with wild-type controls. Notably, *nf1a*^{-/-}; *nf1b*^{-/-} larvae showed some capacity for learning, which likely accounts for their potential to form memories in the presence of Ras pathway inhibitors (Figures 1D–1F). Larvae with at least one wild-type allele of either *nf1a* or *nf1b* did not show a learning deficit, despite dramatic memory deficits (Figure 1C; M.A.W. and E.D.d.G., unpublished data; Shin et al., 2012). It is possible that our nonassociative habituation assay lacks the necessary sensitivity to detect relatively subtle learning deficiencies in larvae with these genotypes. Attenuating Ras signaling by acute pharmacological inhibition of MAPK (U0126) or PI3K (wortmannin) failed to improve the learning deficit of *nf1a*^{-/-}; *nf1b*^{-/-} larvae (Figures 2B and S1B), suggesting that a distinct pathway mediates NF1-dependent learning.

Whole larval lysates revealed reduced cAMP levels in *nf1a*^{-/-}; *nf1b*^{-/-} mutants compared with wild-type controls (*nf1a*^{-/-}; *nf1b*^{-/-}: 33 fmol ± SEM 2.3 versus wild-type: 79 fmol ± SEM 7.8, $p < 0.001$). To determine whether reduced cAMP signaling contributed to the learning deficits in *nf1a*^{-/-}; *nf1b*^{-/-} mutants, we tested whether enhancing cAMP signaling by acute pharmacological inhibition of phosphodiesterase 4 (PDE4) or stimulation of PKA could improve learning. Inhibition of PDE4 by rolipram or roflumilast, or PKA stimulation by 8-Br-cAMP improved learning behavior in *nf1a*^{-/-}; *nf1b*^{-/-} mutants in response to both repetitive visual (Figures 2C–2E) and acoustic (Figures S1C and S1D) stimuli. Treatment with at least 10 μM rolipram, 0.1 μM roflumilast, or 3 μM 8-Br-cAMP improved habituation to wild-type levels. These results provide evidence that cAMP signaling regulates NF1-dependent learning in a vertebrate system.

We next asked whether cAMP signaling regulates NF1-dependent memory in addition to learning. We tested *nf1a*^{-/-}; *nf1b*^{-/-} larvae, which show reduced learning and a failure to recall memory, and *nf1a*^{+/-}; *nf1b*^{-/-} larvae, which learn normally but fail to form memory, and compared them with wild-type controls. Treatment with 10 μM 8-Br-cAMP, a sufficient dose to restore learning in *nf1a*^{-/-}; *nf1b*^{-/-} larvae (Figures 2E and S1D), failed to improve memory recall in either *nf1a*^{+/-}; *nf1b*^{-/-} or *nf1a*^{-/-}; *nf1b*^{-/-} larvae (Figure S2). These results suggest that cAMP signaling regulates NF1-dependent learning but not memory. Moreover, these results indicate that the memory defects in *nf1a*^{-/-}; *nf1b*^{-/-} mutants are not simply attributable to their learning deficit. These data strongly imply that molecularly distinct pathways that control learning and memory are affected in NF1.

Learned behavior requires consolidation to form stable memory. Despite consensus that defective neurofibromin function can result in learning and memory impairments, whether impaired consolidation contributes to memory deficits remains unclear. *nf1a*^{+/-}; *nf1b*^{-/-} larvae learn normally (M.A.W. and E.D.d.G., unpublished data; Shin et al., 2012) but show reduced memory recall (Figure 1C). Therefore, we asked whether reduced

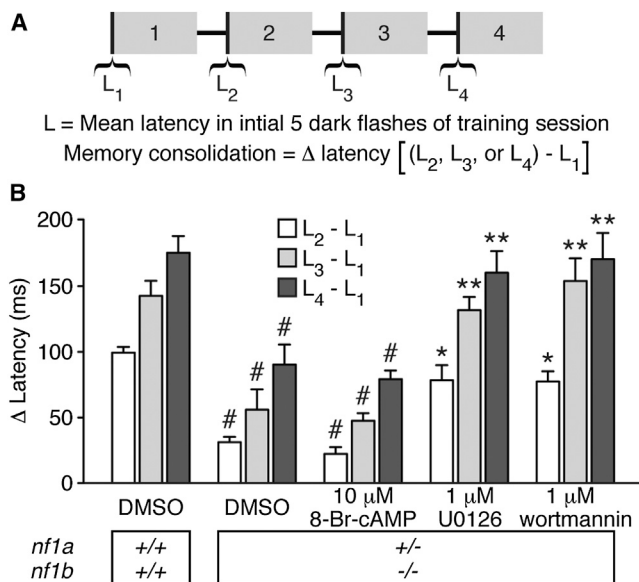


Figure 3. Inhibition of Ras Signaling Improves Memory Consolidation Deficits in *nf1* Mutants

(A) Schematic representation of visual memory consolidation measurement. (B) Mean O-bend latency change comparing responses to dark-flash stimuli 1–5 of sessions 2–4 versus stimuli 1–5 of session 1 ($n = 30$ –139 O-bend maneuvers per genotype/treatment). # $p < 0.001$ versus DMSO-treated wild-type larvae. * $p < 0.01$, ** $p < 0.001$ versus DMSO-treated *nf1a*^{+/-}; *nf1b*^{-/-} larvae. One-way ANOVA. Error bars denote SEM.

See also Figure S3.

memory was due to a consolidation deficit. We determined memory consolidation by calculating the difference between the mean O-bend latency in response to the first five dark-flash stimuli of training session 1 and subsequent training sessions (Figure 3A). Long ISIs between training sessions promote memory consolidation, and therefore spaced training paradigms elicit more stable memory than do massed training paradigms (Beck and Rankin, 1997; Ebbinghaus, 1885). After each session, *nf1a*^{+/-}; *nf1b*^{-/-} larvae showed reduced consolidation compared with wild-type larvae (Figure 3B), suggesting that the memory-recall deficit observed in *nf1a*^{+/-}; *nf1b*^{-/-} larvae (Figure 1C) may be due to a defect in memory consolidation.

To determine the contribution of cAMP and Ras signaling to NF1-dependent memory consolidation, we attempted to improve consolidation in *nf1a*^{+/-}; *nf1b*^{-/-} larvae by pharmacologically enhancing cAMP or attenuating Ras. Enhancing cAMP in *nf1a*^{+/-}; *nf1b*^{-/-} larvae by treatment with 10 μ M 8-Br-cAMP did not increase consolidation (Figure 3B). Pharmacological inhibition of MAPK (1 μ M U0126) or PI3K (1 μ M wortmannin) improved memory consolidation in *nf1a*^{+/-}; *nf1b*^{-/-} larvae to levels indistinguishable from those observed in DMSO-treated wild-type larvae (Figure 3B). These results reveal that deficits in memory consolidation contribute to the etiology of memory dysfunction in NF1 and support a specific role for Ras signaling in mediating NF1-dependent memory formation.

Larvae deficient for *nf1* exhibit learning and memory deficits with characteristics reminiscent of those seen in human NF1

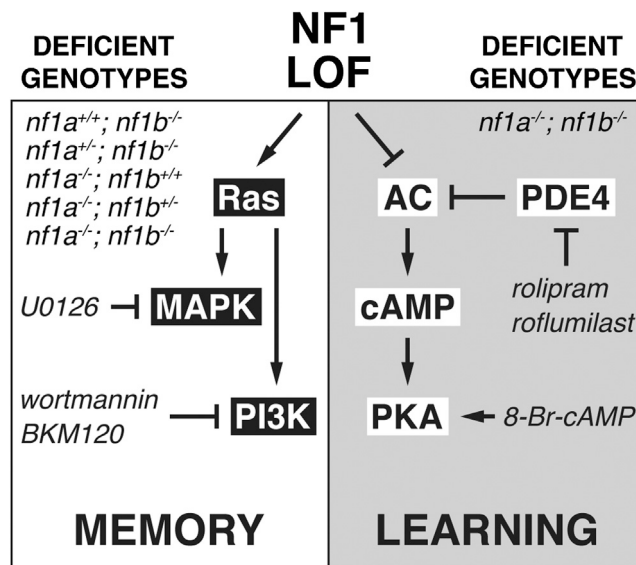


Figure 4. Effects of NF1 Loss of Function on the Ras and cAMP Pathways

The genotypes of the zebrafish *nf1* larvae that exhibited significant memory or learning deficits are shown. The pharmacological agents (italicized) that were used to improve memory or learning in these genotypes, as well as the molecular targets of the agents, are indicated. LOF, loss of function.

patients. We obtained strong evidence in a vertebrate system that NF1 affects at least two distinct signaling pathways that independently modulate learning and memory (Figure 4). A detailed understanding of the structure-function relationship among NF1 mutations, Ras and cAMP signaling, and phenotypes will allow for tailored and personalized therapies for cognitive defects in affected patients. It will also be interesting to determine whether the dynamic regulation of Ras or cAMP signaling in distinct areas of the brain correlates with unique behavioral outcomes. The fact that we observed robust improvements in learning and memory in our experiments even though we used only short-term treatments is encouraging for potential clinical application, and suggests that cognitive defects in this model are not developmental or irreversible. It will be exciting to determine whether these models can be validated in higher vertebrates and whether combination therapy with Ras and cAMP pathway effectors can improve the condition of some NF1 patients.

EXPERIMENTAL PROCEDURES

Generation and Maintenance of Zebrafish

The zebrafish (*Danio rerio*) larvae used in this study were generated from crosses of adults carrying the *nf1a*⁴⁵ and *nf1b*¹⁰ mutant alleles (Shin et al., 2012). Embryos were raised at 28°C in a 14 hr/10 hr light/dark cycle as previously described (Burgess and Granato, 2007a) and all behavioral experiments were conducted with 5 days postfertilization (dpf) larvae. For visual behavioral experiments, larvae were PCR genotyped by clipping a small region of the caudal fin at 3 dpf and genotyping as described previously (Shin et al., 2012). Larvae tested for acoustic habituation were tested individually in a 4 × 4 grid and genotyped after testing. All animal protocols were approved by the University of Pennsylvania Institutional Animal Care and Use Committee.

Behavioral Assays and Analysis

Dark-flash-induced O-bend responses were elicited, recorded, and measured as previously described (Burgess and Granato, 2007a; Wolman et al., 2011). Larvae were trained and tested at a density of 15 larvae per 9 ml E3 in 6 cm Petri dishes and kept in the dishes during training or testing. To elicit memory formation, larvae were exposed to a training paradigm comprised of four 30 min training sessions, each consisting of exposure to a 1 s dark flash delivered every 15 s. Training sessions were separated by 10 min ISIs. After the fourth session and a 1 hr ISI, larvae were exposed to ten dark flashes with 1 min ISIs to evaluate memory recall. To calculate memory recall, the average latency to initiate an O-bend in untrained larvae was subtracted from the latency to initiate an O-bend in trained larvae. Memory consolidation was calculated by subtracting the average latency to initiate an O-bend in response to dark-flash stimuli 1–5 of training session 1 from the latency to initiate an O-bend in response to dark flashes 1–5 of sessions 2–4.

To measure visual short-term habituation, a series of 40 1 s dark flashes were delivered. Stimuli 1–10 were delivered with 30 s ISIs and stimuli 11–40 were delivered with 3 s ISIs. The percentage of habituation was calculated by dividing the mean O-bend responsiveness to stimuli 31–40 by the mean O-bend responsiveness to stimuli 1–10, subtracting this value from 1, and multiplying by 100. An acoustic short-term habituation assay was performed as previously described (Wolman et al., 2011).

Pharmacology

All compounds were added to the larval media 30 min before and throughout the training and testing paradigm. Cycloheximide (C4859; Sigma-Aldrich), U0126 (9903, Cell Signaling Technology), wortmannin (9951; Cell Signaling Technology), BKM120 (S2247; Selleck Chemicals), rolipram (R6520; Sigma-Aldrich), roflumilast (S2131, Selleck Chemicals), and 8-Br-cAMP (B007; BIOLOG Life Science Institute) were dissolved in 100% DMSO and administered in a final concentration of 1% DMSO. Doses of each compound were prescreened for potential effects on baseline O-bend responsiveness to visual stimuli and short-latency C-bend responsiveness to acoustic stimuli. The defined, stereotyped kinematic parameters of both larval maneuvers were also examined (Burgess and Granato, 2007a, 2007b). Selected doses did not change baseline behavior responsiveness or kinematic performance after 30 min or 4 hr of incubation. Immunohistochemistry with anti-phospho-ERK (4377; Cell Signaling Technology) and anti-phospho-(Ser/Thr) PKA substrate (9621; Cell Signaling Technology) was performed on paraffin-embedded larval tissue after fixation in 4% paraformaldehyde, dehydration, and sectioning at 8 μ M thickness in order to demonstrate the pathway specificity of the pharmacologic inhibitors (Figure S3).

SUPPLEMENTAL INFORMATION

Supplemental Information includes three figures and one movie and can be found with this article online at <http://dx.doi.org/10.1016/j.celrep.2014.07.054>.

AUTHOR CONTRIBUTIONS

E.D.d.G. and M.A.W. designed and performed experiments together and wrote the manuscript. M.G. and J.A.E. designed experiments, supervised the work, and edited the manuscript. S.M.M. and T.A.J. contributed reagents and advice on the experimental design and approach.

ACKNOWLEDGMENTS

We thank Tom Look, Kurt Engleka, Kurt Marsden, and Min Min Lu for helpful discussions and technical support. This work was supported by grants from the NIH (2T32 HL007843 to E.D.d.G., R01 HL062974 to J.A.E., R01 MH092257 and HD 37975A11 to M.G., and GM086902 to T.A.J.) and the Department of Defense (NF110108 to J.A.E. and AR1101189 to T.A.J.). S.M. was supported by grants from the FRAXA Research Foundation and the University of Pennsylvania (R25 MH060490, Clinical Research Scholars Program in Psychiatry).

Received: January 24, 2014

Revised: July 20, 2014

Accepted: July 29, 2014

Published: August 28, 2014

REFERENCES

- Armstrong, B.C., Le Bouillier, J.C., and Petit, T.L. (2012). Ultrastructural synaptic changes associated with neurofibromatosis type 1: a quantitative analysis of hippocampal region CA1 in a Nf1(+/-) mouse model. *Synapse* 66, 246–255.
- Bain, J., Plater, L., Elliott, M., Shpiro, N., Hastie, C.J., McLauchlan, H., Klevvernic, I., Arthur, J.S., Alessi, D.R., and Cohen, P. (2007). The selectivity of protein kinase inhibitors: a further update. *Biochem. J.* 408, 297–315.
- Beck, C.D., and Rankin, C.H. (1995). Heat shock disrupts long-term memory consolidation in *Caenorhabditis elegans*. *Learn. Mem.* 2, 161–177.
- Beck, C.D.O., and Rankin, C.H. (1997). Long-term habituation is produced by distributed training at long ISIs and not by massed training or short ISIs in *Caenorhabditis elegans*. *Anim. Learn. Behav.* 25, 446–457.
- Brown, J.A., Gianino, S.M., and Gutmann, D.H. (2010). Defective cAMP generation underlies the sensitivity of CNS neurons to neurofibromatosis-1 heterozygosity. *J. Neurosci.* 30, 5579–5589.
- Brown, J.A., Diggs-Andrews, K.A., Gianino, S.M., and Gutmann, D.H. (2012). Neurofibromatosis-1 heterozygosity impairs CNS neuronal morphology in a cAMP/PKA/ROCK-dependent manner. *Mol. Cell. Neurosci.* 49, 13–22.
- Burgess, H.A., and Granato, M. (2007a). Modulation of locomotor activity in larval zebrafish during light adaptation. *J. Exp. Biol.* 210, 2526–2539.
- Burgess, H.A., and Granato, M. (2007b). Sensorimotor gating in larval zebrafish. *J. Neurosci.* 27, 4984–4994.
- Cichowski, K., and Jacks, T. (2001). NF1 tumor suppressor gene function: narrowing the GAP. *Cell* 104, 593–604.
- Costa, R.M., Federov, N.B., Kogan, J.H., Murphy, G.G., Stern, J., Ohno, M., Kucherlapati, R., Jacks, T., and Silva, A.J. (2002). Mechanism for the learning deficits in a mouse model of neurofibromatosis type 1. *Nature* 415, 526–530.
- Cui, Y., Costa, R.M., Murphy, G.G., Elgersma, Y., Zhu, Y., Gutmann, D.H., Parada, L.F., Mody, I., and Silva, A.J. (2008). Neurofibromin regulation of ERK signaling modulates GABA release and learning. *Cell* 135, 549–560.
- Davis, H.P., and Squire, L.R. (1984). Protein synthesis and memory: a review. *Psychol. Bull.* 96, 518–559.
- Diggs-Andrews, K.A., Tokuda, K., Izumi, Y., Zorumski, C.F., Wozniak, D.F., and Gutmann, D.H. (2013). Dopamine deficiency underlies learning deficits in neurofibromatosis-1 mice. *Ann. Neurol.* 73, 309–315.
- Ebbinghaus, H. (1885). *Memory: A Contribution to Experimental Psychology* (New York: Teachers College, Columbia University).
- Fahsold, R., Hoffmeyer, S., Mischung, C., Gille, C., Ehlers, C., Küçükceylan, N., Abdel-Nour, M., Gewies, A., Peters, H., Kaufmann, D., et al. (2000). Minor lesion mutational spectrum of the entire NF1 gene does not explain its high mutability but points to a functional domain upstream of the GAP-related domain. *Am. J. Hum. Genet.* 66, 790–818.
- Fleming, A., Diekmann, H., and Goldsmith, P. (2013). Functional characterisation of the maturation of the blood-brain barrier in larval zebrafish. *PLoS ONE* 8, e77548.
- Gouzi, J.Y., Moresis, A., Walker, J.A., Apostolopoulou, A.A., Palmer, R.H., Bernardis, A., and Skoulakis, E.M. (2011). The receptor tyrosine kinase Alk controls neurofibromin functions in *Drosophila* growth and learning. *PLoS Genet.* 7, e1002281.
- Guiding, C., McNair, K., Stone, T.W., and Morris, B.J. (2007). Restored plasticity in a mouse model of neurofibromatosis type 1 via inhibition of hyperactive ERK and CREB. *Eur. J. Neurosci.* 25, 99–105.
- Guo, H.F., The, I., Hannan, F., Bernardis, A., and Zhong, Y. (1997). Requirement of *Drosophila* NF1 for activation of adenylyl cyclase by PACAP38-like neuropeptides. *Science* 276, 795–798.

- Guo, H.F., Tong, J., Hannan, F., Luo, L., and Zhong, Y. (2000). A neurofibromatosis-1-regulated pathway is required for learning in *Drosophila*. *Nature* *403*, 895–898.
- Hannan, F., Ho, I., Tong, J.J., Zhu, Y., Nurnberg, P., and Zhong, Y. (2006). Effect of neurofibromatosis type 1 mutations on a novel pathway for adenylyl cyclase activation requiring neurofibromin and Ras. *Hum. Mol. Genet.* *15*, 1087–1098.
- Hegedus, B., Dasgupta, B., Shin, J.E., Emmett, R.J., Hart-Mahon, E.K., Elghazi, L., Bernal-Mizrachi, E., and Gutmann, D.H. (2007). Neurofibromatosis-1 regulates neuronal and glial cell differentiation from neuroglial progenitors in vivo by both cAMP- and Ras-dependent mechanisms. *Cell Stem Cell* *1*, 443–457.
- Ho, I.S., Hannan, F., Guo, H.F., Hakker, I., and Zhong, Y. (2007). Distinct functional domains of neurofibromatosis type 1 regulate immediate versus long-term memory formation. *J. Neurosci.* *27*, 6852–6857.
- Hyman, S.L., Shores, A., and North, K.N. (2005). The nature and frequency of cognitive deficits in children with neurofibromatosis type 1. *Neurology* *65*, 1037–1044.
- Hyman, S.L., Arthur Shores, E., and North, K.N. (2006). Learning disabilities in children with neurofibromatosis type 1: subtypes, cognitive profile, and attention-deficit-hyperactivity disorder. *Dev. Med. Child Neurol.* *48*, 973–977.
- Isenberg, J.C., Templer, A., Gao, F., Titus, J.B., and Gutmann, D.H. (2013). Attention skills in children with neurofibromatosis type 1. *J. Child Neurol.* *28*, 45–49.
- Jayachandran, R., Liu, X., Bosedasgupta, S., Müller, P., Zhang, C.L., Moshous, D., Studer, V., Schneider, J., Genoud, C., Fossoud, C., et al. (2014). Coronin 1 regulates cognition and behavior through modulation of cAMP/protein kinase A signaling. *PLoS Biol.* *12*, e1001820.
- Karlsgodt, K.H., Rosser, T., Lutkenhoff, E.S., Cannon, T.D., Silva, A., and Bearden, C.E. (2012). Alterations in white matter microstructure in neurofibromatosis-1. *PLoS ONE* *7*, e47854.
- Levine, T.M., Materek, A., Abel, J., O'Donnell, M., and Cutting, L.E. (2006). Cognitive profile of neurofibromatosis type 1. *Semin. Pediatr. Neurol.* *13*, 8–20.
- Li, W., Cui, Y., Kushner, S.A., Brown, R.A., Jentsch, J.D., Frankland, P.W., Cannon, T.D., and Silva, A.J. (2005). The HMG-CoA reductase inhibitor lovastatin reverses the learning and attention deficits in a mouse model of neurofibromatosis type 1. *Curr. Biol.* *15*, 1961–1967.
- Liao, J.K., and Laufs, U. (2005). Pleiotropic effects of statins. *Annu. Rev. Pharmacol. Toxicol.* *45*, 89–118.
- Maira, S.M., Pecchi, S., Huang, A., Burger, M., Knapp, M., Sterker, D., Schnell, C., Guthy, D., Nagel, T., Wiesmann, M., et al. (2012). Identification and characterization of NVP-BKM120, an orally available pan-class I PI3-kinase inhibitor. *Mol. Cancer Ther.* *11*, 317–328.
- Peng, S., Yang, X., Liu, G.J., Zhang, X.Q., Wang, G.L., and Sun, H.Y. (2014). The phosphodiesterase-4 inhibitor Ro 20-1724 reverses learning and memory impairments, and down-regulation of CREB in the hippocampus and cortex induced by ketamine anesthesia in immature rats. *J. Neurosurg. Sci.*
- Richter, W., Menniti, F.S., Zhang, H.T., and Conti, M. (2013). PDE4 as a target for cognition enhancement. *Expert Opin. Ther. Targets* *17*, 1011–1027.
- Roberts, A.C., Bill, B.R., and Glanzman, D.L. (2013). Learning and memory in zebrafish larvae. *Front Neural Circuits* *7*, 126.
- Shilyansky, C., Karlsgodt, K.H., Cummings, D.M., Sidiropoulou, K., Hardt, M., James, A.S., Ehninger, D., Bearden, C.E., Poirazi, P., Jentsch, J.D., et al. (2010). Neurofibromin regulates corticostriatal inhibitory networks during working memory performance. *Proc. Natl. Acad. Sci. USA* *107*, 13141–13146.
- Shin, J., Padmanabhan, A., de Groh, E.D., Lee, J.-S., Haidar, S., Dahlberg, S., Guo, F., He, S., Wolman, M.A., Granato, M., et al. (2012). Zebrafish neurofibromatosis type 1 genes have redundant functions in tumorigenesis and embryonic development. *Dis. Model. Mech.* *5*, 881–894.
- Silva, A.J., Frankland, P.W., Marowitz, Z., Friedman, E., Laszlo, G.S., Cioffi, D., Jacks, T., and Bourchouladze, R. (1997). A mouse model for the learning and memory deficits associated with neurofibromatosis type 1. *Nat. Genet.* *15*, 281–284.
- The, I., Hannigan, G.E., Cowley, G.S., Reginald, S., Zhong, Y., Gusella, J.F., Hariharan, I.K., and Bernards, A. (1997). Rescue of a *Drosophila* NF1 mutant phenotype by protein kinase A. *Science* *276*, 791–794.
- Thompson, R.F., and Spencer, W.A. (1966). Habituation: a model phenomenon for the study of neuronal substrates of behavior. *Psychol. Rev.* *73*, 16–43.
- Tong, J., Hannan, F., Zhu, Y., Bernards, A., and Zhong, Y. (2002). Neurofibromin regulates G protein-stimulated adenylyl cyclase activity. *Nat. Neurosci.* *5*, 95–96.
- Walker, J.A., Tchoudakova, A.V., McKenney, P.T., Brill, S., Wu, D., Cowley, G.S., Hariharan, I.K., and Bernards, A. (2006). Reduced growth of *Drosophila* neurofibromatosis 1 mutants reflects a non-cell-autonomous requirement for GTPase-Activating Protein activity in larval neurons. *Genes Dev.* *20*, 3311–3323.
- Walker, J.A., Gouzi, J.Y., Long, J.B., Huang, S., Maher, R.C., Xia, H., Khalil, K., Ray, A., Van Vactor, D., Bernards, R., and Bernards, A. (2013). Genetic and functional studies implicate synaptic overgrowth and ring gland cAMP/PKA signaling defects in the *Drosophila melanogaster* neurofibromatosis-1 growth deficiency. *PLoS Genet.* *9*, e1003958.
- Wolman, M.A., Jain, R.A., Liss, L., and Granato, M. (2011). Chemical modulation of memory formation in larval zebrafish. *Proc. Natl. Acad. Sci. USA* *108*, 15468–15473.